

2012

Experimental investigations on the wake interferences of multiple wind turbines

Ahmet Ozbay
Iowa State University

Follow this and additional works at: <https://lib.dr.iastate.edu/etd>

 Part of the [Aerospace Engineering Commons](#)

Recommended Citation

Ozbay, Ahmet, "Experimental investigations on the wake interferences of multiple wind turbines" (2012). *Graduate Theses and Dissertations*. 12427.
<https://lib.dr.iastate.edu/etd/12427>

This Thesis is brought to you for free and open access by the Iowa State University Capstones, Theses and Dissertations at Iowa State University Digital Repository. It has been accepted for inclusion in Graduate Theses and Dissertations by an authorized administrator of Iowa State University Digital Repository. For more information, please contact digirep@iastate.edu.

Experimental investigations on the wake interferences of multiple wind turbines

by

Ahmet Ozbay

A thesis submitted to the graduate faculty
in partial fulfillment of the requirements for the degree of
MASTER OF SCIENCE

Major: Aerospace Engineering

Program of Study Committee:

Hui Hu, Major Professor

Richard Wlezien

Partha Sarkar

Iowa State University

Ames, Iowa

2012

Copyright © Ahmet Ozbay, 2012. All rights reserved.

TABLE OF CONTENTS

LIST OF FIGURES	iv
LIST OF TABLES	viii
ACKNOWLEDGEMENTS	x
ABSTRACT	xi
CHAPTER 1. OVERVIEW	1
1.1 BACKGROUND INFORMATION	1
1.2 THEORY	3
1.3 EVOLUTION OF WIND ENERGY	9
1.4 WIND FARM AERODYNAMICS	14
1.4.1 WAKE INTERFERENCE EFFECTS	14
1.4.2 ATMOSPHERIC STABILITY EFFECTS	19
1.4.3 COMPLEX TERRAIN (HILLY TERRAIN) EFFECTS	22
1.4.4 TERRAIN ROUGHNESS EFFECTS ON THE INCOMING FLOW	23
CHAPTER 2. WIND FARM ANALYSIS	25
2.1 INTRODUCTION	25
2.2 EXPERIMENTAL SET-UP	26
2.3 EXPERIMENTAL RESULTS AND DISCUSSIONS	29
2.4 CONCLUSION	51
CHAPTER 3. COMPLEX TERRAIN ANALYSIS	52
3.1 INTRODUCTION	52
3.2 EXPERIMENTAL SET-UP	54
3.3 EXPERIMENTAL RESULTS AND DISCUSSIONS	58
3.4 CONCLUSION	74
CHAPTER 4. MULTIPLE WAKE INTERACTIONS	76
4.1 FIVE TURBINES IN A LINE / EFFECT OF SPACING	76
4.1.1 INTRODUCTION	76
4.1.2 EXPERIMENTAL SET-UP	77
4.1.3 EXPERIMENTAL RESULTS AND DISCUSSIONS	80
4.1.4 CONCLUSION	85
4.2 WAKE EFFECTS ON WIND TURBINE PERFORMANCE	86

4.2.1	INTRODUCTION	86
4.2.2	EXPERIMENTAL SET-UP	87
4.2.3	EXPERIMENTAL RESULTS AND DISCUSSIONS	88
4.2.4	CONCLUSION	92
	BIBLIOGRAPHY	93

LIST OF FIGURES

FIGURE 1-1 TYPICAL BOUNDARY-LAYER VELOCITY PROFILE	2
FIGURE 1-2 COMPONENTS OF A TYPICAL HAWT	4
FIGURE 1-3 CONCEPTUAL POWER CURVE FOR A MODERN VARIABLE-SPEED WIND TURBINE	5
FIGURE 1-4 AERODYNAMIC FORCES AND ANGLES ON A TURBINE BLADE	5
FIGURE 1-5 DEPENDENCE OF WIND TURBINE POWER ON THE ROTOR SPEED AND TIP SPEED RATIO (TSR)	7
FIGURE 1-6 GROWTH IN THE SIZE OF WIND TURBINES	9
FIGURE 1-7 INSTALLED WIND ENERGY CAPACITY IN U.S. AND WIND TRAJECTORY UP TO 2030	10
FIGURE 1-8 PREDICTED MEAN ANNUAL WIND SPEED DISTRIBUTION AMONG THE STATES IN U.S.	11
FIGURE 1-9 LAYOUT OF POWER TRANSMISSION LINES	12
FIGURE 1-10 DISTRIBUTION OF INSTALLED WIND POWER CAPACITY AMONG THE STATES IN U.S.	13
FIGURE 1-11 ONSHORE AND OFFSHORE WIND FARMS	14
FIGURE 1-12 CLOUDS FORMED BY THE WAKE OF WIND TURBINES	15
FIGURE 1-13 VELOCITY PROFILE IN THE WAKE OF A SINGLE TURBINE	16
FIGURE 1-14 VISUALIZATION OF TIP VORTICES IN THE NEAR WAKE	17
FIGURE 1-15 TEMPERATURE DISTRIBUTION OF VERTICALLY MOVING AIR	19
FIGURE 1-16 VARIATIONS IN ATMOSPHERIC STABILITY DUE TO DIURNAL CHANGES (THERMAL)	20
FIGURE 1-17 ATMOSPHERIC STABILITY EFFECTS ON WIND TURBINE PERFORMANCE	20
FIGURE 1-18 ATMOSPHERIC STABILITY EFFECTS ON WIND FARM EFFICIENCY	21
FIGURE 1-19 FLOW OVER A STEEP HILL OR 2D-RIDGE	22
FIGURE 1-20 SPEED UP EFFECT ON THE TOP OF THE 2-D RIDGE	22
FIGURE 1-21 ROUGHNESS ELEMENTS (SPIRES, CHAINS AND WOODEN BLOCKS) IN THE ATBL WIND TUNNEL	24
FIGURE 2-1 A PICTURE OF THE TEST SECTION OF THE AABL WIND TUNNEL	27
FIGURE 2-2 THE MEASURED PROFILES OF THE SIMULATED ATMOSPHERIC BOUNDARY LAYER	27
FIGURE 2-3 WIND TURBINE MODEL (LEFT) AND FORCE TRANSDUCER AND WIRING EQUIPMENT UNDERNEATH OF THE MODEL WIND TURBINE (RIGHT)	28
FIGURE 2-4 SIMULATED WIND FARM LAYOUTS (ALIGNED AND STAGGERED) IN THE AABL WIND TUNNEL	29
FIGURE 2-5 POWER SPECTRUM ANALYSIS OF THE MEASURED VOLTAGE FROM TACHOMETER	31
FIGURE 2-6 POWER SPECTRUM ANALYSIS OF MEASURED VOLTAGE FROM TACHOMETER	32
FIGURE 2-7 ALIGNED AND STAGGERED WIND FARM LAYOUT WITH 3D STREAMWISE SPACING AND THE TURBINES IN THE CENTRAL COLUMN OF EACH ROW WERE ANALYZED IN TERMS OF THEIR RELATIVE (NORMALIZED) POWER OUTPUT, ROTATIONAL FREQUENCY AND THRUST FORCE	34
FIGURE 2-8 RELATIVE (NORMALIZED) POWER AND ROTATIONAL FREQUENCY THROUGHOUT THE ROWS OF THE ALIGNED AND STAGGERED WIND FARMS WITH 3D STREAMWISE SPACING FOR THE NO SPIRE FLOW CASE	34
FIGURE 2-9 COBRA PROBE MEASUREMENT LOCATIONS (HORIZONTAL AND VERTICAL)	35

FIGURE 2-10 NORMALIZED VELOCITY DEFICIT PROFILE IN THE VERTICAL ROTOR PLANE	36
FIGURE 2-11 NORMALIZED VELOCITY DEFICIT PROFILE IN THE SPANWISE PLANE	37
FIGURE 2-12 NORMALIZED ADDED TURBULENCE INTENSITY (I_{uu}) PROFILE ON THE ROTOR PLANE	38
FIGURE 2-13 TIME SEQUENCE OF THE MEASURED POWER OUTPUT FOR A TURBINE IN ALIGNED AND STAGGERED WIND FARM LAYOUT WITH 3D STREAMWISE SPACING FOR THE NO SPIRE FLOW CASE	40
FIGURE 2-14 RELATIVE (NORMALIZED) POWER OUTPUT OF A TURBINE LOCATED IN THE CENTER OF THE LAST ROW OF DIFFERENT WIND FARM LAYOUTS FOR THE NO SPIRE FLOW CASE	41
FIGURE 2-15 POWER SPECTRUM ANALYSIS OF THE MEASURED VOLTAGE FROM TACHOMETER	43
FIGURE 2-16 RELATIVE (NORMALIZED) POWER THROUGHOUT THE ROWS OF ALIGNED AND STAGGERED WIND FARMS WITH 3D STREAMWISE SPACING FOR THE SPIRE AND NO SPIRE FLOW CASE	44
FIGURE 2-17 TIME SEQUENCE OF THE MEASURED POWER FOR A TURBINE IN STAGGERED WIND FARM LAYOUT FOR THE SPIRE AND NO SPIRE FLOW CASE	45
FIGURE 2-18 RELATIVE (NORMALIZED) POWER OUTPUT OF THE TURBINE (SHOWN INSIDE THE CIRCLE) FOR DIFFERENT WIND FARM LAYOUTS AND ITS DEPENDENCE ON THE TURBULENCE CHARACTER OF THE INCOMING FLOW	46
FIGURE 2-19 RELATIVE (NORMALIZED) THRUST FORCE THROUGHOUT THE ROWS OF ALIGNED AND STAGGERED WIND FARMS WITH 3D STREAMWISE SPACING FOR THE SPIRE AND NO SPIRE FLOW CASE	47
FIGURE 2-20 TIME SEQUENCE OF THE MEASURED C_F FOR A SINGLE TURBINE FOR THE SPIRE AND NO SPIRE FLOW CASE	48
FIGURE 2-21 TIME SEQUENCE OF THE MEASURED C_F FOR A WIND TURBINE IN ALIGNED AND STAGGERED WIND FARM LAYOUT FOR THE SPIRE FLOW CASE	49
FIGURE 2-22 OVERALL POWER ANALYSIS OF DIFFERENT WIND FARM LAYOUTS FOR THE SPIRE AND NO SPIRE FLOW CASE	50
FIGURE 3-1 SIMULATION OF ATMOSPHERIC BOUNDARY LAYER CONDITIONS IN THE WIND TUNNEL USING SPIRES AND CHAINS	55
FIGURE 3-2 MEASURED PROFILES OF THE NORMALIZED MEAN VELOCITY AND TURBULENCE INTENSITY	55
FIGURE 3-3 SCHEMATIC DRAWING OF A 2D-RIDGE AND SPEED-UP EFFECT ON THE TOP OF THE RIDGE	56
FIGURE 3-4 2D-RIDGE PROFILE WITH WIND TURBINES INSTALLED AROUND THE RIDGE (LEFT) AND COBRA PROBE MEASUREMENT SET-UP ON THE TOP OF THE RIDGE (RIGHT)	56
FIGURE 3-5 THE SCHEMATIC OF THE POWER MEASUREMENT SYSTEM (LEFT) AND UNDERNEATH OF A MODEL WIND TURBINE WITH FORCE TRANSDUCER AND WIRING SYSTEM FOR POWER MEASUREMENT (RIGHT)	57
FIGURE 3-6 1:350 SCALED WIND TURBINE MODEL TO SIMULATE A 2 MW WIND TURBINE WITH 90 M ROTOR BLADES	58

FIGURE 3-7 SCHEMATIC OF THE FLOW OVER STEEP HILL OR RIDGE, SEPARATION IS LIKELY TO OCCUR ON THE LEE SIDE DEPENDING ON THE SLOPE	58
FIGURE 3-8 LOCATIONS WHERE A MODEL WIND TURBINE WAS INSTALLED IN THE FLAT AND COMPLEX (2D-RIDGE) TERRAIN	59
FIGURE 3-9A MEASURED MEAN VELOCITY PROFILE ON THE TOP OF THE 2D-RIDGE IN COMPARISON WITH FLAT TERRAIN FOR THE SPIRE AND NO SPIRE FLOW CASE	60
FIGURE 3-9B FRACTIONAL SPEED UP ($\Delta s = \Delta U/U_0$) ON THE TOP OF THE MODERATE AND HIGH SLOPED 2D-RIDGE FOR THE SPIRE AND NO-SPIRE FLOW CASE	60
FIGURE 3-10 MEASURED TURBULENCE (IUU) PROFILE ON THE TOP OF THE MODERATE AND HIGH SLOPED 2D-RIDGE IN COMPARISON WITH FLAT TERRAIN FOR THE SPIRE AND NO SPIRE FLOW CASE	62
FIGURE 3-11 A SCHEMATIC REPRESENTATION OF A TURBINE LOCATED ON A FLAT AND COMPLEX TERRAIN	62
FIGURE 3-12 POWER SPECTRUM ANALYSIS OF THE MEASURED VOLTAGE FROM THE TACHOMETER FOR A TURBINE IN A FLAT AND COMPLEX (TOP OF THE RIDGE) TERRAIN (NO SPIRE FLOW CASE)	65
FIGURE 3-13 WAKE MEASUREMENTS ON THE TOP OF THE 2D-RIDGE IN THE VERTICAL PLANE FOR DIFFERENT UPSTREAM TURBINE(S) CONFIGURATIONS	67
FIGURE 3-14 NORMALIZED MEAN VELOCITY DEFICIT AND TURBULENCE INTENSITY PROFILE ON THE TOP OF THE MODERATE AND HIGH SLOPED 2D-RIDGE FOR DIFFERENT UPSTREAM TURBINE(S) CONFIGURATIONS (NO SPIRE FLOW CASE)	68
FIGURE 3-15 WAKE MEASUREMENTS OVER A FLAT TERRAIN IN THE VERTICAL PLANE FOR DIFFERENT UPSTREAM TURBINE(S) CONFIGURATIONS	69
FIGURE 3-16 NORMALIZED MEAN VELOCITY DEFICIT AND TURBULENCE INTENSITY PROFILE OVER A FLAT TERRAIN FOR DIFFERENT UPSTREAM TURBINE(S) CONFIGURATIONS (NO SPIRE FLOW CASE)	69
FIGURE 3-17 SCHEMATIC REPRESENTATION OF WAKE EXPANSION OVER A 2D-RIDGE	70
FIGURE 3-18 PERFORMANCE (POWER AND WIND LOADING) MEASUREMENTS ON THE DOWNSTREAM TURBINE FOR DIFFERENT UPSTREAM TURBINE CONFIGURATIONS IN A FLAT TERRAIN	71
FIGURE 3-19 PERFORMANCE (POWER AND WIND LOADING) MEASUREMENTS ON THE DOWNSTREAM TURBINE FOR DIFFERENT UPSTREAM TURBINE CONFIGURATIONS IN COMPLEX (2D-RIDGE) TERRAIN	72
FIGURE 4-1 A SCHEMATIC REPRESENTATION OF TWO TURBINES IN TANDEM ARRANGEMENT	76
FIGURE 4-2 A SCHEMATIC REPRESENTATION OF FIVE TURBINES WITH 3D STREAMWISE SPACING IN TANDEM ARRANGEMENT	77
FIGURE 4-3 FIVE TURBINES IN TANDEM ARRANGEMENT WITH 3D SPACING (LEFT) AND SPIRES AT THE ONSET OF THE TEST SECTION OF THE WIND TUNNEL (RIGHT)	78
FIGURE 4-4 NORMALIZED MEAN VELOCITY AND TURBULENCE INTENSITY PROFILES OF THE SIMULATED ATMOSPHERIC BOUNDARY LAYER	79
FIGURE 4-5 NORMALIZED (RELATIVE) POWER AND THRUST FORCE VARIATION FOR DIFFERENT TURBINE SPACING	80

FIGURE 4-6 VARIATION OF THE POWER OUTPUT OF THE WIND TURBINE WITH DIFFERENT LOADING IN EACH ROW FOR THE SPIRE AND NO SPIRE FLOW CASE	81
FIGURE 4-7 NORMALIZED (RELATIVE) POWER AND THRUST FORCE VARIATION THROUGHOUT THE ROWS	82
FIGURE 4-8 POWER SPECTRUM ANALYSIS OF THE MEASURED VOLTAGE FROM TACHOMETER FOR THE SPIRE AND NO SPIRE FLOW CASE (COMPARISON BETWEEN THE TURBINES LOCATED IN THE 1ST AND THE LAST (5TH) ROW)	83
FIGURE 4-9 TIME SEQUENCE OF THE MEASURED POWER OUTPUT OF THE TURBINE LOCATED IN THE 1ST AND LAST (5TH) ROW FOR THE SPIRE AND NO SPIRE FLOW CASE	84
FIGURE 4-10 TWO TURBINES IN TANDEM ARRANGEMENT WITH UPSTREAM TURBINE YAWED WITH 50° ON THE TURNTABLE	87
FIGURE 4-11 MEASURED PROFILES OF NORMALIZED MEAN VELOCITY AND TURBULENCE INTENSITY	87
FIGURE 4-12 A SCHEMATIC OF TWO TURBINES (YAWING THE UPSTREAM TURBINE) IN TANDEM ARRANGEMENT WITH DIFFERENT SPACING	88
FIGURE 4-13 VARIATION IN THE POWER OUTPUT AND ROTATIONAL FREQUENCY OF THE UPSTREAM TURBINE AT VARIOUS YAW ANGLES FOR THE NO SPIRE (LOW TURBULENCE) CASE	89
FIGURE 4-14 NORMALIZED (RELATIVE) POWER OF THE UPSTREAM TURBINE AT VARIOUS YAW ANGLES FOR THE SPIRE AND NO SPIRE FLOW CASE	89
FIGURE 4-15 NORMALIZED (RELATIVE) POWER OF THE DOWNSTREAM TURBINE AT $X/D=2$ AND $X/D=4$ WITH THE FIRST UPSTREAM TURBINE OPERATING AT VARIOUS YAW ANGLES	90
FIGURE 4-16 VARIATION IN THE TOTAL POWER OUTPUT FROM TWO TURBINES AT VARIOUS UPSTREAM YAW ANGLES DEPENDING ON THE SEPARATION DISTANCE FOR THE NO SPIRE FLOW CASE	91
FIGURE 4-17 VARIATION IN THE TOTAL POWER OUTPUT FROM TWO TURBINES AT VARIOUS UPSTREAM YAW ANGLES DEPENDING ON THE SEPARATION DISTANCE FOR THE SPIRE FLOW CASE	92

LIST OF TABLES

TABLE 1-1 TERRAIN CLASSIFICATION DUE TO DAVENPORT (WIERINGA, 1992)	2
TABLE 1-2 LEADING COUNTRIES IN THE WIND ENERGY AND THEIR WIND POWER CAPACITY	12
TABLE 2-1 VARIATION IN THE MEASURED POWER OUTPUT AND ROTATIONAL FREQUENCY OF A WIND TURBINE IN DIFFERENT WIND FARM LAYOUTS FOR THE NO SPIRE FLOW CASE	33
TABLE 2-2 MEASURED POWER OUTPUT AND DEVIATIONS IN THE POWER OUTPUT OF A TURBINE IN STAGGERED AND ALIGNED WIND FARM LAYOUT WITH 3D STREAMWISE SPACING FOR THE NO SPIRE FLOW CASE	40
TABLE 2-3 VARIATION IN THE MEASURED POWER OUTPUT OF A WIND TURBINE IN DIFFERENT WIND FARM LAYOUTS FOR THE SPIRE AND NO SPIRE FLOW CASE	42
TABLE 2-4 MEASURED POWER OUTPUT AND DEVIATIONS IN THE POWER OUTPUT OF A TURBINE IN STAGGERED WIND FARM LAYOUT FOR THE SPIRE AND NO SPIRE FLOW CASE	44
TABLE 2-5 MEASURED C_F AND DEVIATIONS IN C_F OF A WAKE-FREE TURBINE FOR THE SPIRE AND NO SPIRE FLOW CASE	48
TABLE 3-1 COMPARISON OF WIND TURBINE PERFORMANCES AT LOCATION 1 AND LOCATION 2 IN THE FLAT AND COMPLEX TERRAIN FOR THE SPIRE AND NO SPIRE FLOW CASE	59
TABLE 3-2 FRACTIONAL SPEED UP (AT THE HUB HEIGHT) ON THE TOP OF THE MODERATE AND HIGH SLOPED 2D-RIDGE	61
TABLE 3-3 PERFORMANCE OF A TURBINE (AVERAGE POWER OUTPUT WITH THE DEVIATIONS) ON A FLAT AND COMPLEX TERRAIN FOR THE SPIRE AND NO SPIRE FLOW CASE	63
TABLE 3-4 MODEL WIND TURBINE PERFORMANCE IN FLAT AND COMPLEX (TOP OF A 2D-RIDGE) TERRAIN FOR THE SPIRE AND NO SPIRE FLOW CASE	66
TABLE 3-5 WAKE EFFECTS ON THE PERFORMANCE (POWER) OF A DOWNSTREAM TURBINE DEPENDING ON DIFFERENT UPSTREAM TURBINE SPACING FOR THE SPIRE AND NO SPIRE FLOW CASE IN A FLAT TERRAIN	71
TABLE 3-6 WAKE EFFECTS ON THE PERFORMANCE (WIND LOADING) OF A DOWNSTREAM TURBINE DEPENDING ON DIFFERENT UPSTREAM TURBINE SPACING FOR THE SPIRE AND NO SPIRE FLOW CASE IN A FLAT TERRAIN	72
TABLE 3-7 WAKE EFFECTS ON THE PERFORMANCE (POWER) OF A DOWNSTREAM TURBINE IN A COMPLEX (TOP OF A 2D-RIDGE WITH MODERATE AND HIGH SLOPE) TERRAIN DEPENDING ON DIFFERENT UPSTREAM TURBINE SPACING FOR THE SPIRE AND NO SPIRE FLOW CASE	73
TABLE 3-8 WAKE EFFECTS ON THE PERFORMANCE (WIND LOADING) OF A DOWNSTREAM TURBINE IN A COMPLEX (TOP OF A 2D-RIDGE WITH MODERATE AND HIGH SLOPE) TERRAIN DEPENDING ON DIFFERENT UPSTREAM TURBINE SPACING FOR THE SPIRE AND NO SPIRE FLOW CASE	74
TABLE 4-1 PERCENT DECREASE (%) IN THE POWER AND THRUST FORCE FOR THE SPIRE AND NO SPIRE FLOW CASE DEPENDING ON THE SPACING BETWEEN TURBINES	80

TABLE 4-2 PERFORMANCE OF THE TURBINE (AVERAGE POWER OUTPUT WITH THE DEVIATIONS) LOCATED IN THE 1ST AND LAST (5TH) ROW FOR THE SPIRE AND NO SPIRE FLOW CASE

ACKNOWLEDGEMENTS

I have been indebted in the preparation of this thesis to my major professor, Dr. Hui Hu, whose patience and kindness, as well as his academic experience, have been invaluable to me. It was an honor for me to study under his assistance and to be one of his research students. I am extremely grateful to Dr. Zifeng Yang and Dr. Wei Tian for their great contributions to my study. I want to thank all the students in my research group who shared their comments and ideas that I made use of. I also appreciate the assistance I received from Bill Rickard and Jim Benson during my experiments in the wind tunnel. In addition, I would like to thank our graduate secretary, Dee Pfeiffer, for answering my endless questions about the graduate program and helping me get through tough times.

I have been extremely fortunate to have the support of a very special friend, Farid Huseynov, who helped me stay sane through my graduate study.

My parents, Akif and Sema Ozbay, and my sister, Asli Ozbay, have been a constant source of support – emotional, moral and of course financial – during my years as a graduate student, and this thesis would certainly not have existed without them.

My fiance, and my future wife, Hilal has been, always, my pillar, my joy and my guiding light, and I thank her.

ABSTRACT

In this study, a wind tunnel investigation was carried out to investigate the wake interferences of multiple wind turbines sited over flat and complex (2D-Ridge) terrains in order to understand the physics behind the wind farm design optimization for higher power yield and better durability. The experiments were conducted in Aerodynamic/Atmospheric Boundary Layer (AABL) Wind Tunnel with an array of model wind turbines over flat and complex terrains with non-homogenous surface winds. The effects of the turbine spacing and the wind farm layout on the wake interferences were investigated among multiple wind turbines sited over flat and complex (2D-Ridge) terrains.

The characteristics of the surface winds (mean velocity and turbulence profiles) were quantified by using cobra probe in order to elucidate the interaction between atmospheric boundary layer and wind farms. The detailed flow field measurements were correlated with the dynamic wind loads as well as the power outputs of the wind turbine models. Thus, different wind farm layouts (aligned and staggered) were analyzed in terms of their performance.

The effects of the characteristics of the incoming atmospheric boundary layer (mean velocity and turbulence intensity profiles) on the performance of the individual wind turbines and on the array efficiency of different wind farm layouts were also investigated.

The results obtained from the present study shed light on how complex dynamics of the wind farms could be affected by different factors such as the wind farm configuration, turbine spacing, incoming flow character, topography of the terrain (complex terrains) and operating conditions of the upstream turbines.

CHAPTER 1. OVERVIEW

1.1 BACKGROUND INFORMATION

Air flows from higher to lower pressure fields due to the pressure gradient. The movement of air caused by the differences in the air pressure is the formal definition of the wind. There are two major driving mechanisms generating large scale winds;

- Rotation of the earth (Coriolis effect)
- Uneven heating of Earth's surface resulting air density gradients – horizontal and vertical motion of air

In order to exploit the energy of the wind, wind turbines operate in the Earth's boundary layer called Atmospheric Boundary Layer (ABL) which is the lowest part of the atmosphere. Since it is very close to the Earth's surface, it is directly affected from the frictional and viscous effects of the surface depending on the type of the surface. Different surfaces have different effects on the wind flow. Thus, the thickness of the Atmospheric Boundary Layer (ABL) varies depending on the type of the terrain. The boundary layer is thinner over smooth surfaces (sea, ocean or ice) and much thicker over rough surfaces such as hilly, forested or urban terrains with buildings. The Atmospheric Boundary Layer (ABL) thickness could be as shallow as 50 m in wintertime Arctic and as deep as 2 km in the tropics.

The boundary layer thickness is defined as the distance from the ground where $U(x, y) = 0.99 U(x)$, $U(x, y)$ is the velocity inside the boundary layer and $U(x)$ is the free stream velocity. Inside the boundary layer, the flow is dominated by surface friction and viscous effects. The flow velocity on the surface is zero due to the no-slip condition, the flow inside the boundary layer is characterized by the strong velocity gradients especially closer to the ground (10% of the thickness of the BL) – the flow velocity increases with increasing height within the boundary layer as shown in Figure 1-1.

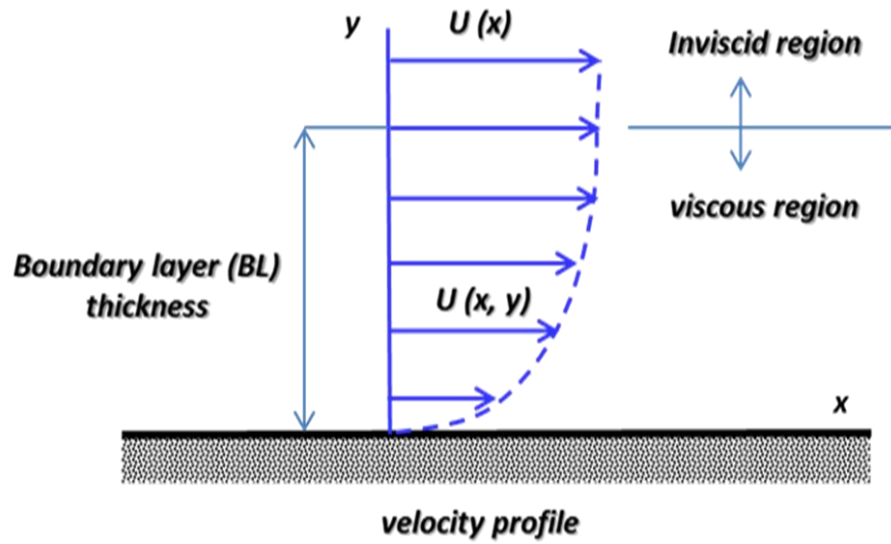


Figure 1-1 Typical boundary-layer velocity profile

The velocity profile inside boundary layer (BL) is defined by the logarithmic law depending on the roughness length (m) of the terrain. Thus, the velocity profile in the boundary layer varies depending on the type of the terrain.

no.	class name	Roughness length: m	landscape features
1	sea	0.0002	<i>open water, tidal flat, snow with fetch above 3 km</i>
2	smooth	0.005	<i>featureless land, ice</i>
3	open	0.03	<i>flat terrain with grass or very low vegetation, airport runway</i>
4	roughly open	0.10	<i>cultivated area, low crops, obstacles of height H separated by at least 20 H</i>
5	rough	0.25	<i>open landscape, scattered shelter belts, obstacles separated by 15 H or so</i>
6	very rough	0.5	<i>landscape with bushes, young dense forest etc. separated by 10 H or so</i>
7	closed	1.0	<i>open spaces comparable with H, e.g. mature forest, low-rise built-up area</i>
8	chaotic	over 2.0	<i>irregular distribution of large elements, e.g. city center, large forest with clearings</i>

Table 1-1 Terrain classification due to Davenport (Wieringa, 1992)
(Linacre & Geerts, 1999)

Roughness length (m) is used to define the surface roughness for different terrains (Table 1-1). As the roughness of the terrain increases, the flow velocity tends to decrease in the boundary layer especially at the first 10% of the thickness of the boundary layer.

$$\text{Log wind profile: } U = \frac{U_*}{k} \ln \frac{z}{z_0} \quad \text{for neutral stability} \quad (\text{eq. 1-1})$$

Where U_* is the shear velocity (m/s), k is Von Karman's constant (0.40) and z_0 is the surface roughness (m). The formula also takes the stability conditions of the atmosphere into account with a stability term (including Monin – Obukhov stability parameter). However, for neutral stability conditions, stability term drops out.

The wind velocity profile in the Atmospheric Boundary Layer (ABL) can be approximated using the log wind profile equation (eq. 1-1). According to the equation, wind velocity increases logarithmically with increasing height within the boundary layer depending on the surface roughness and atmospheric stability. However, the equation above accounts for the neutral stability (adiabatic) conditions (stability term drops out). Power law is generally used as a substitute for log wind profile to determine the velocity profile in the absence of surface roughness and atmospheric stability information.

$$\text{Power law wind profile: } U = U_r \times \left(\frac{z}{z_r}\right)^\alpha \quad \text{for neutral stability} \quad (\text{eq. 1-2})$$

Where U_r is the reference velocity at the reference height z_r and α is the power exponent commonly assumed to be constant (1/7) in wind resource assessments.

The turbulence in the Atmospheric Boundary Layer (ABL) leads to fluctuations in the wind speed and direction which makes the siting and design of wind turbines very crucial for efficient power production.

1.2 THEORY

Wind turbines operate inside the Atmospheric Boundary Layer (ABL) in order to generate electricity by extracting the power available in the wind. A typical horizontal axis wind turbine (HAWT) has thousands of different components. Three main parts of a typical wind turbine;

- Rotor or blades (3 bladed for most commercial wind turbines)

It converts the kinetic energy available in the wind to the rotational energy

- Driving train (Hub + Nacelle)

It has gearbox and generator (converting mechanical energy to electrical energy)

- Tower

It supports rotor, drive train and all the other equipments

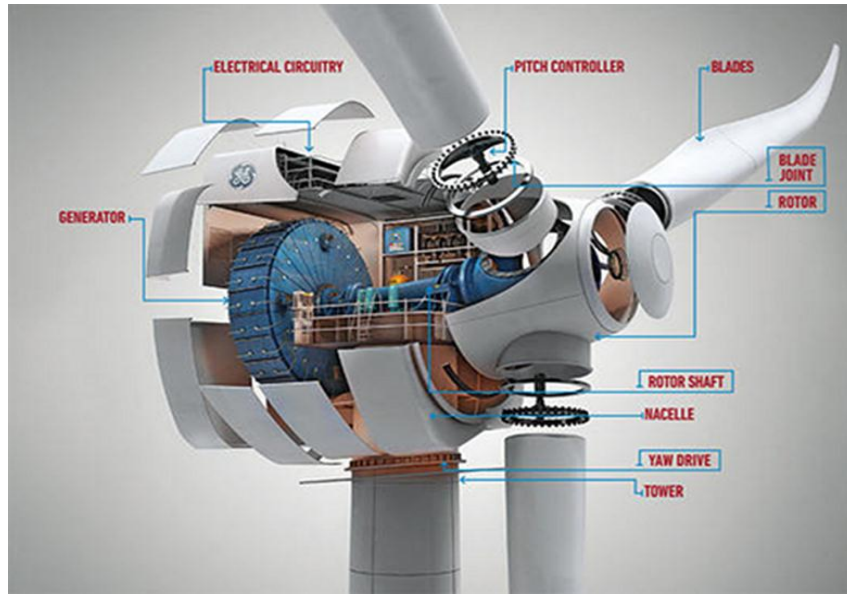


**Figure 1-2 Components of a typical HAWT
(Pacella, 2010)**

The main components of a typical Horizontal Axis Wind Turbine (HAWT) is shown in Figure 1-2. As the wind flows through the rotor, the blades start to rotate. The speed at which the turbine first starts to rotate and generate power is defined as the cut-in speed (3-5 m/s). As the wind speed rises above the cut-in speed, the level of electrical power output increases rapidly (proportional to the cube of incoming velocity). However, the power output of a turbine does not go beyond the limit which is set by the capacity of the generator. This limit is called the *rated power output*. At higher wind speeds, turbines are designed to limit the power to the rated power output by rotating the blades around its longitudinal axis (pitch controller), so no further increase can be seen in the power output (Figure 1-3).

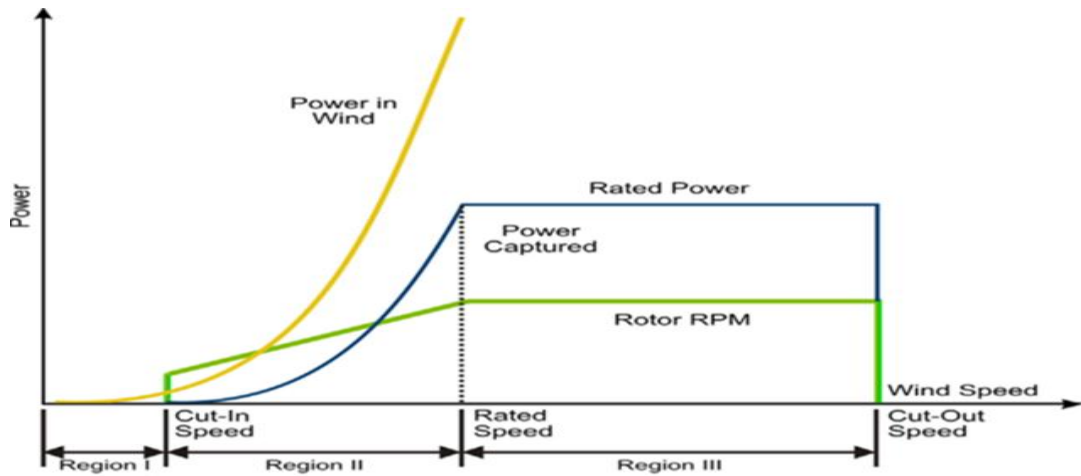


Figure 1-3 Conceptual power curve for a modern variable-speed wind turbine (20% Wind Energy by 2030, 2008)

Pitching of the blades or changing the pitch angle of the blades (pitch angle is the angle between the blade chord line and its axis of rotation) is crucial for protecting the structural integrity of the wind turbine especially at higher wind speeds due to the fact that extreme forces acting on rotor blades may cause overloading of rotor, gearbox and generator.

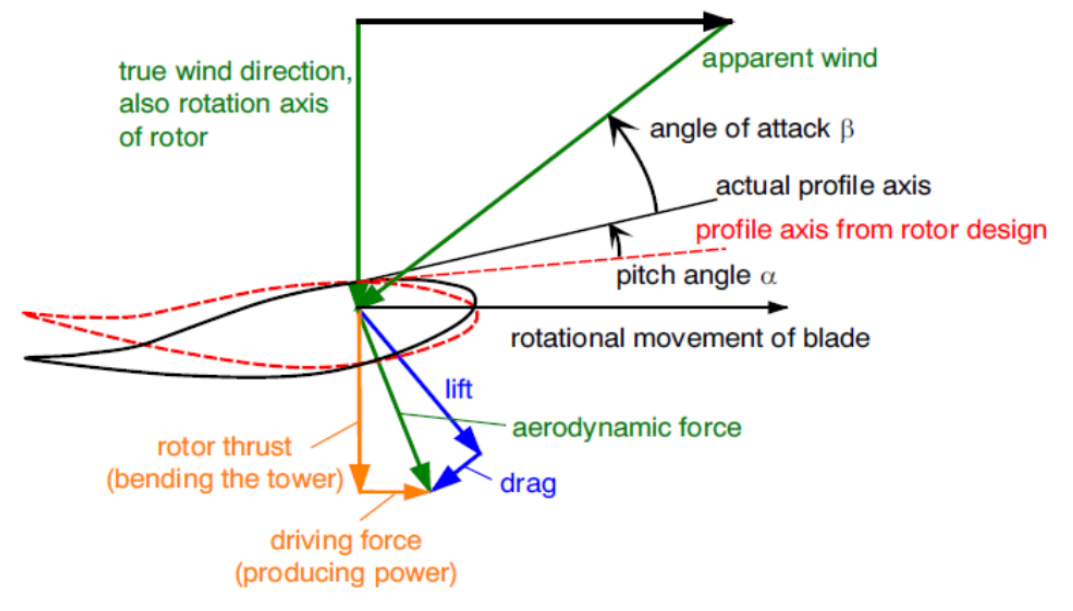


Figure 1-4 Aerodynamic forces and angles on a turbine blade (Hoffmann, 2002)

The power generated by the wind turbines increases with increasing wind speed. However, at strong winds, wind turbines are exposed to excessive forces which may cause catastrophic damages. Therefore, pitching the blades (increasing the pitch angle α in Figure 1-4) protects the wind turbine at strong winds through pitch control or active stall control to keep the power output at its optimum range.

Pitch control: At higher wind speeds, in order not to exceed the rated power output level, blades are pitched out of the wind through the gears in the hub of the rotor (through electrical controls using step motors). It is used to keep the rotor speed in the optimum range for varying wind speeds. In an emergency shutdown or at stronger winds, feathering the blades ($\alpha=90^\circ$) minimizes the angle of attack, thereby reduces the lift and increases the drag generated by the blades.

Active stall control: It is an alternative method, increasing the angle of attack of wind turbine blade until the point where blade stalls (active stall at $\alpha=0^\circ$). Due to stall, lift is decreased and drag is increased – decreasing the torque on the blades and power output as well.

Therefore, above the optimum wind speed, the blades are typically pitched either into the wind (feathering) or away from the wind (active stall) to provide a safe and efficient operating condition for the wind turbine. The effects of pitching on a wind turbine can be summarized as;

- Optimizing the power output
- Preventing the overloading of the rotor, gearbox and generator

In order to describe the relation between the wind speed (U – m/s) and the rotation of the rotor (Ω - rad/s), a non-dimensional term called Tip Speed Ratio (TSR) is used. It is an important parameter which is related to the power output of the wind turbine.

$$\text{Tip Speed Ratio (TSR)} = \frac{\Omega D}{2U} \quad (\text{eq. 1-3})$$

Wind turbines are designed to operate at its optimum Tip Speed Ratio (TSR) to extract as much power as possible from the incoming flow. Optimum TSR for modern wind turbines with three rotor blades is over the range 5 – 7 (Figure 1-5).

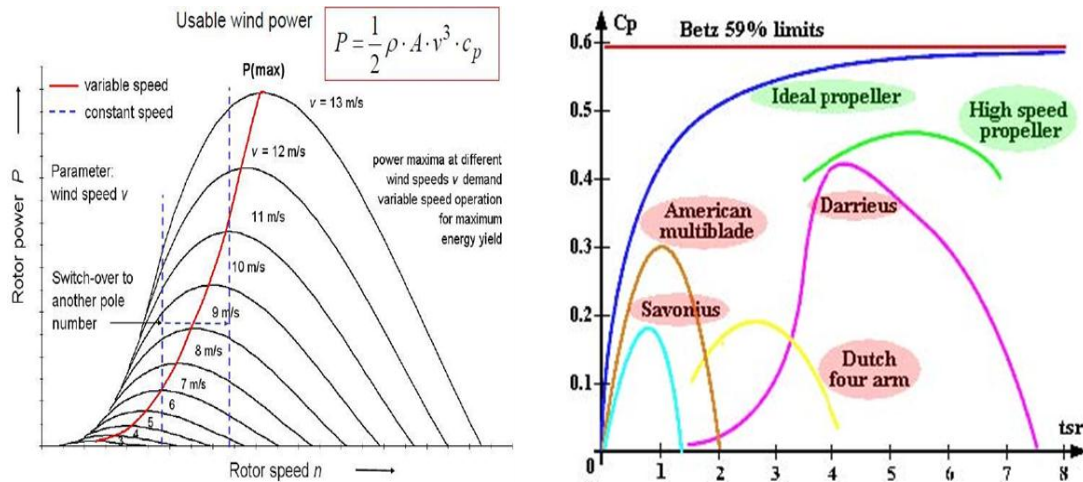


Figure 1-5 Dependence of wind turbine power on the rotor speed and tip speed ratio (TSR) (FS Turbines Aerodynamic Efficiency Improvement) (left) and (Fink, 2005) (right)

If a rotor operates below its optimum TSR then it will disturb less flow thus extract less power. If it operates above its optimum TSR, it acts like a solid wall obstructing the wind flow thereby reducing the power. Turbines operating at greater TSRs than the optimum range face with;

- Higher rotational speeds at the blade tip
- Higher levels of noise and vibration,
- Reduced rotor efficiency and overloading of the rotor, gearbox and generator

Thus, wind turbines should operate at its optimum TSR to extract the power available in the wind efficiently.

The power output of a wind turbine is proportional to the cube of the wind speed proving that the wind speed is playing a key role on the performance of wind turbines. As the wind speed increases, rotor speed (Ω - rad/s) also increases thereby increasing the power output of the wind turbine. Most of the commercial-scale wind turbines operate in the range of 5 – 22 rpm. For a commercial turbine with a rotor diameter of 90 meters, blade tip speed exceeds 90 meters per second if it was to rotate at more than 20 rpm. As a result of higher blade tip speeds, leading edge of the blades will suffer from erosion. In addition to that, this will also contribute to the noise generation.

The gearbox inside the nacelle of the wind turbine converts the slow (5 – 22 rpm), high-torque rotation of the turbine into much faster rotation of the generator. The generator-required speed for energy production is around 1000 to 1600 rpm. Gearboxes used in modern

utility wind turbines with rated power output of MWs are the weakest component of wind turbines and they are likely to fail in five years and have to be replaced (Ragheb & Ragheb, 2010) (A gearbox replacement can cost up 10% of the original construction cost). Therefore, direct drive wind turbines market is growing in the recent years eliminating the need for a gearbox. This technology is attractive for offshore applications since accessing offshore turbines is much more difficult for the replacement of gearboxes. The direct drive technology offers more efficient (higher power output) and reliable (lowering the mechanical maintenance with longer life) wind turbines making direct drive market a highly competitive market including the top wind turbine manufacturers (Transparency Market Research, 2012).

Wind turbines today have speed controller coupled with pitch controller, variable – speed pitch controlled wind turbines. In lower wind speeds, speed controller can adjust the rotational speed of rotor in order to maintain optimum TSR and increase the efficiency of the turbine.

$$\text{Power available in the wind} = P_{\text{available}} = \frac{1}{2} \rho S U^3 \quad (\text{eq. 1-4})$$

Efficiency of a wind turbine can be defined as the percent of power a wind turbine can extract from the power available in the wind. This is limited by what is called the Betz limit. According to the Betz limit, a wind turbine can extract maximum 59% of energy available in the wind. Modern wind turbines today operate in the range of 35 % – 45 % capacity.

$$\text{Efficiency of a wind turbine } (C_p) = \frac{P_{\text{turbine}}}{P_{\text{available}}} = \frac{P_{\text{turbine}}}{\frac{1}{2} \rho S U^3} \quad (\text{eq. 1-5})$$

Rotor diameter (D) of the wind turbine is important for wind energy production. As the rotor diameter of the wind turbine increases, swept area (S) of the rotor increases thereby increasing the power available in the wind. However, increase in the diameter of the wind turbine rotor will add additional costs such as transportation, manufacturing, maintenance, etc.

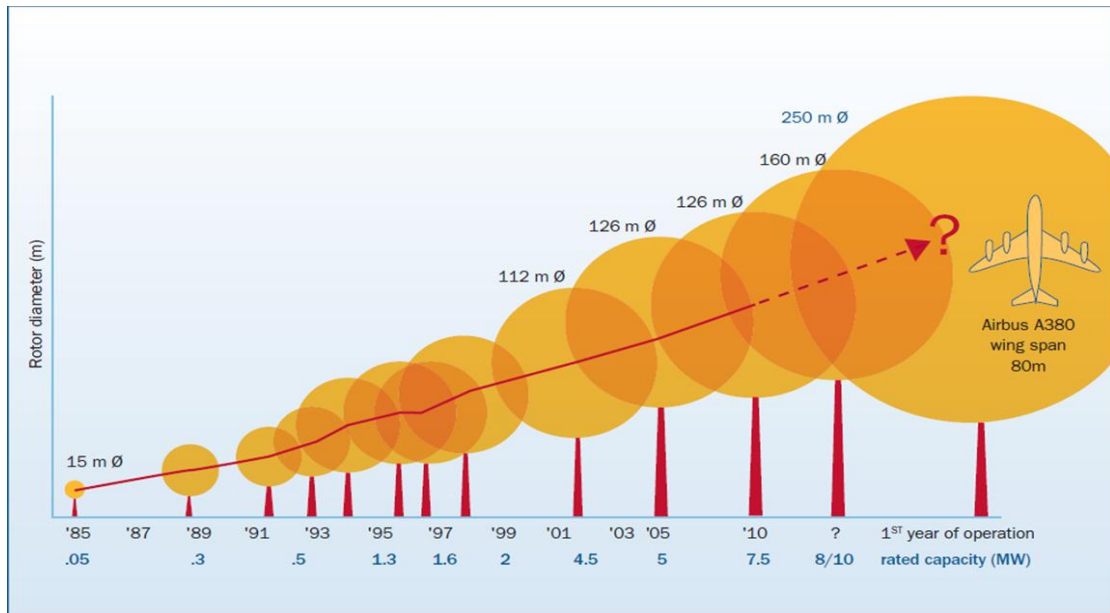


**Figure 1-6 Growth in the size of wind turbines
(Beurskens, 2005)**

Figure 1-6 shows the growth in the size of wind turbines over the years (projected after 2010). The largest wind turbine built today is the Enercon E-126 with a rotor diameter of 126 meters. It was first installed in Germany in 2007 with a capacity of 7+ MW.

Top 3 wind turbine manufacturers in the world:

- Vestas Wind Systems (Denmark)
- General Electric (GE) Wind Energy (U.S.)
- Sinovel Wind Energy (China)

Most of the commercial-scale turbines manufactured and installed in the wind farms have a capacity of 2MW with a rotor diameter ranging between 70-90 meters. Each one will produce enough energy for the annual needs of 500-600 average sized homes. A wind turbine roughly costs \$2 Million per MW to install with an average life span of 20-30 years. In comparison to fossil sources, wind turbine technology requires higher initial investment per MW installed as mentioned above, roughly around \$2 Million per MW; however, wind costs are much more competitive on a life-cycle cost basis with minimal operating expenses.

1.3 EVOLUTION OF WIND ENERGY

Today, 80% of the energy in the world is produced from the fossil sources. However, the world is running out of fossil sources with the environmental concerns about their

consumption due to CO₂ emission. In the near future, the world is going to face with the lack of non-renewable energy sources. Thus, renewable energy will play an important role solving the energy demand in the future. Together with hydro and solar power, wind energy is becoming one of the most promising renewable energy having the potential to contribute substantially to high demand of energy in the world.

Wind is a renewable and sustainable energy resource obviously reducing the CO₂ emission and saving the natural resources. It is cheaper especially after installing the entire infrastructure. However, the variation in the wind speed and direction in the nature affects the amount of electricity produced by wind turbines. Thus, efficiency and reliability are two major concerns about the wind energy. However, understanding the nature of the wind will help convert these concerns into advantages.

Although wind energy is environment-friendly, there are some environmental concerns (danger for wild life, disturbance due to noise and sight) related to the use of wind turbines for wind energy production.

Today, wind energy is providing 2%-3% of total U.S. electricity generation. Wind energy is starting to play a vital role in today's energy market with the advancements in the wind turbine technology. According to a report prepared by the U.S Department of Energy, wind energy has a great potential to satisfy the increasing energy demand of U.S. An interesting scenario in the report is that the contribution of wind energy to the U.S electricity supply will increase up to 20% in 2030.

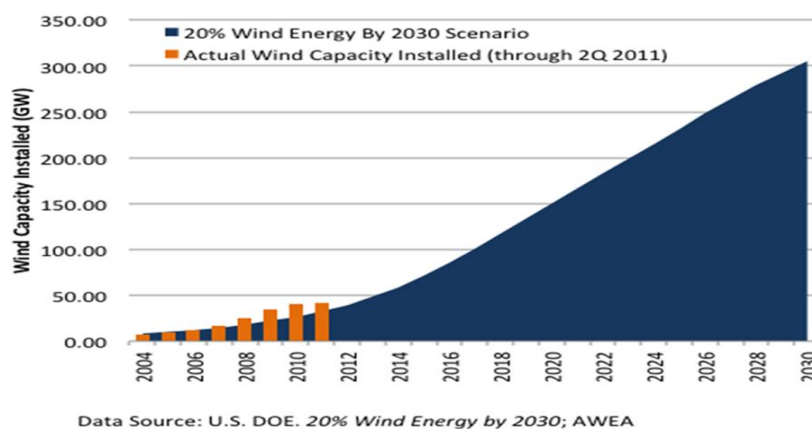


Figure 1-7 Installed wind energy capacity in U.S. and wind trajectory up to 2030 (20% Wind Energy by 2030, 2008)

Figure 1-7 shows the current wind energy capacity (around 45 GW) installed in the U.S. together with the 20% wind trajectory contained in the DOE report. According to the DOE report, the wind energy capacity installed in the U.S. will increase up to 300 GW by 2030 and U.S. has enough wind energy resources to make this scenario go through.

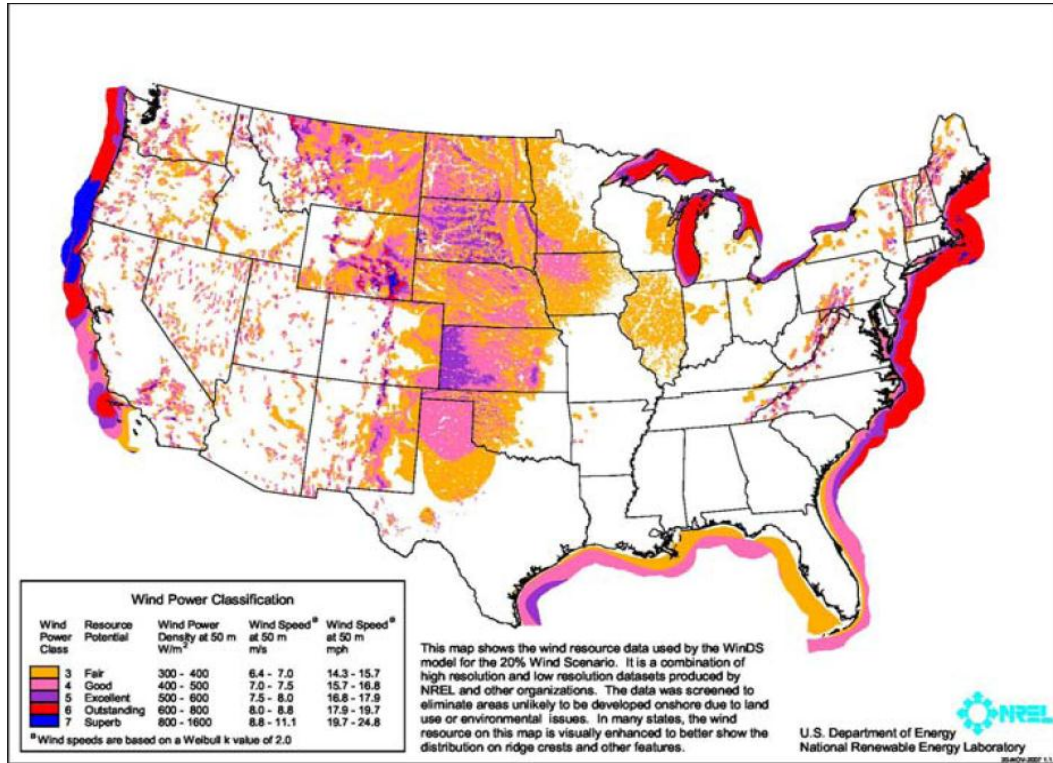


Figure 1-8 Predicted mean annual wind speed distribution among the states in U.S. (20% Wind Energy by 2030, 2008)

Figure 1-8 shows the predicted mean annual wind speeds at 50 meter (m) height. The areas with annual average wind speeds around 6.5 m/s and greater are generally considered to have a wind resource suitable for the wind development.

Although U.S. has enough wind resources to generate 20% of the projected electricity demand by 2030, transmission capacity is not enough to carry the electricity produced.

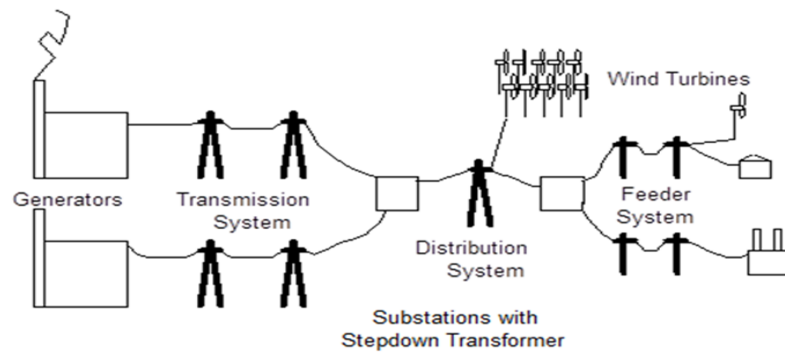


Figure 1-9 Layout of power transmission lines
(Manwell, McGowan, & Rogers, 2010)

Transmission systems use high voltage to reduce the losses in the power transmission lines distributing the power over a large region. Location of usable wind resources do not allow wind turbines to be easily tied into high voltage transmission system (100kV – 400kV). Wind turbines are mostly connected to the distribution system (2.4kV – 40kV) or into feeder systems (480V) as shown in Figure 1-9 (Manwell, McGowan, & Rogers, 2010).

Some of the best wind resources in U.S. are located in areas remote from the largest load centers and markets for electricity. It will be easier to access the wind energy by expanding and upgrading transmission systems, especially for the populated areas where electricity demand is greatest.





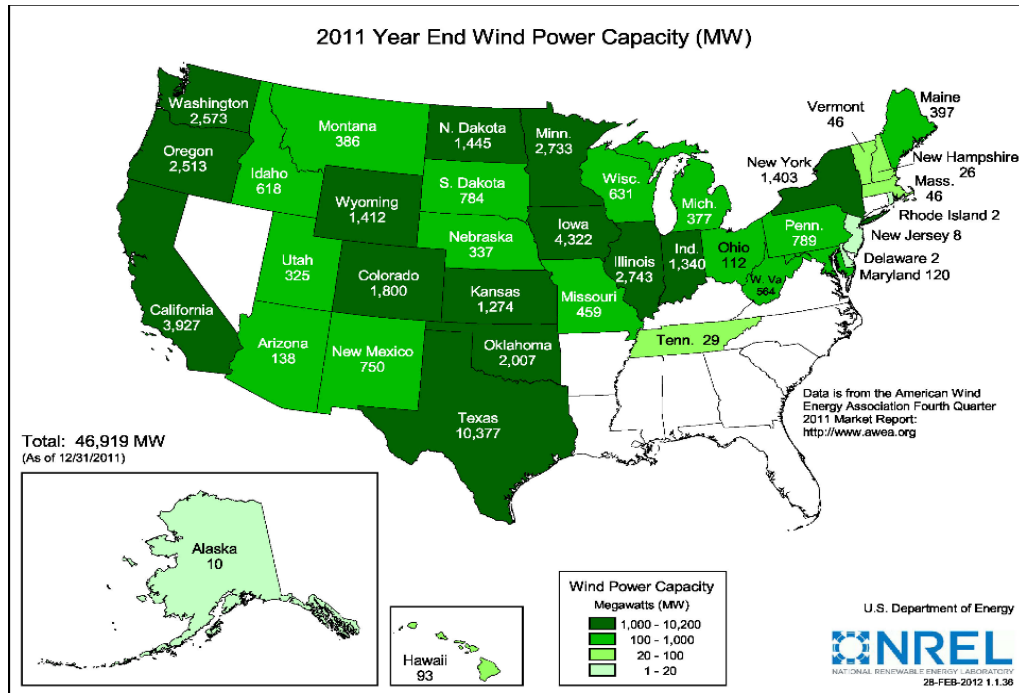
Country	Continent	Capacity (MW, 2011)
 China	Asia	62,733
 USA	North America	46,919
 Germany	Europe	29,060
 Spain	Europe	21,674

Table 1-2 Leading countries in the wind energy and their wind power capacity
(Major Wind Energy Countries, 2012)

Table 1-2 is showing the four major wind energy countries with their current wind power capacities. China is leading with its more than 60 GW of installed wind power capacity and U.S. is following China with 47 GW of wind power capacity. Germany and Spain are the two European countries coming after U.S. with their capacity of 29 GW and 22 GW, respectively.



**Figure 1-10 Distribution of installed wind power capacity among the states in U.S.
(U.S. Department of Energy, 2012)**

The distribution of installed wind power capacity among the states in U.S. is shown in Figure 1-10.

Top 3 states in terms of installed wind power capacity:

- TEXAS (10377 MW) – World’s largest wind farm is located in Texas (Roscoe wind farm, 627 installed wind turbines with a capacity of 782 MW)
- IOWA (4322 MW)
- CALIFORNIA (3927 MW)

These 3 states constitute 40% of the overall wind power capacity in the U.S.

Although Iowa is the second biggest wind power market among the states after Texas, Texas is almost five times bigger with much more population than Iowa. When a comparison is made on the wind power density (installed wind power capacity (kW) /state area (km²)) between Iowa and Texas, the wind power density for Iowa (30kW/ km²) is remarkably higher for a small Midwest state compared to Texas (14.9 kW/ km²).

Iowa now gets a higher percentage of its power from the wind more than any other state in U.S. According to EIA (Energy information Administration), reported by the American

Wind Energy Association, Iowa has reached the milestone of 20% so that wind is providing one fifth of the state's energy needs.

1.4 WIND FARM AERODYNAMICS

This paper is primarily focused on the Horizontal Axis Wind Turbines (HAWT). There are several factors affecting the performance of wind turbines especially in a large wind farm consisting hundreds of turbines and covering larger areas of land (onshore) or water (offshore) as shown in Figure 1-11.



Figure 1-11 Onshore and offshore wind farms

Siting of wind turbines in a wind farm is very crucial for the efficiency of turbines. Wake interference effects on the wind turbines located downstream inside the wind farm should be taken into account during the siting of the wind turbines. Spacing between the turbines together with the layout of the wind farm (staggered or aligned) are important parameters need to be considered while placing the wind turbines in a wind farm.

It is also important to know how a turbine interacts with the atmospheric boundary layer (atmospheric stability, complex terrain, incoming flow characteristics etc.) including the natural life around it.

1.4.1 WAKE INTERFERENCE EFFECTS

The wake interference effects inside a wind farm are vital especially for the turbines located in the subsequent downstream rows due to the fact that wake and wake interaction

effects in a wind farm (Figure 1-12) not only severely influence the overall power production but also reduce the life-time of the wind turbines.



Figure 1-12 Clouds formed by the wake of wind turbines

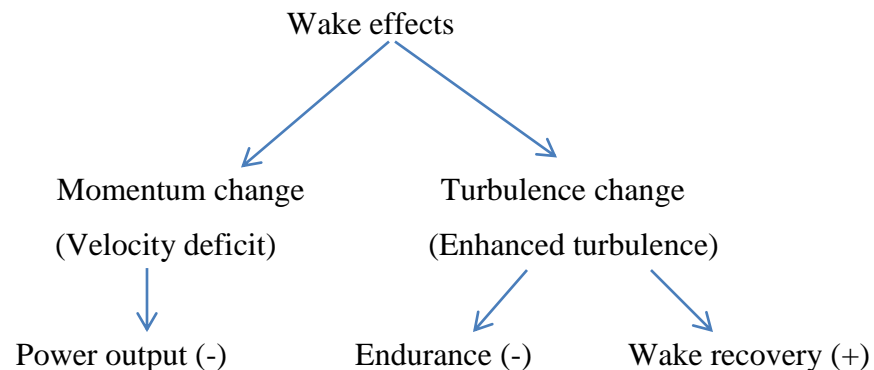
The wind turbine wake is characterized by two parameters,

- Velocity deficit

Reduced power output for downstream turbines

- Enhanced turbulence

Dynamic loading (fatigue) on the blades reducing the life-time of wind turbine; however, high turbulence levels in the atmosphere for large wind farms will make the wake recovery faster hence increasing the efficiency of wind farms



The upstream turbines extract the energy available in the wind so that the wind will lose some of its kinetic energy (Betz limit) leading to reduced wind speed in the wake. Thus, downstream turbines experience loss in their power output due to the velocity deficit. Power

losses due to wake effects in the wind farm will go up to 23% depending on the spacing and alignment of wind turbines (Adaramola & Krogstad, 2011; Barthelmie, et al., 2009; Dahlberg & Thor, 2009; Beyer, Pahle, Schmidt, Waldl, & de Witt, 1994).

Losses can be significantly higher especially for the first turbine immediately downstream of the most upstream turbine depending on the spacing of the turbines. Then, the loss in the successive turbines is much smaller since the wind speed profile and the turbulence levels inside the wind farm will reach an equilibrium value (Sanderse, 2009). This equilibrium value can be reached after several rows depending on the spacing and arrangement of turbines in a wind farm and after that downstream turbines operate approximately at constant power output.

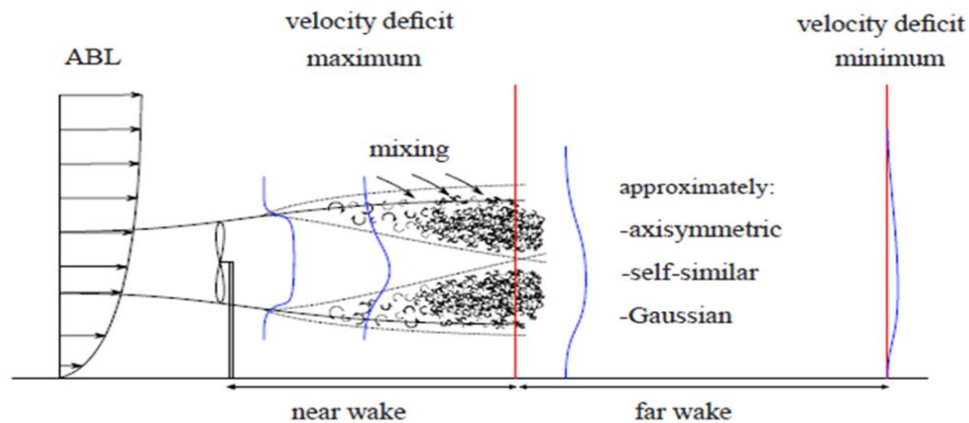


Figure 1-13 Velocity profile in the wake of a single turbine (Sanderse, 2009)

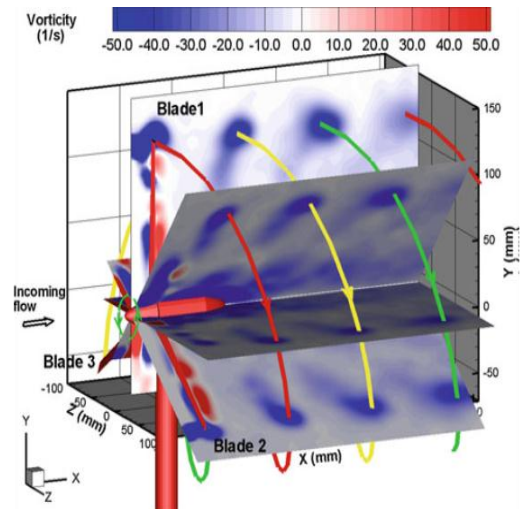
Figure 1-13 shows the velocity profile in the wake of a single turbine. The wake is divided into two parts; near wake and far wake. In the near wake ($1D - 2D$), geometry of turbine (blades aerodynamics, tower effects and vortices shedding from the blade tips) determines the shape of the flow field. The far wake is the region in which geometry of turbine is no more dominant on the flow field; however, wake interference and topographical effects play an important role in that region (Vermeer, Sorensen, & Crespo, 2003). As it is seen from Figure 1-13, the velocity deficit in the wake starts to recover in the far wake and have an axisymmetric Gaussian shaped profile. In addition, the shear layer formed starting from the near wake and extends (expands at the same time) up to the far wake due to the velocity difference between the air inside and outside the wake. In this region, the flow is

highly turbulent (turbulent eddies) and the turbulent mixing mechanism is dominant. As the momentum is transferred to the wake by this mechanism, wake expands and velocity deficit is reduced in the downstream distances (Sanderse, 2009).

As the rotor blades rotate, vortices from the tip and root of the blades start to shed from the rotor. The tip vortices form the helical vortex system rotating in the opposite direction relative to the rotor. Tip vortices, located in the shear layer, are the main sources of the turbulence in the wake together with the nacelle, tower, turbulent boundary layer leaving the blades and the ambient turbulence (Sanderse, 2009). In addition, tip vortices in the wake of a single turbine are visualized (Figure 1-14) using smoke and high resolution Particle Image Velocimetry (PIV) techniques in order to better understand the formation and evolution of helical tip vortices and the turbulent wake structure (Hu, Yang, & Sarkar, 2011; Massouh & Dobrev, 2007; Vermeer, Sorensen, & Crespo, 2003).



Tip vortices visualized with smoke (Alfredsson et al., 1979)



3D wake structure behind a model wind turbine – PIV (Hu et al., 2011)

Figure 1-14 Visualization of tip vortices in the near wake

The effect of enhanced turbulence in the wake is essential for the downstream turbines in a wind farm. Downstream turbines will experience dynamic loading (fatigue) on the blades reducing the life-time of the wind turbine. According to the measurements on the Vindeby farm in Denmark, there is a significant fatigue loading increase of 80% in the downstream turbine (Sanderse, 2009; Adaramola & Krogstad, 2011). However, higher turbulence levels in the atmosphere triggers the turbulent mixing mechanism enabling a faster wake recovery. This effect is more pronounced in onshore wind farms compared to offshore wind farms. In

offshore (low terrain roughness) wind farms, wake effects are more persistent due to lower turbulence levels.

Spacing between the turbines in a wind farm is essential in reducing the power losses due to wake effects (velocity deficit and enhanced turbulence). However, wind tunnel investigations on the wind turbine wakes showed that even at 20D stream-wise spacing, wake effects are still observed in the velocity distribution behind the wake of a single turbine (Chamorro & Porte-Agel, 2010a). Meneveau and Meyers (2012) suggested that optimal average stream-wise spacing is considerably higher (15D) than currently used in wind farm implementations (7D). However, putting the turbines far apart in a wind farm is not always possible due to space and economic constraints.

Wind farm layout (staggered or aligned) also plays an important role on the efficiency of wind turbines in a wind farm. Chamorro, Arndt, and Sotiropoulos (2011) found out that staggered configuration leads to improved overall power output of the wind farm on the order of 10% in comparison to the aligned configuration with the same stream-wise and span-wise spacing. Each turbine in the staggered layout experiences the wake of the upstream turbine over a distance of twice as much as compared to aligned layout. Thus, wake recovery occurs over longer distances in staggered case which increases the efficiency of the wind farm. However, highest dynamic loads (fatigue) on a downstream turbine occur when a rotor is only partially immersed in the wake of an upstream turbine due to the non-uniform distribution of turbulence on the rotor plane (Madsen, Larsen, & Thomsen, 2005).

Adaramola and Krogstad (2011) proposed a way to improve the array efficiency. Their idea was to increase the overall power output of a wind farm by changing the operating conditions of upstream turbines (changing pitch angle, tip speed ratio (TSR) or yaw angle). They used two model wind turbines and by changing the yaw angle of the upstream turbine, they found out that total power output from the two turbines could be increased by about 12% for a yaw angle of 30°. They also indicated that operating the upstream turbine at an appropriate yaw angle will reduce the space requirement for the wind farm.

1.4.2 ATMOSPHERIC STABILITY EFFECTS

Atmospheric stability has a significant effect on the characteristics of incoming ABL flow and the structure of wind turbine wakes. Based on thermal stability, ABL can be classified as stable, unstable and neutral.

For the stable case (at night),

- Air does not tend to move vertically
- Little vertical mixing occurs (low turbulence)

For the neutral case (some periods in the morning and evening),

- Air will not move vertically unless an external force is applied
- Some vertical mixing occurs

For the unstable case (in the afternoons),

- Air is moved vertically and it tends to move in the same direction
- Strong vertical mixing occurs (high turbulence)

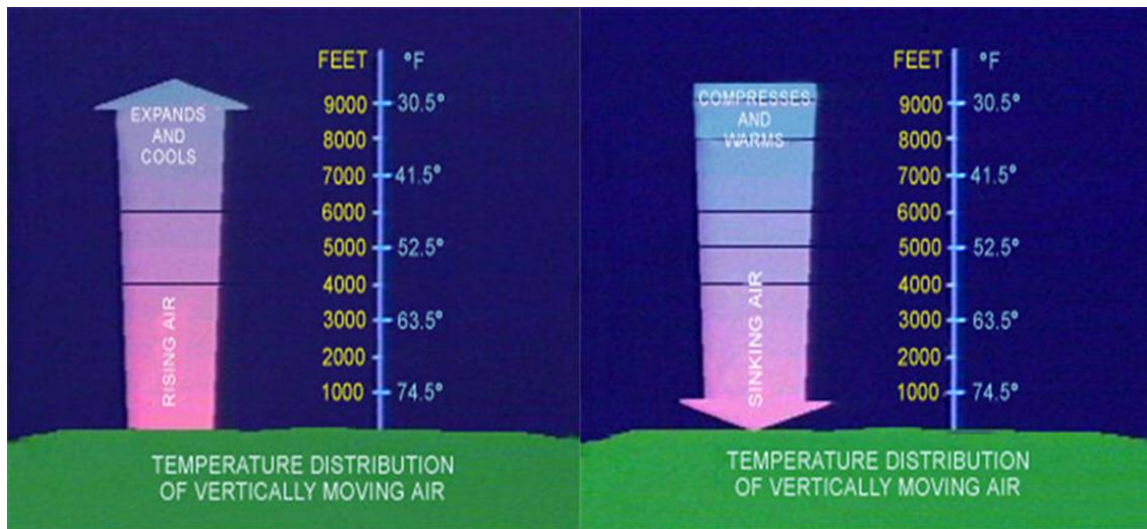


Figure 1-15 Temperature distribution of vertically moving air (Jenkins, 2008)

If the temperature of the air is higher than the temperature of the surroundings, it rises. As it rises, the air expands and cools. If the temperature of the air is less than the temperature of the surroundings, it sinks. As it sinks, the air compresses and warms (Figure 1-15).

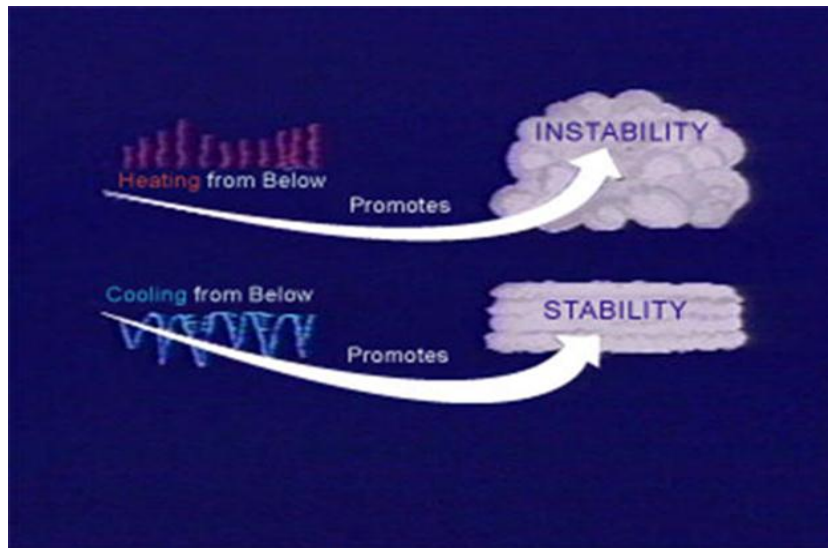


Figure 1-16 Variations in atmospheric stability due to diurnal changes (thermal) (Jenkins, 2008)

As shown in Figure 1-16, heating from below promotes instability – observed in the afternoons during the day and cooling from below promotes stability – observed at nights.

Atmospheric stability is an important parameter affecting the turbulence and wind shear in the lower atmosphere where wind turbines are located. Thus, atmospheric stability effects on the performance of the wind turbines, through the mechanisms of turbulence and wind shear, cannot be neglected. Variations in the power generation will go up to 20% due to the atmospheric stability (Wharton & Lundquist, 2010).

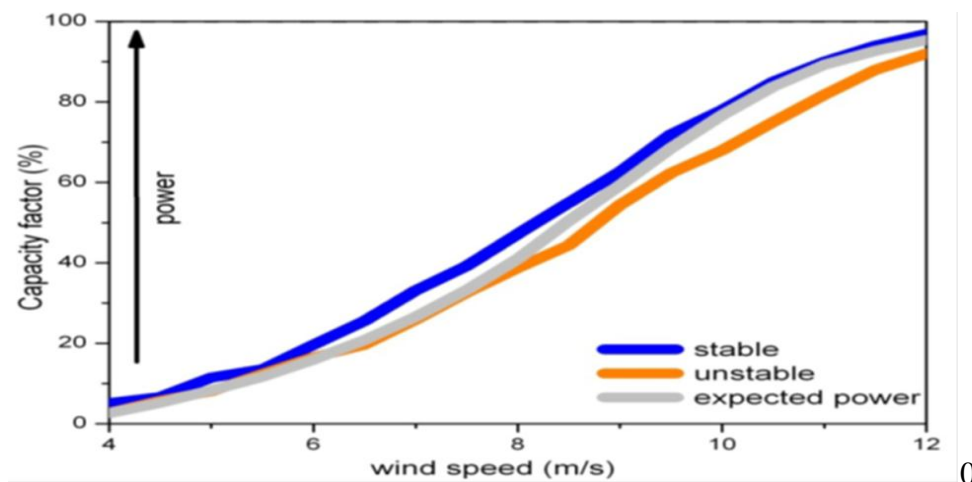


Figure 1-17 Atmospheric stability effects on wind turbine performance (Wharton & Lundquist, 2010)

Wharton and Lundquist (2010) also found out that power generated under stable conditions is higher compared to the power generated under strongly unstable conditions (Figure 1-17). Amount of power produced by the wind turbines decreases as the atmospheric stability changes from stable to convective (highly unstable) regimes. Since vertical mixing is dominant for unstable case, wind shear is less pronounced for the wind turbines. Thus, higher amounts of wind shear (stable) in the rotor disk leads to higher power performance.

There are also strong indications that atmospheric stability has an impact on the wake phenomena (wake recovery) especially in the wind farms, affecting the wind farm array efficiency.

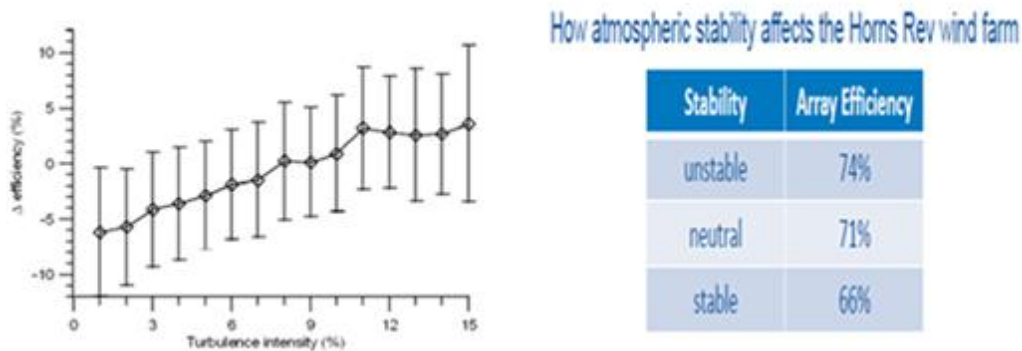


Figure 1-18 Atmospheric stability effects on wind farm efficiency (Jensen, 2007)

Efficiency of wind farm arrays improves as atmosphere stability changes from stable to convective (highly unstable). The high turbulence intensity levels in the incoming velocity profile make the wake recover faster due to turbulent mixing process. The measurements at the Horns Rev wind farm also show that wind farm efficiency increased from 66% to 74% as the stability changed from stable to highly unstable (Figure 1-18) (Jensen, 2007).

1.4.3 COMPLEX TERRAIN (HILLY TERRAIN) EFFECTS

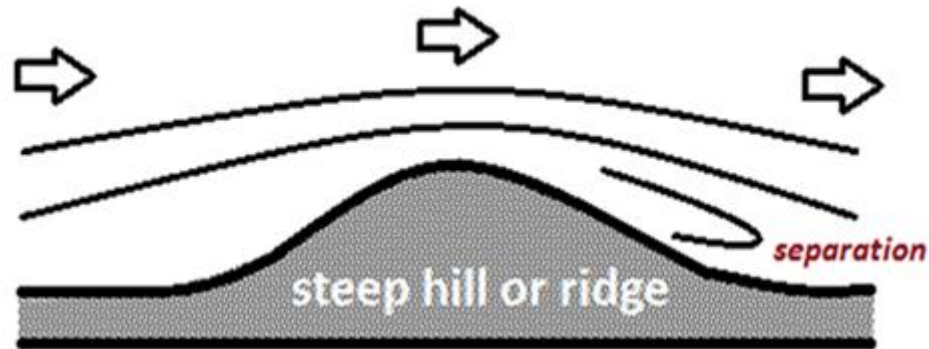


Figure 1-19 Flow over a steep hill or 2D-ridge

As the wind turbine market gets bigger and bigger, wind turbines are placed in a variety of different terrains with complex topography as shown in Figure 1-19. Although the flow character over flat terrain is well known, there is still too much to learn about the flow characteristics over complex terrain such as hills, ridges and escarpments and their interactions with the wind turbines.

Since wind turbines generate power proportional to the cube of the incoming velocity profile, the wind speed is an essential parameter affecting the performance of a wind turbine. The flow over the complex terrains such as hills or ridges will experience higher wind speeds especially on the top of the hills or ridges (Figure 1-20). This will lead to a significant increase in the power output and wind loading of the turbine placed on the top of hills or ridges. However, this speed-up effect is influenced by several factors including the slope and the terrain roughness.

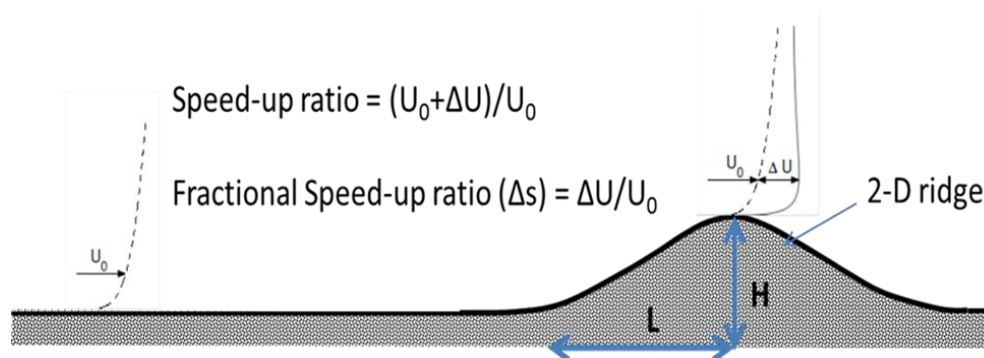


Figure 1-20 Speed up effect on the top of the 2-D ridge

The speed-up of the flow is dependent on the average slope and largest speed-ups are observed at moderate slopes (Arya, Introduction to Micrometeorology, 1988). When the slope of the hill is steep enough ($>20^\circ$ or $H/L > 0.36$), the separation occurs on the lee side of the hill. The separation region can be defined as the region with strong adverse pressure gradients causing velocity deficits and enhanced turbulence levels. The turbines placed within the separation region will suffer from highly turbulent flow shortening the life-time of the turbine and reduced wind speeds reducing the power output of the turbine.

Another factor affecting the flow over complex terrains is the surface roughness. Venas (1998) indicated that increased surface roughness promotes separation. Furthermore, Cao and Tamura (2007) investigated the effects of varying roughness on the flow over 2D low hill with a slope of 12° . They found out that flow field over a low hill is very sensitive to the change in the surface roughness (surface roughness is changed by adding/removing roughness blocks). They also studied the flow over a steep hill (Cao & Tamura, 2006) and observed that the upstream surface condition plays an important role on the speed-up over the hill as well as the surface condition of the hill.

1.4.4 TERRAIN ROUGHNESS EFFECTS ON THE INCOMING FLOW

For the wind tunnel experiments, roughness elements (chains, blocks, spires etc.) are used in order to simulate atmospheric boundary layer flow conditions with logarithmic velocity profile (Figure 1-21).

These roughness elements are used to obtain a logarithmic velocity profile similar to the one in atmospheric boundary layer of the earth. In addition, they also change the turbulence intensity levels of the incoming flow. The spires are placed at the onset of the test section of the wind tunnel and they act like a vortex generator and add turbulence to the flow. As mentioned in Adaramola and Krogstad (2011), higher turbulence generated by surface roughness elements in the incoming flow will cause a reduction in the power output of the upstream turbine; however, the turbulent mixing mechanism in the wake of the upstream turbine makes the wake recover faster thereby decreasing the loss in the power output of downstream turbine (increased overall efficiency in high turbulent flow) (Meada, Yokota, Shimizu, & Adachi, 2004). This effect is also observed in unstable atmospheric conditions

(compared to stable conditions) and onshore wind farms (compared to offshore) where ambient turbulence is comparable higher.

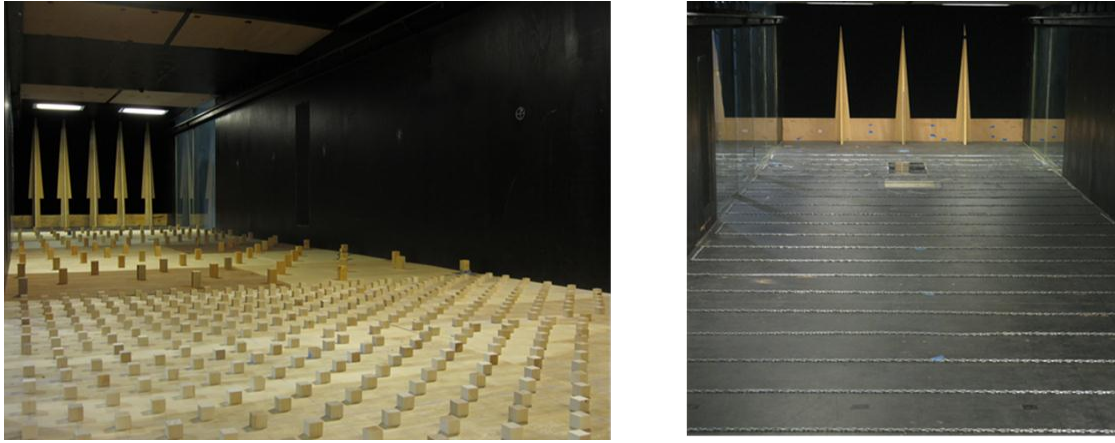


Figure 1-21 Roughness elements (spires, chains and wooden blocks) in the ATBL Wind Tunnel

To sum up, the described factors affecting the complex dynamics of wind farms;

- Turbine layout (aligned or staggered) and spacing
- Inflow character (turbulence and velocity profile)
- The topography of the terrain (complex terrain – hills or ridges)
- Operating conditions of the upstream turbines
- Thermal stability (stable, unstable or neutral)

The first four factors are going to be investigated and analyzed (AABL Wind Tunnel Testing) in the following chapters, assuming neutral stability conditions in the Wind Tunnel.

CHAPTER 2. WIND FARM ANALYSIS

2.1 INTRODUCTION

Wind energy, as a renewable energy source, has been playing an important role in the worldwide energy production in the recent years. Effective use of wind energy will provide clean and environmental friendly solutions for energy production thereby alleviating dependence on hydrocarbons and reducing CO₂ emissions. Today, only 2% of U.S. electricity is coming from the wind power; however, according to the U.S. Department of Energy, wind power could provide 20% of U.S. electricity by 2030. This goal can be achieved by increasing the number of wind power generation facilities (wind farms) installed in onshore or/and offshore. Larger wind farms necessitates the installation of wind turbines in large arrays which raises the concerns about the overall efficiency of the wind farms since wind turbines operating within an array will experience power losses up to 40% (Barthelmie, Folkerts, Ormel, & et al., 2003; Corten, Schaak, & Hegberg, 2004) and enhanced fatigue loads up to 80% (Sanderson, 2009). Those two effects are mainly because of the two characteristics of wind turbine wakes; velocity deficit and enhanced turbulence intensity. When inflow and surface conditions and their interactions with the wind turbine wakes are also taken into account, the study of the flow inside the wind farms is really complex but an interesting research area both experimentally and numerically.

Since wind turbines are operating inside the atmospheric boundary layer, the flow characteristics inside the wind farm are affected from strong vertical velocity and turbulence gradients inherent in the layer. It is important to simulate the atmospheric boundary layer in wind tunnel testing to really understand how it interacts with the wind farm. Understanding this interaction is essential for determining and optimising the wind farm performance. Wind turbine siting plays an important role for the wind farm performance. Maximizing the energy production and ensuring the structural integrity of wind turbines in a wind farm are two key parameters need to be considered when optimizing the wind farm layout.

There have been several numerical and experimental studies in order to understand the turbulent flow patterns on the wind turbine wakes. For example, Wu and Porté-Agel (2010) used large-eddy simulation to simulate the wake of a wind turbine developed in a neutrally-stratified turbulent boundary layer flow and compare the results with wind tunnel

measurements. Chamorro and Porté-Agel (2008) performed a wind tunnel study to investigate the effects of boundary layer turbulence and surface roughness (smooth and rough) on the wake structure of a wind turbine model under neutral conditions. Later in 2010, they investigated the effects of different atmospheric stability conditions (neutral and stable) on the wake structure of a single wind turbine over a smooth surface (Chamorro & Porté-Agel, 2010a) and also studied the mean velocity distribution and turbulence intensity in aligned wind farm layouts with different streamwise spacing (Chamorro & Porté-Agel, 2010b). Chamorro, Arndt, and Sotiropoulos (2011) investigated the turbulent flow characteristics in a staggered wind farm placed inside a boundary layer under thermally neutral conditions and compared with the aligned configuration. They found out that staggered layout is more efficient in terms of the overall power performance and overall levels of maximum turbulence intensity are significantly lower when compared to the aligned counterpart. In addition, Lebron et al. (2009) conducted Particle Image Velocimetry (PIV) measurements in the last row of a 3*3 wind farm array on different planes surrounding the center wind turbine and investigated the turbulent flow features within the wind turbine array thereby providing vital information for wind farm optimization. Furthermore, Hu, Yang, and Sarkar (2011) have done PIV measurements to clearly understand the turbulent wake flow characteristics and wake structure (formation of helical tip vortices) behind wind turbines.

In the present study, multiple wake interference effects on different wind farm layouts were investigated for different inflow turbulence levels in the Atmospheric Boundary Layer Wind Tunnel.

2.2 EXPERIMENTAL SET-UP

3-bladed horizontal axis wind turbine (HAWT) models were placed in a large-scale Aerodynamic/Atmospheric Boundary layer (AABL) Wind Tunnel located at the Aerospace Engineering Department of Iowa State University with the goal of investigating the multiple wake interactions in wind farm with different configurations. The AABL wind tunnel is a closed circuit wind tunnel with a test section of 20m and a cross section of 2.4m*2.3m. Figure 2-1 shows a picture of the test section of AABL wind tunnel with several wind turbine models mounted on the wind tunnel floor. A turbulent boundary layer was developed with the help of spires at the beginning of the test section and the wind tunnel floor was covered

with the chains in order to simulate the flow conditions similar to AABL under thermally neutral conditions. Spires are used to change the inflow conditions to observe the effect of high velocity and turbulence intensity gradients in our study. Figure 2-2 shows the measured normalized mean velocity and turbulence intensity profiles at the furthest downstream wind turbine location in Figure 2-1 by using cobra probe with no turbines installed.

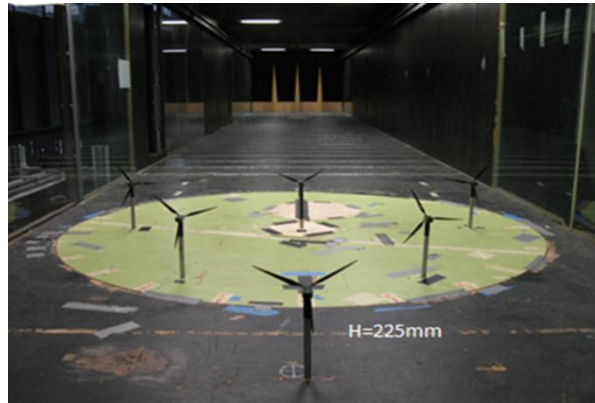


Figure 2-1 A picture of the test section of the AABL Wind Tunnel

Two different inflow conditions were used; spire or high turbulence case (17% at hub height) and no spire or low turbulence case (10% at hub height). The purpose was to study the effect of different incoming flow characteristics on the wind farm efficiency for different wind farm layouts.

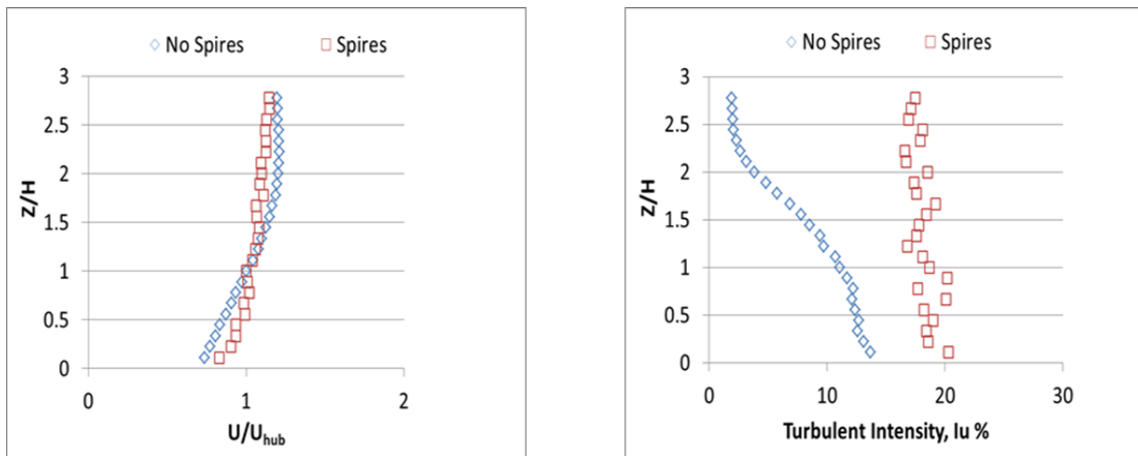


Figure 2-2 The measured profiles of the simulated atmospheric boundary layer

In Figure 2-3 (left), wind turbine model used for the study was shown on the left. The 3 bladed horizontal wind turbine rotors have a diameter of 254 mm and the tower is 225 mm high with a pitch angle of 10° . All model wind turbines used in the wind farm experiments

are of the same kind and have the same dimensions. They are scaled down 350 times from the real life length scales.



Figure 2-3 Wind turbine model (left) and force transducer and wiring equipment underneath of the model wind turbine (right)

High-sensitivity force transducer was connected to the underneath of the installed wind turbine as shown in Figure 2-3 (right) in order to measure the dynamic wind loads acting on the wind turbine. Besides, the electrical voltage through the DC motor installed inside the turbine nacelle was measured for different resistance values ranging from 1ohm to 1000ohm. Resistance was adjusted by using a variable resistance box connected to the DC motor via special wiring equipment. Electrical power output of a wind turbine was then calculated.

During the experiments, turbine angular velocity was also measured using the Monarch Instrument Tachometer. FFT analysis of voltage time series taken from the tachometer was used to obtain the turbine angular velocity. Also power, force and angular velocity measurements for a specific turbine were all taken at the same time in order to be consistent with the measurements and save time. During the experiments, the dynamic wind loads data were acquired for 60 seconds at a sampling rate of 1 kHz. Power and angular velocity data were taken for 120 seconds at the same sampling rate.

Three different wind farm configurations were used in the study. Two of the layouts are aligned and one is staggered. For all these configurations, crosswind distance between the wind turbines is constant and three rotor diameters (3D). For aligned configurations, three (3D) and six (6D) rotor diameters were used as downwind distance. Nine of the wind turbine models were used to simulate aligned wind farm models in a 3*3 array. For staggered

configuration, three rows of wind turbine models were placed in the wind tunnel floor $3/2$ wind turbines for each row with a three diameters ($3D$) of downwind distance.

Aligned wind farm

(a)

- 3 wind turbines for each row with a cross-distance of $3D$
- 3 rows of wind turbines with a streamwise distance of $3D$

(b) – shown in Figure 2-4 on the left

- 3 wind turbines for each row with a cross-distance of $3D$
- 3 rows of wind turbines with a streamwise distance of $6D$

Staggered wind farm

(c) – shown in Figure 2-4 on the right

- $3/2$ wind turbines for each row with a cross distance of $3D$
- 3 rows of wind turbines with a streamwise distance of $3D$



a) ALIGNED WIND FARM (6D)



b) STAGGERED WIND FARM (3D)

Figure 2-4 Simulated wind farm layouts (aligned and staggered) in the AABL Wind Tunnel

2.3 EXPERIMENTAL RESULTS AND DISCUSSIONS

Inside a wind farm, the effects of the multiple wake interactions are more pronounced especially on the downstream turbines. These effects will significantly reduce the power output of the downstream wind turbines up to 40% depending on the spacing and alignment of wind turbines in an array (Barthelmie, Folkerts, Ormel, & et al., 2003; Corten, Schaak, & Hegberg, 2004)

Power output of a wind turbine is indirectly related to its rotational frequency (f or Ω – rev/s) as mentioned in Chamorro, Arndt, and Sotiropoulos (2011). They conducted a rough

first-order analysis to relate the differences in the rotational frequency of the turbines in different wind farm layouts (staggered or aligned) to the power differences between these layouts. Thus, different wind farm layouts will be compared in terms of their efficiency just by analyzing the change in the rotational frequency of turbines throughout the rows.

$$\Delta \left(\frac{P_i}{P_1} \right) = 3 \left(\frac{f_i}{f_1} \right)^2 \Delta \left(\frac{f_i}{f_1} \right) \quad (\text{eq. 2-1})$$

It is assumed that the changes in Tip Speed Ratio (TSR) and Power Coefficient (C_p) are negligible compared to the changes in the wind speed while deriving the equation (2-1) above. In the formula, i denotes the number of the rows in the wind farm and 1 denotes the turbine in the first row. For the i^{th} row in the formula, they used the last row of the wind farm (10th row) since the turbine in the last row is more vulnerable to the multiple wake effects within the wind farm so it will be a good indicator of overall wind farm performance when comparing staggered and aligned configurations. Chamorro, Arndt, and Sotiropoulos (2011) compared the performance of staggered and aligned wind farm layouts (10 rows of wind turbines with the same spacing; 5D in streamwise and 4D in spanwise). They found out that staggered wind farm is more efficient than the aligned one and the power difference is roughly %15 between aligned and staggered configuration.

Our experiment differs in some ways from the experiments of Chamorro, Arndt, and Sotiropoulos (2011). First, the model wind turbines used in our experiments is much bigger (the diameter of wind turbines they used is around 128 mm, whereas our model wind turbines have a diameter of 254 mm). Second, they took advantage of using smaller wind turbines and simulated bigger wind farm layouts with 10 rows with larger streamwise and spanwise spacing. Thus, the flow conditions inside the wind farm are expected to approach the case of large wind farms.

In our experiment, we measured the rotational frequency of the wind turbine located in the center of the last row (3th row) for each case (staggered and aligned configurations). Then, we measured the individual rotational frequency (alone) of the turbine at the same location without any wake effects (removing all the other turbines). It is more accurate than measuring it for the wind turbine in the first row because of the fact that the wind speed will decrease in the downstream direction due to the pressure gradients in the wind tunnel and

especially in the wind farm simulations with 10 rows; this will be more pronounced for the downstream wind turbines.

Rotational frequency of the wind turbines was measured by using optical tachometer. The voltage time series from the tachometer were recorded and angular frequency was obtained from FFT (Fast Fourier Transform) analysis of the voltage time series.

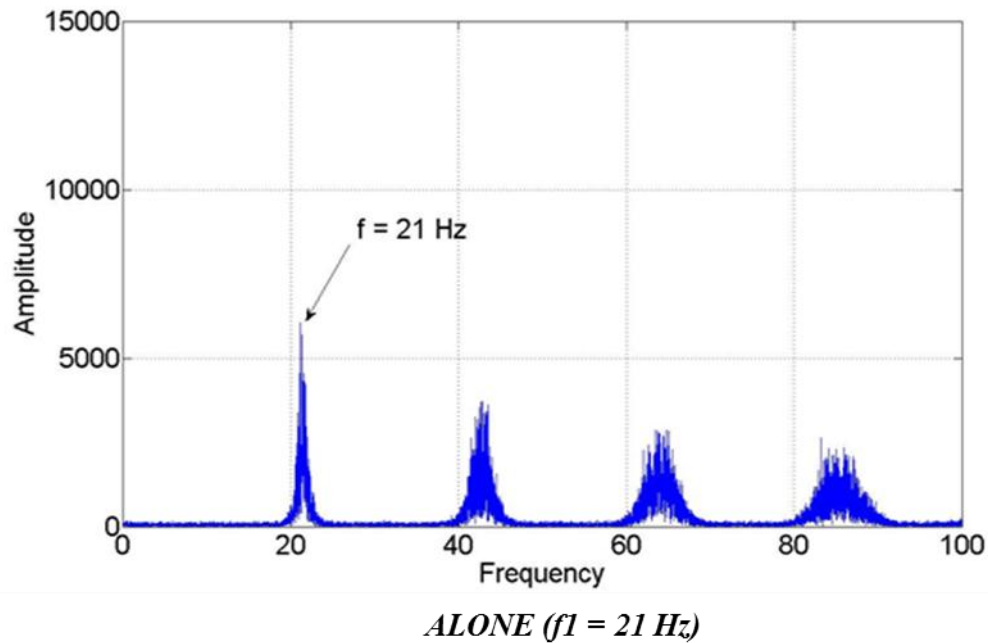
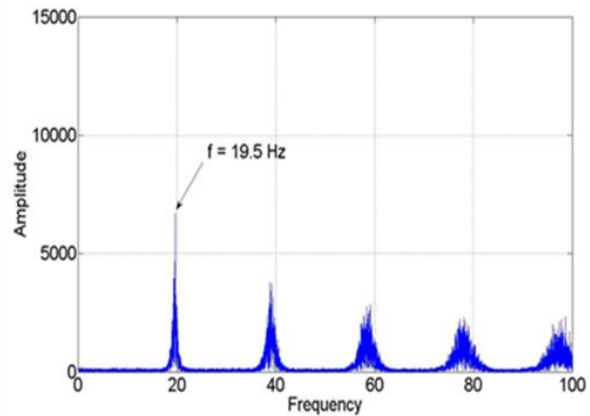
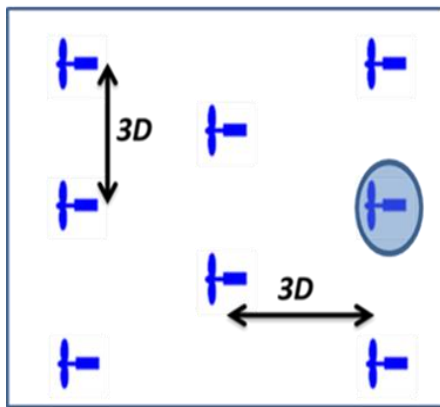
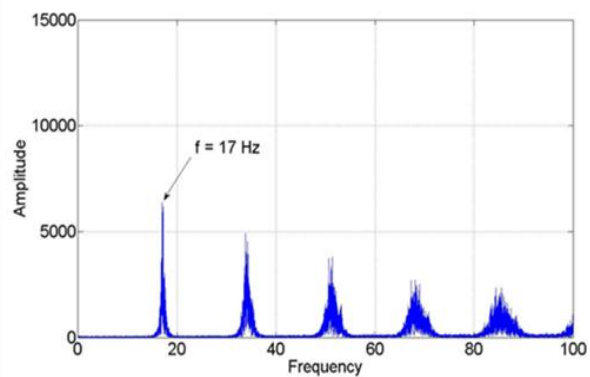
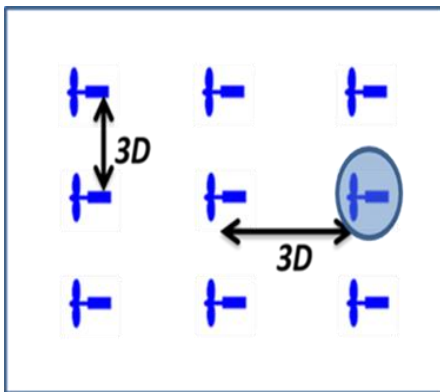


Figure 2-5 Power spectrum analysis of the measured voltage from tachometer (single turbine under no wake effect) for the no spire flow case

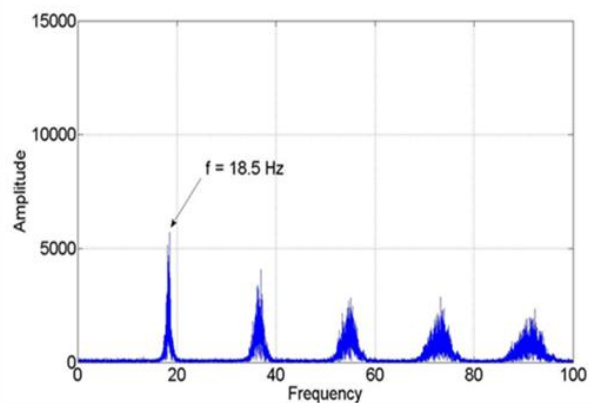
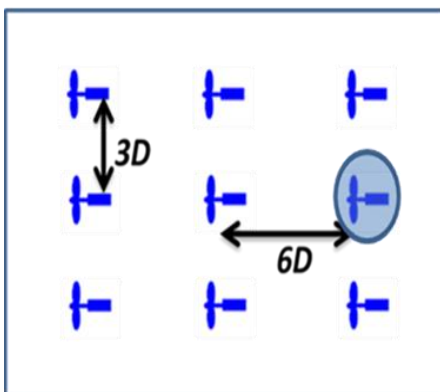
Figure 2-5 shows the amplitude versus frequency plot for the turbine (alone) without any wake effects (obtained from FFT analysis in MATLAB). As it can be seen from Figure 2-5, a dominant peak in the amplitude is identified at a frequency of 21 Hz which corresponds to the rotational frequency of the model wind turbine. Other peaks observed at the multiples of the rotational frequency representing the harmonic frequencies.



STAGGERED 3D SPACING ($f = 19.5$ Hz) ($f/f1=0.925$)



ALIGNED 3D SPACING ($f = 17$ Hz) ($f/f1=0.8$)



ALIGNED 6D SPACING ($f = 18.5$ Hz) ($f/f1=0.88$)

Figure 2-6 Power spectrum analysis of measured voltage from tachometer (turbine in the center of the last row of different wind farm layouts) for the no spire flow case

The effect of multiple wake interactions on the rotational frequency of the most downstream turbine in different wind farm configurations are shown in Figure 2-6.

Using equation 2-1 given by Chamorro, Arndt, and Sotiropoulos (2011), the power difference between staggered and aligned cases with the same streamwise (3D) and spanwise (3D) spacing is calculated.

$$\Delta\left(\frac{\Omega_i}{\Omega_1}\right) = \left(\frac{f}{f_1}\right)_{\text{stag}} - \left(\frac{f}{f_1}\right)_{\text{alig}} = 0.925 - 0.8 = 0.125$$

$$\Delta\left(\frac{P_i}{P_1}\right) = 3 \times 0.8^2 \times 0.125 = \mathbf{0.24}$$

Power increment for the staggered layout is roughly around 0.24, meaning that staggered layout is more efficient than the aligned one on the order of 20% under similar turbine spacing.

Last row, middle turbine (no spire)	Alone (wake free)	Aligned (3D)	Staggered (3D)	Aligned (6D)
Power*1000(mWatts)	<i>2.45</i>	<i>1.50</i>	<i>1.86</i>	<i>1.89</i>
Rotational Frequency (Hz)	<i>21</i>	<i>17</i>	<i>19.5</i>	<i>18.5</i>

Table 2-1 Variation in the measured power output and rotational frequency of a wind turbine in different wind farm layouts for the no spire flow case

Power output measurements were also taken from the wind turbine (last row, middle turbine) for each layout and the results were compared with the rotational frequency measurements as tabulated in Table 2-1. Although equation 2-1 is derived from a simple first-order analysis based on assumptions, it perfectly fits with the power measurements on the power difference between staggered and aligned cases. Since the power output of the turbine increased from 1.50 mWatts to 1.86 mWatts for the staggered layout, the increase in the power output is $(1.86-1.50)/1.50 = 0.24$ i.e. 24% higher power output in the staggered layout compared to the aligned one with similar turbine spacing. The power difference is higher than what Chamorro, Arndt, and Sotiropoulos (2011) found (15%) due to the differences in experimental set up mentioned earlier in the chapter.

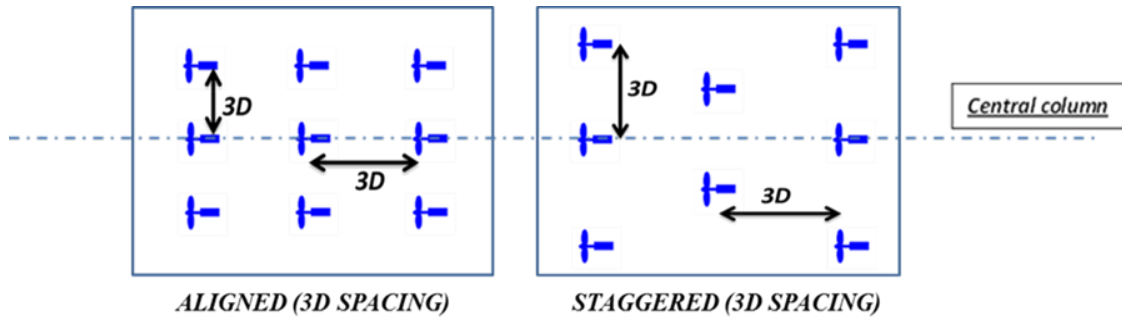


Figure 2-7 Aligned and staggered wind farm layout with 3D streamwise spacing and the turbines in the central column of each row were analyzed in terms of their relative (normalized) power output, rotational frequency and thrust force

Normalized rotational frequency and power output of the wind turbines in the staggered and aligned wind farm throughout the rows of the central column, as shown in Figure 2-7, were measured. Staggering helps the turbine in the last row experience the wake of the upstream turbine over a distance twice as much as compared to the aligned layout. Thus, wake has twice as much distance to recover for the staggered case thereby increasing the power output of the downstream turbine. However, downstream turbine is partly influenced by the wake of the upstream staggered neighbor turbines.

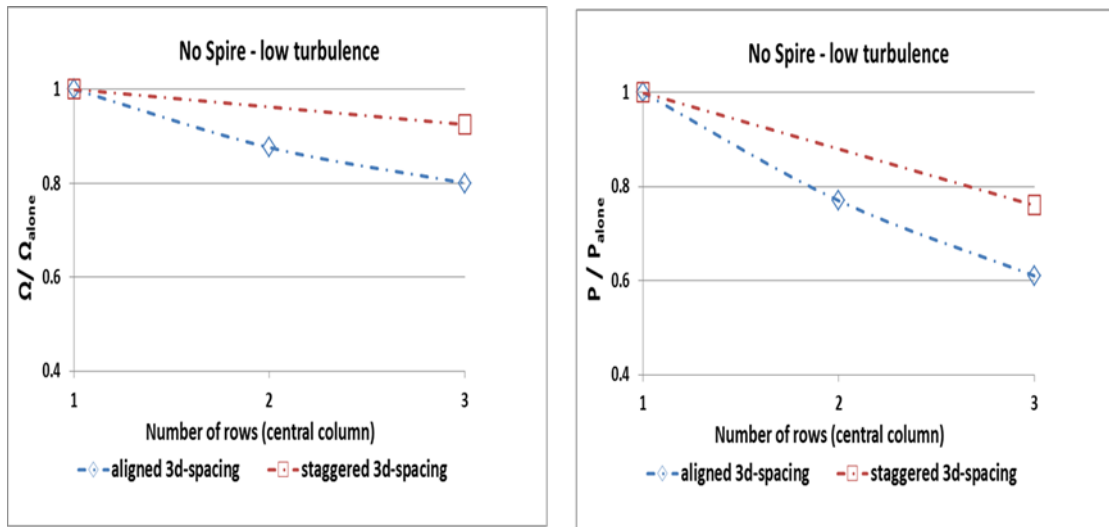


Figure 2-8 Relative (normalized) power and rotational frequency throughout the rows of the aligned and staggered wind farms with 3D streamwise spacing for the no spire flow case

It can be deduced from Figure 2-8 that the turbine in the last row of staggered wind farm is showing almost the same performance with the turbine in the second row of the aligned

one proving that staggering reduced the multiple wake effects making the wake profile similar to the wake of a single turbine.

Furthermore, cobra probe measurements were done for the vertical profiles (mean velocity and turbulence intensity) in the center column of the wind farm layouts (shown as circles in Figure 2-9) at incremental steps of one inch on the rotor plane of the model wind turbine due to the fact that wind profile across the entire rotor is vital for the performance of the wind turbines.

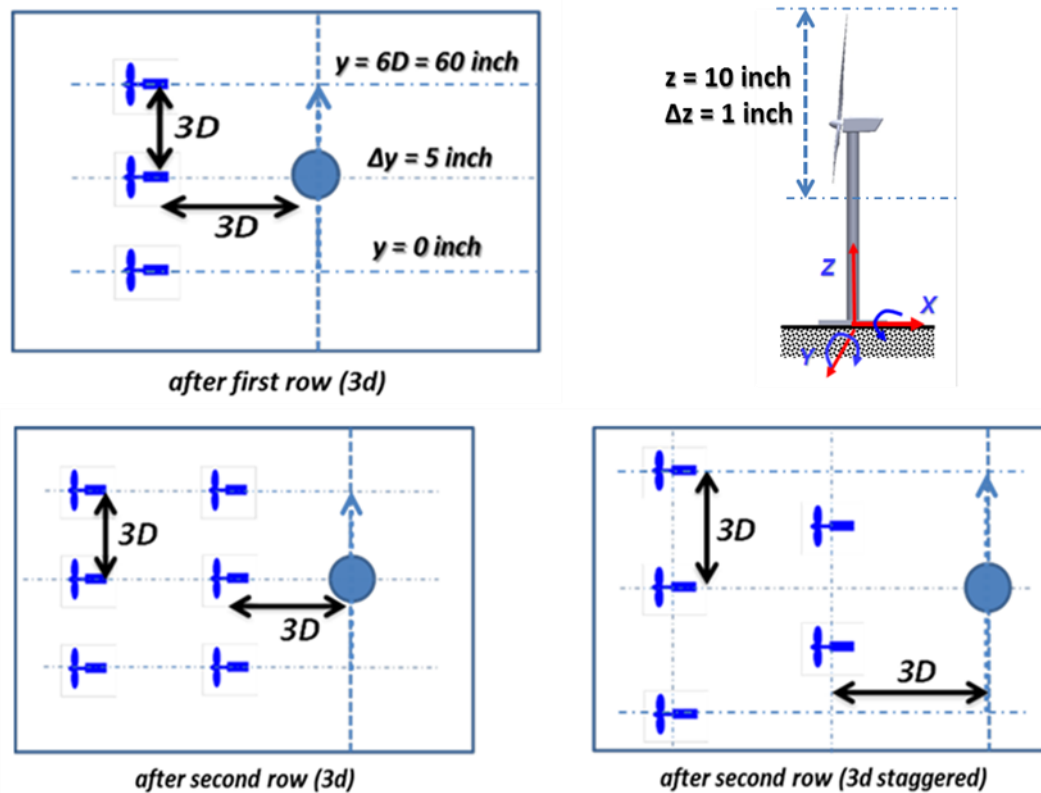


Figure 2-9 Cobra probe measurement locations (horizontal and vertical)

Cobra probe measurements also included the spanwise planes located in the second row and the third row of the aligned and staggered cases as shown in Figure 2-9. The measurements were taken at incremental steps of 5 inch covering the span of the wind farm ($6D = 60$ inch).

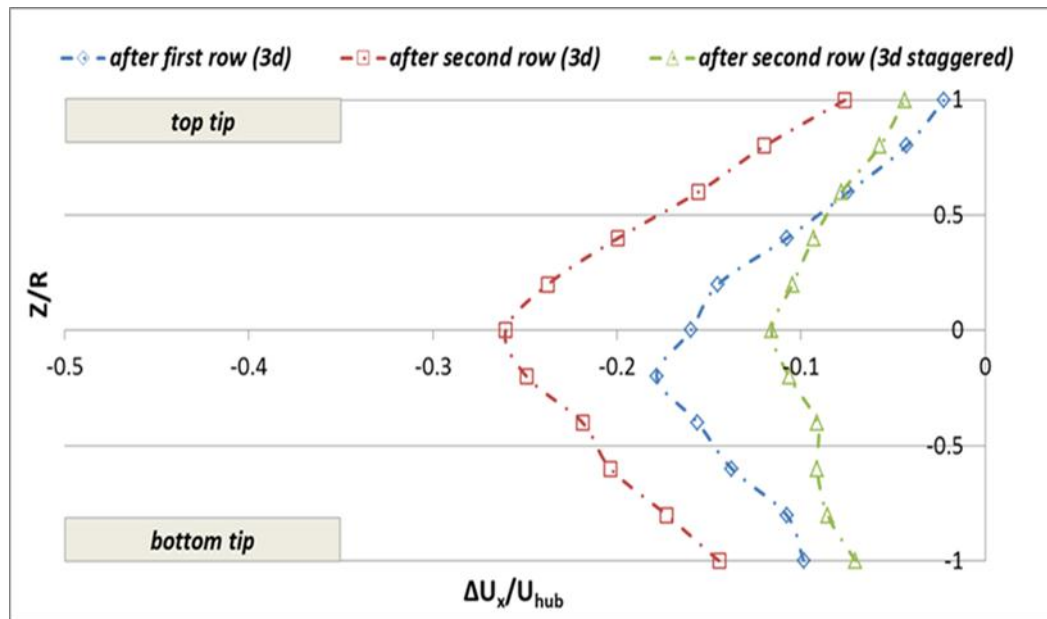


Figure 2-10 Normalized velocity deficit profile in the vertical rotor plane

Normalized velocity deficit on the vertical rotor plane is plotted in Figure 2-10 for the three cases shown in Figure 2-9. The shape of the normalized velocity deficit $[(U_{\text{wake}} - U_{\text{alone}})/U_{\text{hub}}]$ is nearly axisymmetric as it is also pointed out by Chamorro and Porte-Agel (2009). They found out that the velocity deficit shows a reasonable symmetric shape between the top and bottom tip heights. However, the symmetry is degraded below the hub height due to the presence of the tower and the ground effects as well.

Velocity deficit in the wake is more pronounced at the hub height ($Z/R=0$) or below the hub height ($Z/R<0$). The effect of tower is clearly observed on the velocity deficit difference between top and bottom tips of the wind turbine model (velocity deficit is relatively higher in the bottom tip of the wind turbine due to the existence of tower).

The normalized velocity deficit after the second row (corresponding to the last row of the wind farm layouts) is greater for the aligned configuration. The turbine in the last row receives a flow with a significant velocity deficit of roughly 25% for aligned configuration; however, for staggered configuration where centerline turbine is absent, velocity deficit is recovered more than 10%.

It can also be deduced from the normalized velocity deficit profile that the velocity deficit profile in the last row of the staggered layout - after second row (3d staggered) - is similar to the profile of the wake of a single turbine - after first row (3d) - even showing less velocity

deficit throughout the rotor plane due to the fact that wake is recovered over a distance twice as much in the staggered layout compared to the aligned one. However, the wake generated by the staggered neighbor turbines still influences the wind profile in the last row.

Since power is proportional to the cube of the wind speed, normalized velocity deficit profile throughout the rotor plane is a good indicator of the performance of the turbine at that location. Thus, the normalized velocity deficit profiles obtained for staggered and aligned layout (center of the last row) were in good agreement with the power output measurements of the turbines installed in the same location. For staggered case, more than 10% recovery in the velocity deficit was observed when compared to the aligned wind farm configuration substantially affecting the power output of the staggered layout – improved power output (approximately 24%).

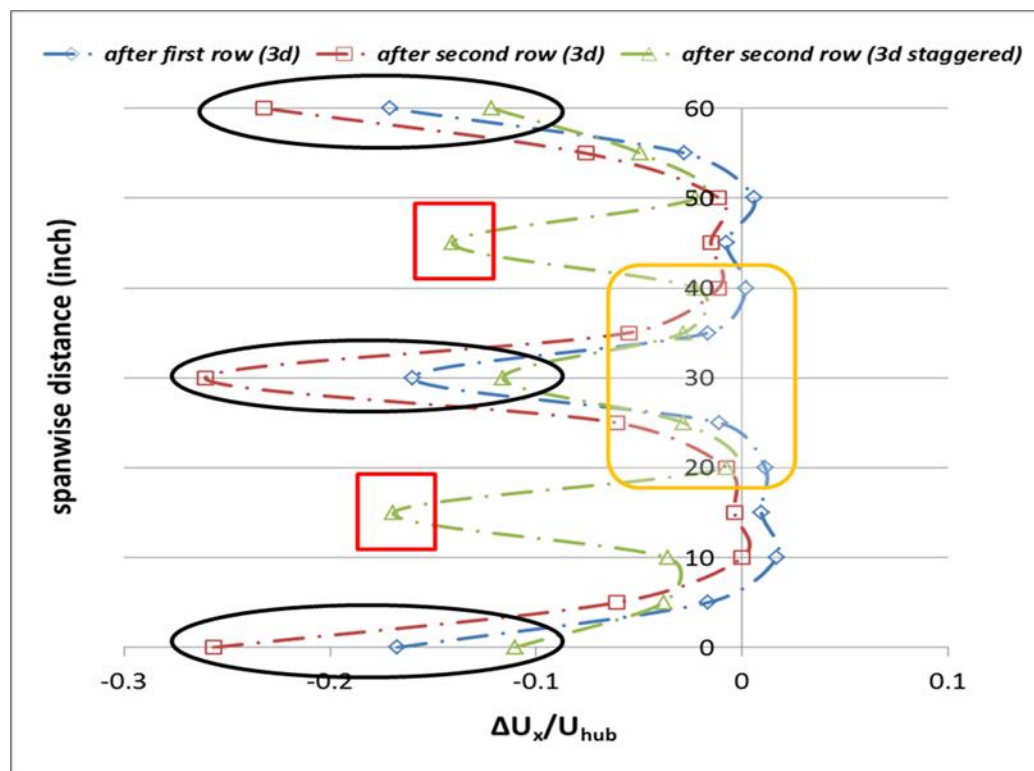


Figure 2-11 Normalized velocity deficit profile in the spanwise plane

Spanwise distribution of normalized velocity deficit for different configurations is shown in Figure 2-11. For aligned wind farm configuration with 3D stream-wise spacing, velocity deficit behind the first row is around 15% and behind the second row, it will go up to 25%. For the staggered layout, last row (0-30-60 inch), indicated inside black ellipses in Figure 2-

11, experiences less velocity deficit (around 12%) due to the staggered upwind wind turbines in the second row where centerline turbine is absent. Wake effects of staggered turbines in the second row can be seen in the last row; however, no turbines located in that locations (15-45 inch), indicated inside red squares in Figure 2-11 so that wake recovers over distances twice as much as compared to the aligned case thereby increasing the power output of wind turbines located downstream. Thus, the overall power output of wind farm is increased.

The spanwise variation of the normalized velocity deficit also gives crucial information about the wake expansion. If we have a closer look at the central plane (20-40 inch), the region indicated by yellow rectangular line in Figure 2-11, wake expands more in the last row of the aligned wind farm compared to the staggered one. In addition, wake expansion in the last row (after second row) of staggered layout is similar (slightly larger) to the wake expansion in the wake of the first row.

Another essential factor affecting the performance of the wind turbines in a wind farm is the turbulence generated by the upstream turbines. This will trigger dynamic loading on the turbine blades drastically shortening the life-time of the turbines especially for the downstream turbines in large wind farms.

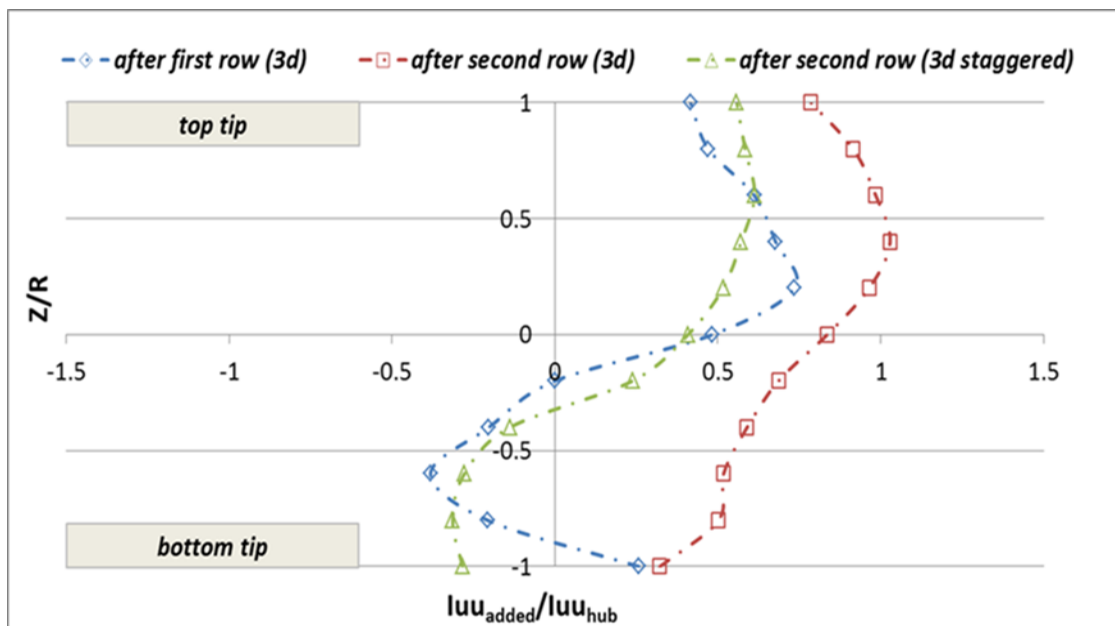


Figure 2-12 Normalized added turbulence intensity (I_{uu}) profile on the rotor plane

Normalized added turbulence intensity profile is plotted in Figure 2-12. The added turbulence is calculated in the following way;

$$I_+^2 = I_{\text{wake}}^2 - I_0^2 \quad (\text{eq. 2-2})$$

Where I_0 is the ambient turbulence without any wake effects, I_{wake} is the overall turbulence generated in the wake and I_+ is the added turbulence in the wake. The distribution of added turbulence intensity on the rotor is non-axisymmetric (non-Gaussian), as seen from Figure 2-12, due to the boundary layer effects as also proposed by Chamorro and Porte-Agel (2009).

Added turbulence is more pronounced above the hub height ($Z/R > 0$) due to the large enhancement of turbulence levels in the upper part of the wake. It can be deduced from Figure 2-12 that enhanced turbulence levels are observed especially for the lower part of upper wake region (Z/R is between 0 and 0.5) due to the fact that the disturbances generated by the blade root vortices and nacelle is stronger. As a matter of fact, the disturbances generated by the blade tips (tip vortices) do not contribute much to the turbulence levels in the wake. This could be related to the blade aerodynamics since the model turbine rotor blades are getting very thin at the tips so the generated tip vortices are not strong and broken down easily in shorter distances. In addition, negative values observed in the normalized added turbulence intensity is due to the fact that the presence of turbine leads to a reduction in the turbulence levels compared to the turbulence levels near the ground (Chamorro & Porte-Agel, 2009).

In staggered configuration (green dotted line), the turbulence levels produced on the rotor plane is similar to those produced on the wake of a single turbine (blue dotted line). Chamorro, Arndt, and Sotiropoulos (2011) also found out that the maximum level of turbulence in a staggered layout is very similar to the wake of a single wind turbine. Furthermore, overall levels of turbulence intensity is significantly higher in the aligned case (red dotted line) when compared to the staggered configuration (green dotted line) because in staggered layout, wake of upstream turbine has more space (twice as long as the aligned case) to recover.

Wind turbine in the last row of the staggered case is also influenced by the turbulence produced by upstream staggered neighbors. In terms of the overall turbulence characteristics,

it is clear from Figure 2-12 that this effect is not very important when compared to the diminished wake effect from the aligned upstream one. However, non-uniform distribution of the turbulent intensity is more pronounced in the staggered case (green dotted line) (showing similarity with the wake profile of a single wind turbine) when compared to the aligned case (red dotted line). This will impose a higher dynamic loading on the wind turbine blades in a staggered layout, increasing the fluctuations in the power output. Furthermore, highest dynamic loads on a downstream turbine occur when a rotor is only partially immersed in the wake of an upstream turbine (Sanderse, 2009) and this will drastically reduce the life-time of wind turbines (Madsen, Larsen, & Thomsen, 2005).

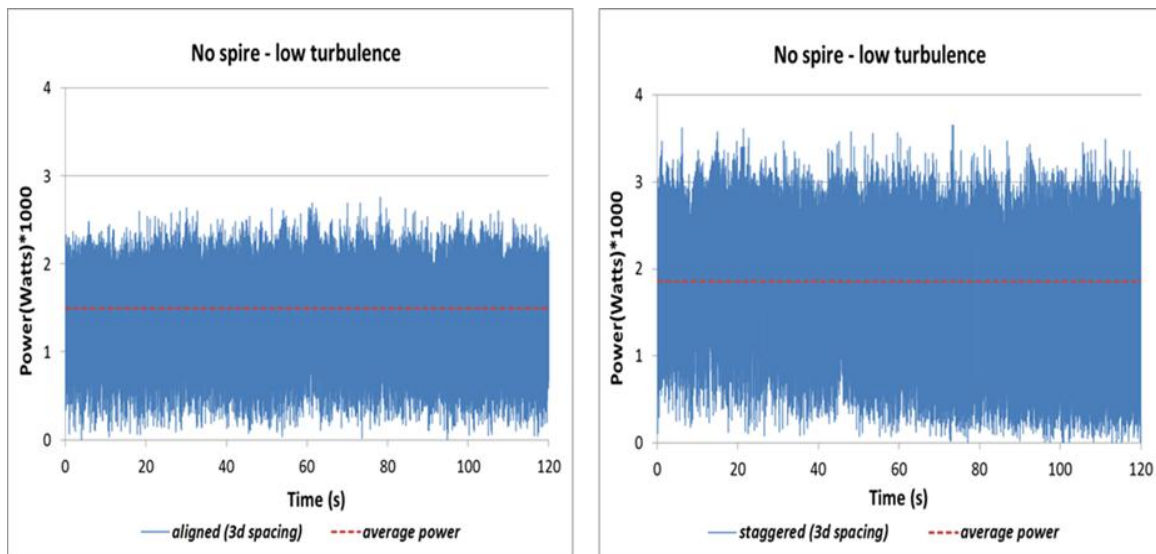


Figure 2-13 Time sequence of the measured power output for a turbine in aligned and staggered wind farm layout with 3D streamwise spacing for the no spire flow case

Figure 2-13 illustrates the instantaneous power output reading for the center turbine in the last row of aligned and staggered configurations with 3D streamwise spacing.

Last row, middle turbine (no spire)	Aligned 3D-spacing	Staggered 3D-spacing
Average power*1000 (mWatts)	<i>1.50</i>	<i>1.86</i>
Standard deviation (std)	<i>0.40</i>	<i>0.58</i>
A.F. (std / average power)	<i>0.27</i>	<i>0.31</i>

Table 2-2 Measured power output and deviations in the power output of a turbine in staggered and aligned wind farm layout with 3D streamwise spacing for the no spire flow case

In the staggered layout, average turbine power output is 24% higher in comparison to the aligned one. However, the fluctuations in the power output also increase with increasing average turbine power output as it is seen from the calculated standard deviation values shown in Table 2-2. The amplitude of fluctuations (A.F.) is calculated by the ratio of the standard deviation in the power output to the average power output. 4% increase was observed in the amplitude of fluctuations for staggered configuration compared to the aligned one. Although the turbulence levels observed in the staggered case is lower compared to the aligned case, the fluctuations in the power output is greater for the staggered case mainly due to the non-uniform distribution of turbulence on the rotor plane (Figure 2-12). Thus, the effects of the generated turbulence by the upstream staggered turbines cannot be underestimated (partly shadowing).

Furthermore, it was also found out that staggered layout with 3D streamwise spacing has slightly greater effect on the rotational frequency of the wind turbine than aligned layout with 6D streamwise spacing. It was also pointed out by Coeffe (2011) that staggering has a larger effect on the rotational frequency than increasing the streamwise distance. However, the power measurements for the last row-middle turbine did not show any significant difference between staggered 3D-spacing and aligned 6D-spacing wind farms (Figure 2-14).

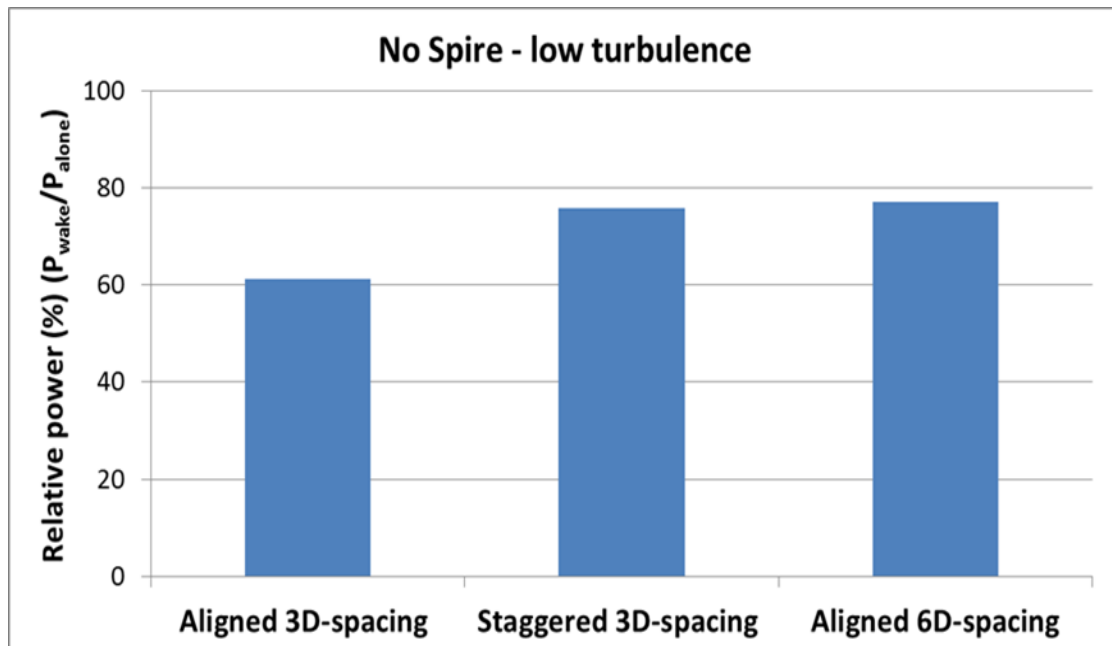


Figure 2-14 Relative (normalized) power output of a turbine located in the center of the last row of different wind farm layouts for the no spire flow case

Figure 2-14 represents the relative power output of the last row – middle turbine for different wind farm layouts. It can be deduced from the measurements that the maximum power output loss is observed in aligned 3D-spacing case (around 40%). Staggering the turbines or increasing the streamwise spacing between the turbines can be used to increase the overall wind farm efficiency. The results of the performance of a single turbine located in mid-last row illustrate that the turbine is performing almost the same for staggered 3D-spacing and aligned 6D-spacing case (the loss is slightly higher than 20%). However, it is not always possible in a wind farm to put turbines far apart from each other due to space and economic constraints. In addition, the power density (overall power output of the wind farm / area covered by wind farm) tends to get smaller as the streamwise spacing between turbines is increased. All these factors make staggering more advantageous over increasing the streamwise spacing for optimization.

The effects of the turbulence character of the incoming flow were also investigated in this study using spires at the beginning of the test section. The turbulence intensity (I_{tu}) at the hub height is 10% for no spire – low turbulence case and 17% for spire – high turbulence case. Spires not only enhance the turbulence intensity of the flow but also reduce the mean flow speed thereby degrading the performance of the wind turbines. However, it will also increase the efficiency in large wind farms making the wake recover faster due to the turbulent mixing. This effect is more pronounced for onshore wind farms with unstable atmospheric conditions (high turbulence) compared to the offshore wind farms with stable atmospheric conditions (low turbulence).

last row, middle turbine	Alone (wake free)	Aligned 3D-spacing	Staggered 3D-spacing	Aligned 6D-spacing
Power*1000 (mWatts) (no spire)	2.45	1.50	1.86	1.89
Power*1000 (mWatts) (spire)	1.68	1.10	1.51	1.44

Table 2-3 Variation in the measured power output of a wind turbine in different wind farm layouts for the spire and no spire flow case

Table 2-3 illustrates the change of the power output of turbine, located in the center of the last row, for different layouts in the spire and no spire flow case. There is an obvious

reduction in the power output of turbine for high turbulence (spire) case. This is due to the reduced velocity (up to 11% at the top tip height for wake free profile). In addition, fluctuations in the velocity (turbulence) on the rotor could be another factor degrading the performance of turbine. Assuming that the turbine operate at its rated power output, fluctuations in the velocity will cause fluctuations in the power output of the turbine; however, fluctuations do not go beyond the rated power output so fluctuations occur below the rated power output thereby reducing the power output of the turbine.

The effect of staggering on the rotational frequency of the wind turbine was mentioned earlier in this chapter for low turbulence case (no spire). Even, the performance of wind turbine in different layouts was inferred from the change in the rotational frequency of the turbine and compared with the actual power output readings from the turbine. However, for the spire case, rotational frequency oscillates in a wide range due to highly turbulent character of the flow and makes it impossible for an accurate estimate (Figure 2-15).

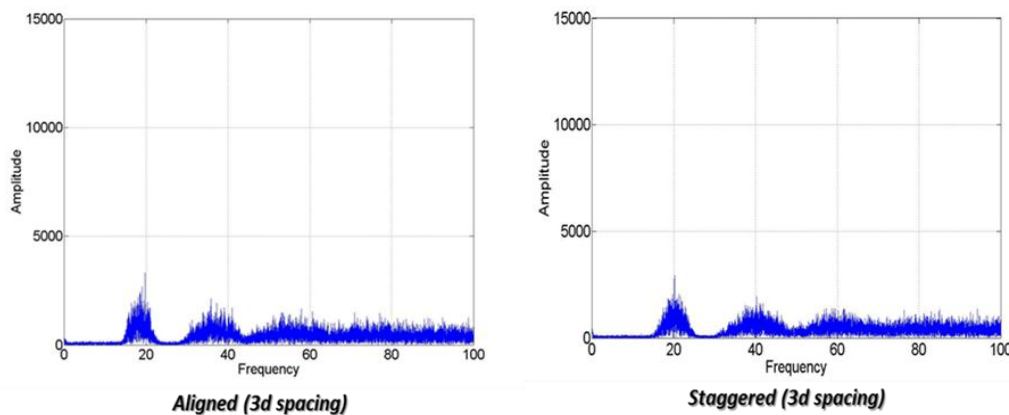


Figure 2-15 Power spectrum analysis of the measured voltage from tachometer (turbine in the center of the last row of staggered and aligned layouts) for the spire flow case

Unlike the no-spire case, no significant differences observed between aligned and staggered layouts for highly turbulent flow (spire) case. The frequency of the turbine oscillates in a large range between 15-25 Hz and does not show any significant difference for aligned and staggered configurations. However, a slight shift to the right (increasing) was observed in the frequency range of the staggered layout (Figure 2-15).

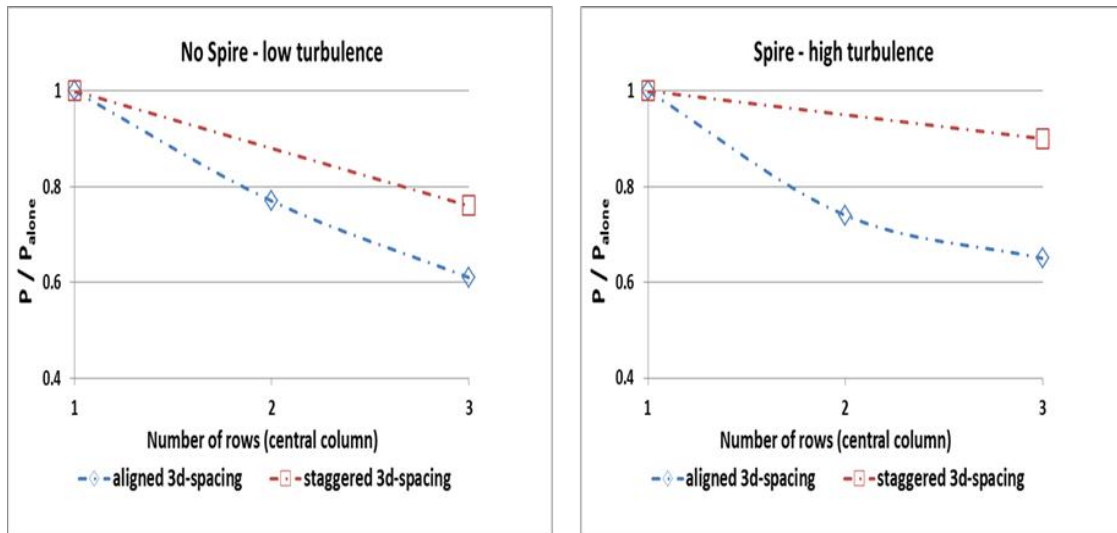


Figure 2-16 Relative (normalized) power throughout the rows of aligned and staggered wind farms with 3D streamwise spacing for the spire and no spire flow case

Figure 2-16 illustrates the change in the relative power output of turbines throughout the rows of central column for the spire and no spire cases. The effect of turbulence on the wind farm efficiency can be seen on the relative power output of the turbine located in the last row. Efficiency of wind farms in both configurations increase in the high turbulence case due to the turbulent mixing effect. This effect enables the wake recover faster. However, in highly turbulent flow, turbines suffer from enhanced turbulence levels causing fluctuations in the power output.

In addition, the rate of increase (in transition from low turbulence to high turbulence case) in the relative power output for the staggered case is greater compared to that for the aligned case (Figure 2-16).

	Staggered 3D-spacing	
	No Spire	Spire
last row, middle turbine		
Average power*1000 (mWatts)	<i>1.86</i>	<i>1.51</i>
Standard deviation (std)	<i>0.58</i>	<i>0.83</i>
A.F. (std / average power)	<i>0.31</i>	<i>0.55</i>

Table 2-4 Measured power output and deviations in the power output of a turbine in staggered wind farm layout for the spire and no spire flow case

Table 2-4 shows how the power output of a turbine (located in the center of the last row) is influenced by the turbulence character of the incoming flow for the staggered layout. Highly turbulent (spire case) incoming flow degrades the performance of the wind turbine due to the reduction in the wind speed and increases the amplitude of fluctuations (A.F.) in the power output as well.

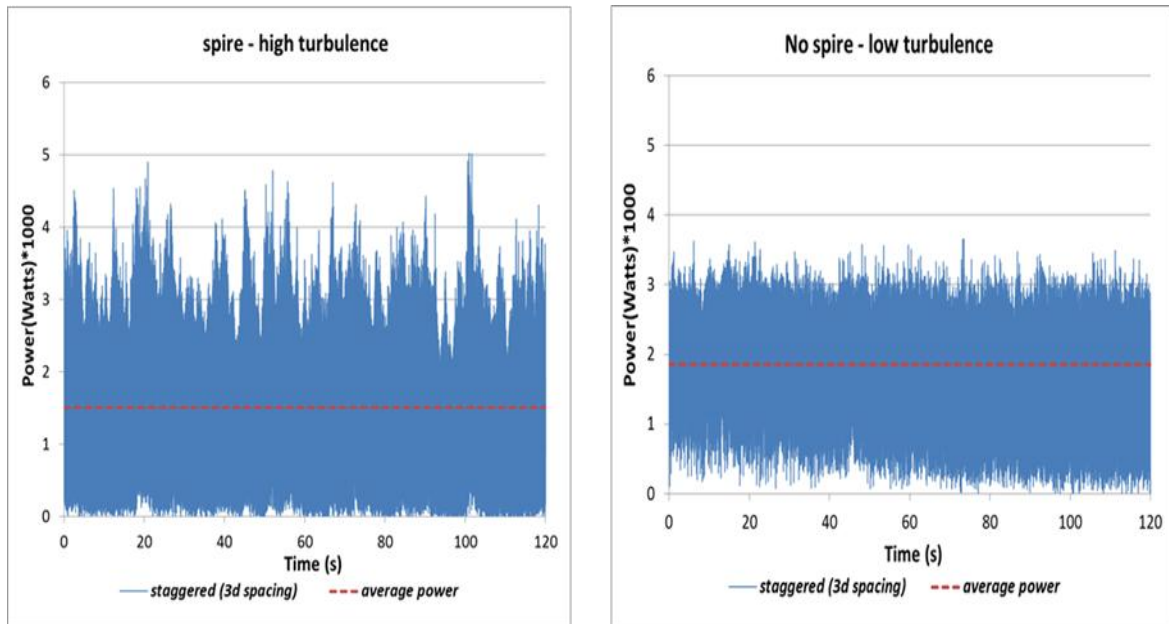


Figure 2-17 Time sequence of the measured power for a turbine in staggered wind farm layout for the spire and no spire flow case

In Figure 2-17, the instantaneous power output of the wind turbine (located in the center of the last row in staggered wind farm) for the spire and no spire cases was shown. For the spire case, the flow is highly turbulent and unsteady causing greater fluctuations in the instantaneous power output readings of the wind turbine in comparison to the no spire case, even fluctuations are sometimes two times greater than the average power output value.

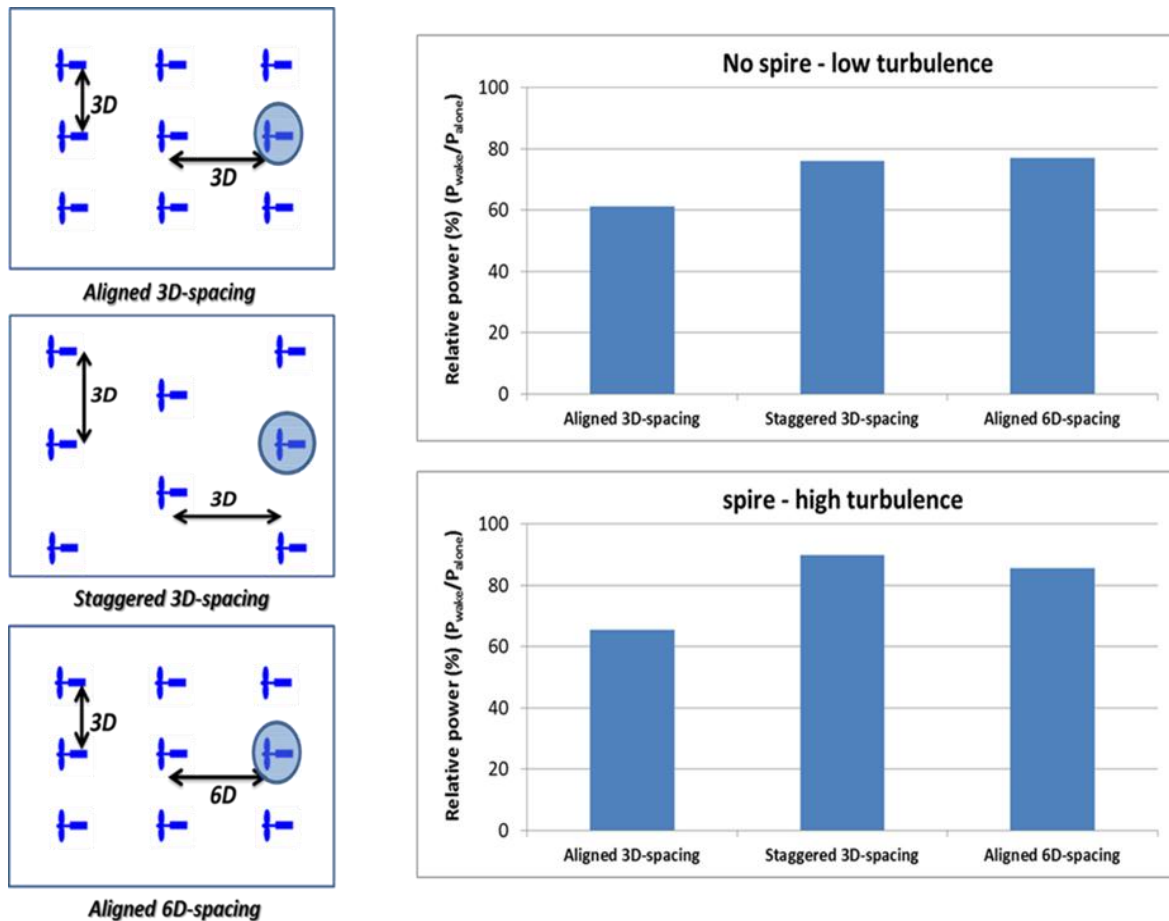


Figure 2-18 Relative (normalized) power output of the turbine (shown inside the circle) for different wind farm layouts and its dependence on the turbulence character of the incoming flow

Figure 2-18 tells more about the efficiency of different wind farm layouts and compares the effects of turbulence on these layouts. It can be deduced from Figure 2-18 that staggered wind farm is more efficient than the aligned with the same turbine spacing. In addition, the efficiency of aligned layout with streamwise spacing twice as much as compared to staggered layout is almost the same as the efficiency of the staggered one. Thus, the power density (overall power output of the wind farm / area covered by wind farm) is greater for staggered layout, saving money and space.

For the spire (high turbulence) case, the effect of turbulent mixing helps the wake recover faster, thereby increasing the efficiency of the wind farm layouts as it can be seen from Figure 2-18. The effect of turbulence on the efficiency is more pronounced in the staggered

wind farm since relative power output of the turbine increases from 76% to 90%. However, turbulence has a very little effect on aligned layout with 3D streamwise spacing.

Up to now, the analysis was mainly focused on the power output of the turbines. However, force acting on a wind turbine in the prevailing wind direction (thrust force) is another parameter that can be used to define the performance of a wind turbine.

$$P = 0.5 \times C_p \times \rho \times S \times V^3 \quad (\text{eq. 2-3})$$

$$F = 0.5 \times C_f \times \rho \times S \times V^2 \quad (\text{eq. 2-4})$$

Power (P) and thrust force (F) are parameters, which are dependent on the incoming velocity (V) profile. However, power is dependent on the cube of the wind speed, whereas thrust force is dependent on the square of the wind speed as shown in equations in 2-3 and 2-4. Thus, the effect of reduced velocity on the power output is greater compared to its effect on the thrust force.

$$\Delta P \sim |\Delta V|^3 > \Delta F \sim |\Delta V|^2$$

For example, 10% decrease in the wind speed will lead to approximately 19% decrease in the thrust force and 27% decrease in the power output. This is just a rough estimation based on the hub height velocity; however, wind speed varies throughout the rotor due to boundary layer effects.

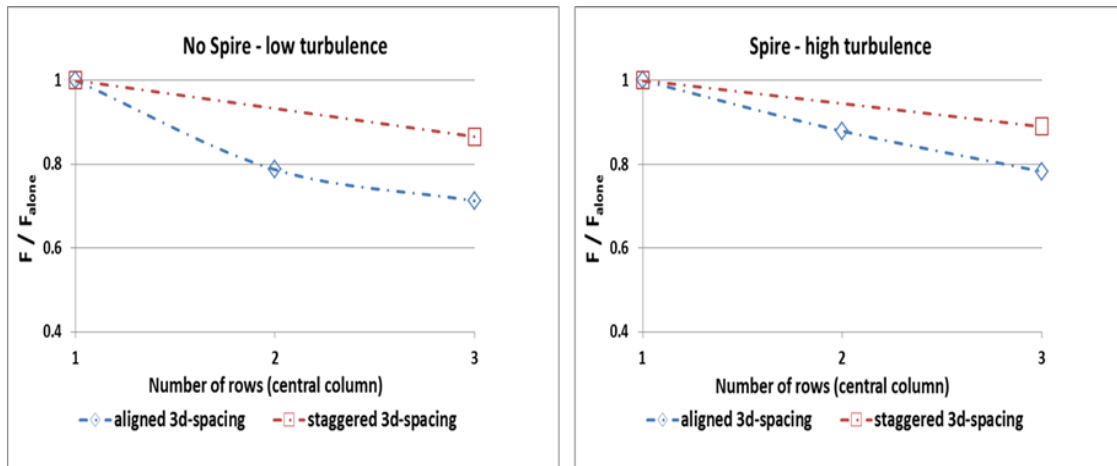


Figure 2-19 Relative (normalized) thrust force throughout the rows of aligned and staggered wind farms with 3D streamwise spacing for the spire and no spire flow case

Change in the relative thrust force acting on the turbines throughout the rows in the central column of aligned and staggered wind farm with the same spacing (3D) is shown in Figure 2-19. The results are in agreement with the normalized power output results

throughout the rows. The wake effects in the last row are more pronounced in the aligned 3D-spacing leading to a greater reduction in the thrust force and the power output of the turbine compared to the staggered one. However, the reduction in the power output is larger than the reduction in the thrust force due to the fact that the effect of reduced velocity on the power output is greater compared to its effect on the thrust force.

Highly turbulent incoming flow tends to improve the efficiency of the wind farm by reducing the wake effects (turbulent mixing). This will lead to an increase in the normalized power output and thrust force of the turbine that can be easily seen on the turbine located in the last row.

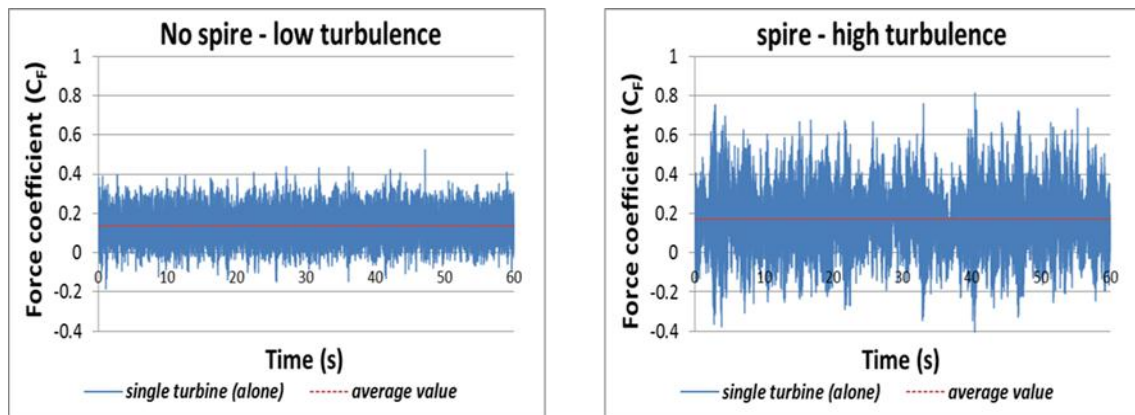


Figure 2-20 Time sequence of the measured C_F for a single turbine for the spire and no spire flow case

The effect of turbulence on the instantaneous wind loads (thrust force) of a wake-free wind turbine model was shown in Figure 2-20. It can be seen clearly that instantaneous wind loads acting on the wind turbine model were found to be highly unsteady for the spire (high turbulence) case with deviations up to four times as much as the average value. This kind of unsteady loading will cause dynamic loading (fatigue) on the blades thus reducing the life-time of the turbine drastically. Table 2-5 presents the statistical proof by calculating the amplitude of fluctuations (A.F.) for the spire and no spire case.

	Single turbine (alone)	
	No Spire	Spire
Last row, middle turbine		
Force coefficient (C_F)	0.136	0.170
Standard deviation (std)	0.071	0.144
A.F. (std / average C_F)	0.52	0.85

Table 2-5 Measured C_F and deviations in C_F of a wake-free turbine for the spire and no spire flow case

Two important concerns arise from the instantaneous wind loading plots; one is why we keep getting higher average thrust force from the spire (high turbulence) case although the flow velocity is reduced. Another one is the negative force values observed during fluctuations in the wind loading, meaning that force is acting in the opposite direction with respect to the prevailing wind. These two concerns need to be investigated in detail for future studies.

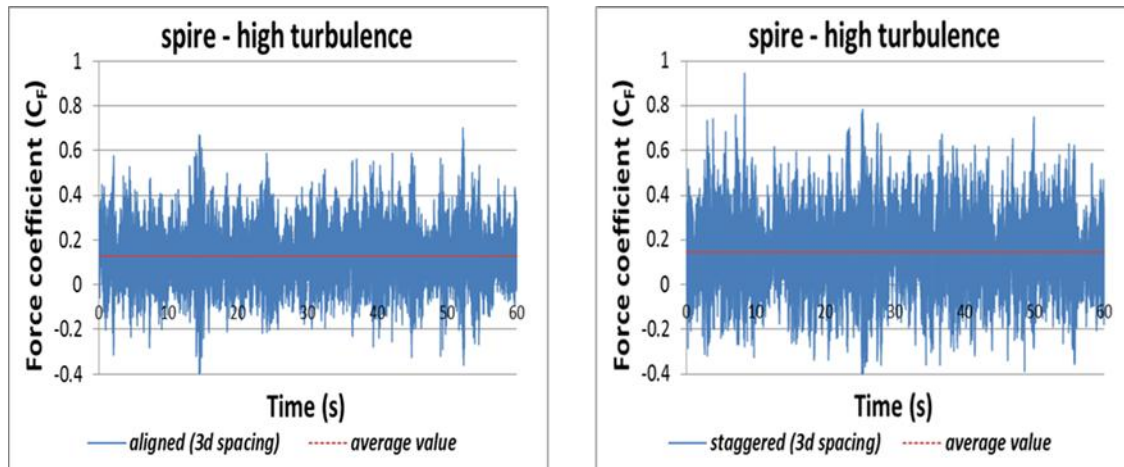


Figure 2-21 Time sequence of the measured C_F for a wind turbine in aligned and staggered wind farm layout for the spire flow case

Figure 2-21 shows the instantaneous wind loading (thrust force) on the wind turbine (located in the center of the last row of aligned and staggered layouts) for the spire case. It can be seen from Figure 2-21 that, the fluctuations in the staggered case is higher compared to the aligned case. This has already mentioned earlier in this chapter that non-uniform distribution of the turbulent intensity is more pronounced in the staggered case due to the partly shadowing effect from the staggered upstream turbines. However, the thrust force acting on the turbine is higher for the staggered layout in agreement with the power output results, making the staggered layout more efficient than aligned one with similar turbine spacing.

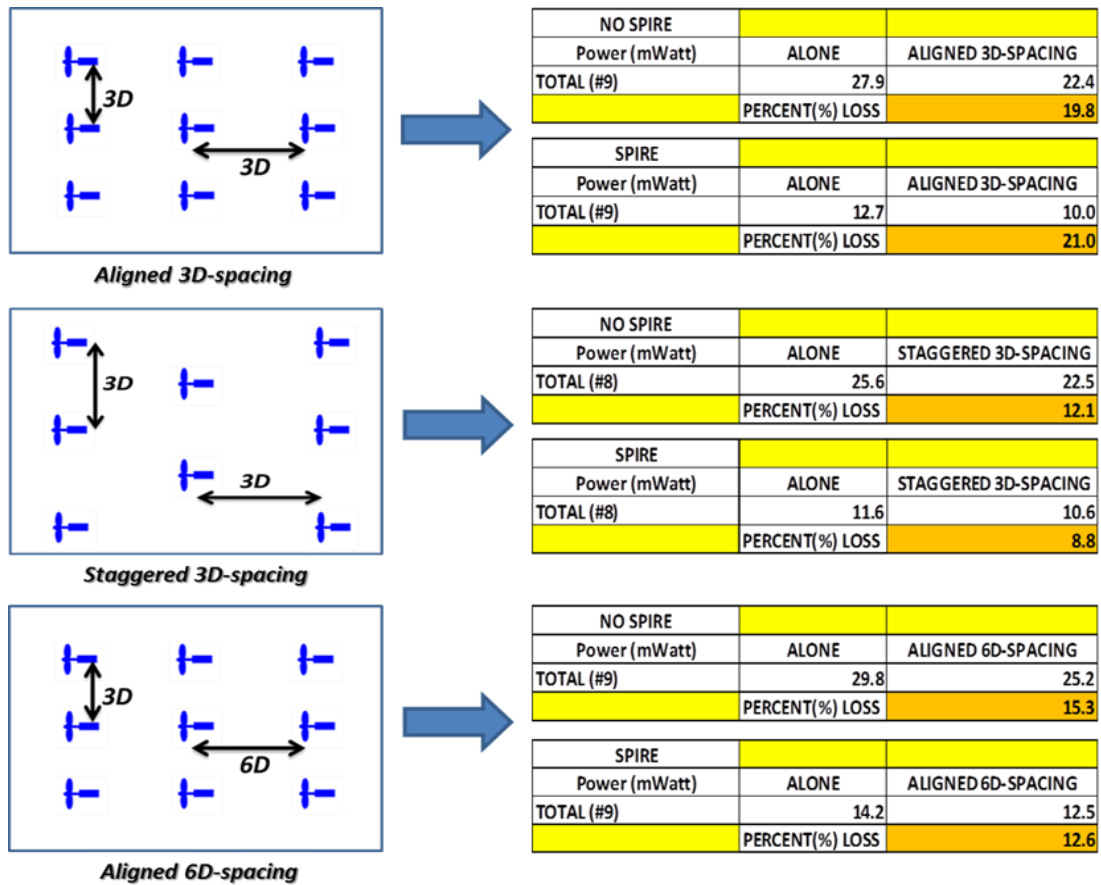


Figure 2-22 Overall power analysis of different wind farm layouts for the spire and no spire flow case

In a wind farm, power losses due to wake effects can be up to 23% depending on the wind farm layout and spacing between the wind turbines (Adaramola & Krogstad, 2011; Barthelmie, et al., 2009; Dahlberg & Thor, 2009; Beyer, Pahkle, Schmidt, Waldl, & de Witt, 1994).

According to the experimental results shown in Figure 2-22, staggered 3D-spacing wind farm is the most efficient farm with a power loss around 12% for the no spire case and 9% for the spire case. Maximum power loss is observed in aligned 3D-spacing wind farm with a power loss on the order of 20%. Increasing the streamwise spacing in aligned 6D-spacing wind farm improved the efficiency of the wind farm (up to 7% improvement compared to the aligned 3D-spacing). However, staggering has stronger effect on the wind farm efficiency than increasing the streamwise spacing in a wind farm.

The turbulence character of the incoming flow significantly affects the efficiency of wind farm. High levels of turbulence (spire case) increases the efficiency of the wind farm due to

the faster wake recovery (turbulent mixing). The improvement in the wind farm efficiency due to turbulence is more pronounced for aligned 6D-spacing and staggered 3D-spacing wind farms which was around 3%. However, no improvement observed in the efficiency of aligned 3D-spacing wind farm. In addition, turbulence degrades the performance of the wind turbines thereby reducing the power output of the overall wind farm.

2.4 CONCLUSION

Staggered wind farm is more efficient than the aligned one with similar streamwise and spanwise turbine spacing. Staggering is more effective on the wind farm efficiency than increasing the spacing between turbines in a wind farm.

The staggered wind farm generates less turbulence; however, the fluctuations in the power output is higher compared to aligned one due to partly shadowing from neighboring staggered wind turbines which leads to a significant change in the turbulence levels throughout the rotor.

Reynolds number ($6 \cdot 10^4 < Re < 10^5$) (Re based on hub height velocity and rotor diameter) for the wind turbine model used in the experiment is very small when compared to real wind turbines. Typical Reynolds number range for operating wind turbines are around $5 \cdot 10^5$ - $10 \cdot 10^6$. This would be the reason for smaller power output readings from model wind turbines.

Turbulence is significantly effective on the wind farm efficiency especially for staggered configuration since wake recovers faster in turbulent flow due to efficient mixing.

For the spire (high turbulence) case, levels of fluctuations in the power output of wind turbines inside the farm are significantly higher and it will also impose dynamic loading on the blades, thereby causing a significant reduction in the life-time of the turbines.

Increasing the wind farm capacity (adding more rows) would be helpful for future studies in order to simulate larger wind farms and understand the development of turbulent boundary layer in such big farms.

CHAPTER 3. COMPLEX TERRAIN ANALYSIS

3.1 INTRODUCTION

Wind turbines can be placed in complex terrains as well as flat terrains due to the increasing number of wind farms installed all around the world. This makes understanding the turbulent flow character over complex terrains (hills, escarpments, cliffs, 2D-Ridges, etc.) a vital issue for energy production in wind farms.

Wind turbines operate in order to extract energy available in the wind (limited by Betz limit, a wind turbine can extract maximum 59% of energy available in the wind). Available energy in the wind is dependent on several factors:

Swept area of the wind turbine (S): The area swept by wind turbine blades. It is directly related to the power output of the wind turbine. As the rotor diameter gets larger, the wind turbine can extract more energy from the wind.

Density of air (ρ): The kinetic energy (KE) in the wind depends on the density of air - mass per unit of volume. Density of air depends on its temperature, pressure and humidity. Air density decreases with increasing humidity and temperature; however, it increases with increasing pressure. The more the air gets dense, the more energy available in the wind to be extracted by a wind turbine.

The velocity profile of incoming flow (U): The wind speed is extremely important for energy production. Hub height velocity (U_{hub}) is generally used as a reference to define the incoming velocity for the wind turbines. However, the mean velocity profile throughout the rotor plays a key role in the power output of the wind turbine. In addition, the fluctuations in the mean velocity profile throughout the rotor is a sign of turbulence in the air which is also a crucial parameter affecting the life-time of a wind turbine as well as its power output.

As it is explained in detail above, the power available in the wind is dependent on the velocity and density of incoming air and swept area of the wind turbine. Especially power is proportional to the cube of velocity (hub height velocity) meaning that even a small increase in velocity will result in a larger gain in power or vice versa. That makes the site selection (topography) very important for the energy production especially for larger wind farms.

Complex terrains used for defining the terrains where separation is likely to occur. Complex terrains take advantage of speed-up effects that the topography produces so these

kinds of terrains with high wind speeds have great potential for energy production. However, the speed-up over a complex terrain such as hills or 2D-ridges is influenced by several factors: surface roughness, upstream terrain and the slope. Thus, previous experimental studies investigated the effects of slope and shape of the 2D hills, surface roughness and combination of hills on the flow. Arya, Capuano, and Fagen (1987) observed that speed-up of the flow on the hill tops were proportional to the average slope and largest speed-ups are observed over hills of moderate slope. The hills with moderate slope do not have any significant separation on the lee side. As the slope increases, flow on the lee side of the hill starts to separate and produces a wake characterized by reduced mean flow and enhanced turbulence. Behind long steep ridges, the wake region may extend to ten hill heights in the downstream direction (Arya, 1988). It has also been shown by Kaimal and Finnigan (1994) that both for naturally shaped and triangularly shaped two-dimensional ridges, the critical angle for steady separation is around 18° - 20° . When the downstream slope of the hill is steep enough ($>20^{\circ}$), the turbines located on the lee side of the hill experiences wind shear and turbulence reducing the life-span and efficiency of the turbine. In addition, surface roughness is an important factor affecting the flow over complex terrains. Increased surface roughness promotes separation diminishing the wind momentum near the ground and thus reducing its capacity to overcome the adverse pressure gradient (Venas, 1998). For a corresponding very rough ridge, the critical angle for separation can be reduced. Furthermore, Cao and Tamura (2007) investigated the effects of varying roughness on the flow over 2D low hill with a slope of 12° . They studied four different cases; a smooth hill in rough flow, a rough hill in smooth flow, a smooth hill in smooth flow and a rough hill in rough flow. It was seen that wake structure is significantly changed by adding /removing roughness blocks and flow field over a low hill is very sensitive to the change in surface roughness.

In our present work, we performed a wind tunnel study on investigation of wind flow over 2D-Ridge ($H/L=0.22$ with a slope of 12° - moderate slope) and ($H/L=0.41$ with a slope of 22° - high slope) to understand the effects of the hill slope on the flow character and how it affects the performance of wind turbines placed on the top of the 2D-Ridge. We also investigated the wake effects and how the wake generated by the upstream turbines (placed with different stream-wise spacing) interact with the flow over the 2D-ridge. In addition, we

compared the results with those obtained in flat terrain since it is very important to see cons-pros of both complex and flat terrains in terms of their influence on the wind turbine performance.

It was also observed during the experiments that turbines located on the lee part of the 2D-ridge did not operate during the experiments for both moderate and high slope cases because of the separation region on the lee side of the ridge with reduced mean flow velocity and enhanced turbulence. However, increasing the wind speed in the wind tunnel would be helpful for future studies in order to observe the effect of separation on the performance of the wind turbine located on the lee side of the ridge having different slopes.

For high sloped ridge, separation is more pronounced on the lee side; however, this effect can change the flow field over the entire ridge due to large scaled pressure gradient developed around the hill. For high sloped ($\alpha=22^\circ$) ridge, the effect of flow separation on the performance of the wind turbine sited on the top of the 2D-ridge was more pronounced compared to moderate sloped ($\alpha=12^\circ$) ridge during the experiments.

Vertical profiles of mean flow velocity and turbulence character of the flow on the top of 2D-ridge were measured by cobra probe (multi-hole pressure probe). These profiles helped us comprehend the power output and dynamic load measurements of the wind turbine installed on the top of the ridge.

Furthermore, spires are used at the onset of the test section of the wind tunnel to change the incoming flow character. We investigated how increased levels of turbulence in the flow will affect the flow over 2D-ridges having different slopes.

3.2 EXPERIMENTAL SET-UP

Experiments were carried out in AABL closed circuit wind tunnel at Iowa State University. Test section is 20m long and a cross section of 2.4m*2.3m. Spires are used to change the turbulence character of the inflow and first ten meters of the test section surface was covered with chains as a roughness element so as to simulate the atmospheric boundary conditions showing log-wind velocity profile. The flow is generated by an electric fan located downstream of the test section, and the wind speed is changed by changing the rotational frequency of the fan. In our experiments, rotational frequency is kept at 5.5 Hz.

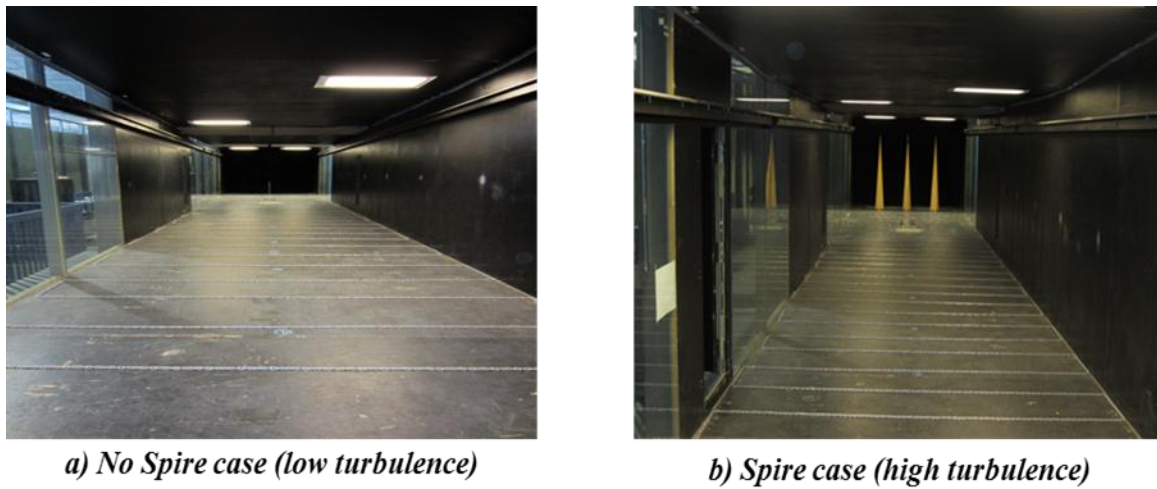


Figure 3-1 Simulation of atmospheric boundary layer conditions in the wind tunnel using spires and chains

Figure 3-1 illustrates the test section of AABL wind tunnel. Spires are used to change the incoming flow characteristics. Figure 3-2 shows the measured profiles of normalized flow velocity and turbulence intensity for two cases; spire and no spire cases. Hub height ($Z/H=1$) turbulence intensity for no spire case is around 10%; however, for spire case, turbulence intensity goes up to 17% at the hub height.

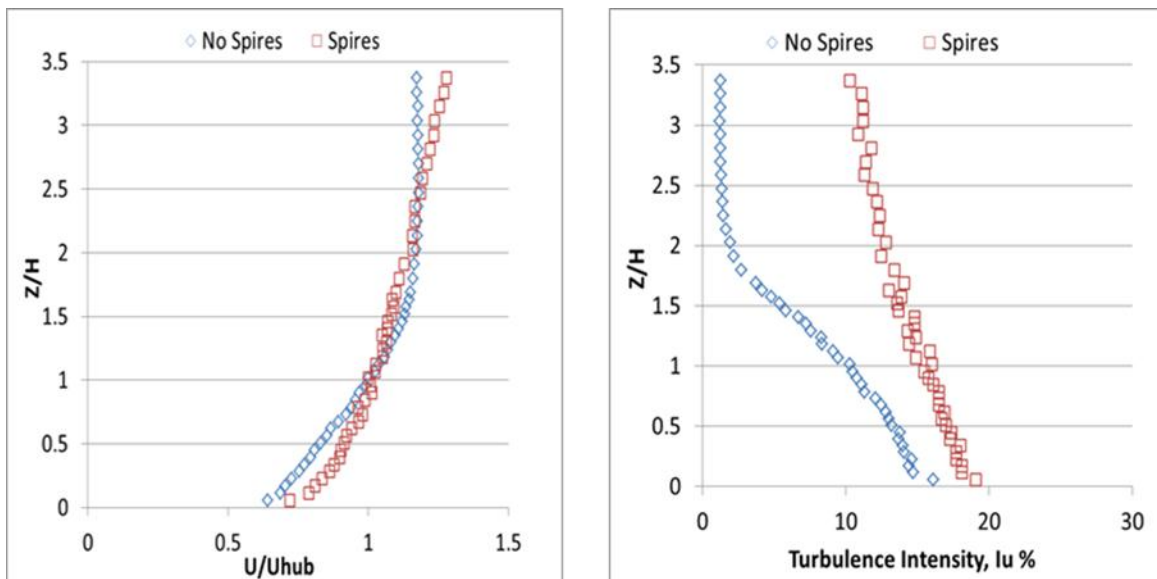


Figure 3-2 Measured profiles of the normalized mean velocity and turbulence intensity

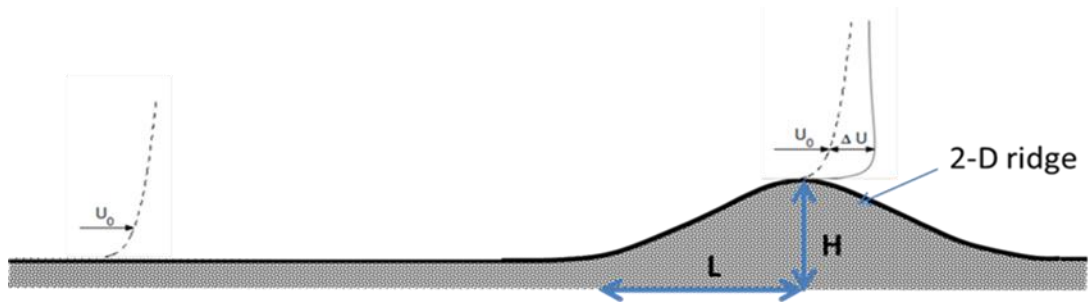


Figure 3-3 Schmeatic drawing of a 2D-Ridge and speed-up effect on the top of the ridge

Two different 2D-Ridge profiles were used in the experiments.

- Moderate slope 2D-Ridge ($H/L=0.22$, slope= 12°)
- High slope 2D-Ridge ($H/L=0.41$, slope= 22°)

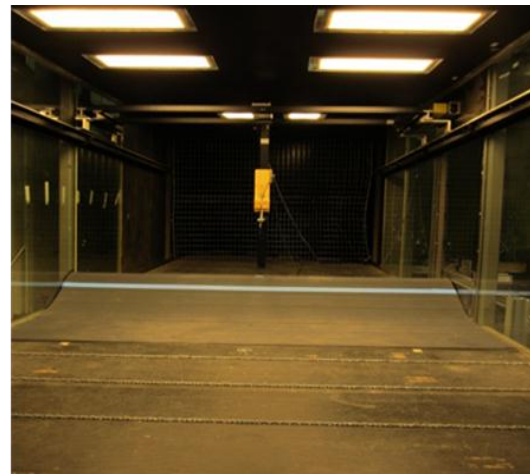


Figure 3-4 2D-Ridge profile with wind turbines installed around the ridge (left) and cobra probe measurement set-up on the top of the ridge (right)

Purpose of the experiment:

a) Investigate the flow characteristics (mean velocity profile and turbulence intensity) on the top of the 2D-Ridge and compare them with measurements for the flat terrain - observation of speed-up and reduced turbulence levels on the top of the 2D-Ridge.

b) Investigate the effect of ridge slope ($\alpha=12^\circ$ and $\alpha=22^\circ$) on the flow over the ridge and on the performance of the wind turbine on the top of the ridge (speed up is directly affected from the slope and flow tends to separate at higher slopes thus reducing the speed-up on the top of the ridge).

c) Investigate how the wake of an upstream turbine with different stream-wise spacing (3D and 6D) affects the wind turbine on the top of the 2D-Ridge and compare with the wake effects in the flat terrain via cobra probe measurement and wind turbine power output and wind loading analysis

d) Investigate how the turbulent character of upstream flow affects the flow over the 2D-Ridge and compare with the flat terrain case.

Power output and Wind loading measurements

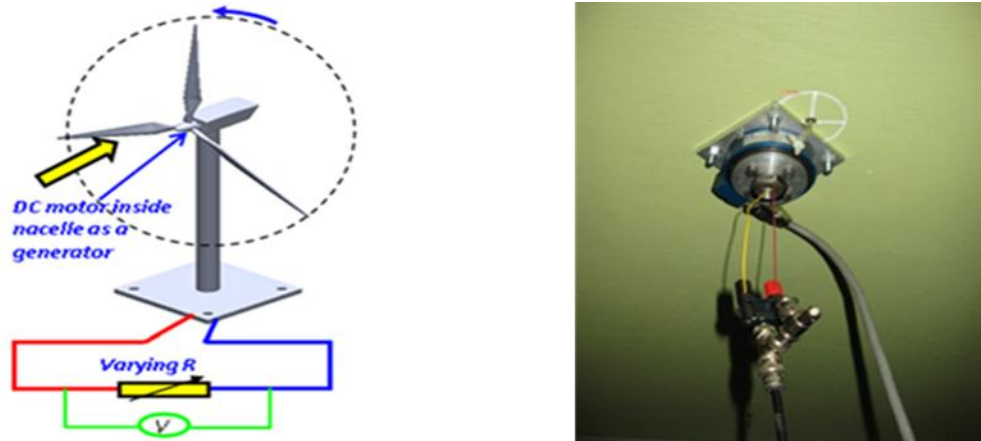


Figure 3-5 The schematic of the power measurement system (left) and underneath of a model wind turbine with force transducer and wiring system for power measurement (right)

As the flow goes through the rotor of the model wind turbine, blades start to rotate and electrical voltage through the DC motor installed inside the nacelle was measured under different loading (resistance ranging from 1ohm to 1000ohm) conditions. Resistance was adjusted by using a variable resistance box connected to the DC motor via special wiring equipment. Then electrical power output is calculated. Sampling frequency is 1 kHz with sampling time of 120 seconds.

JR3 Force/Moment transducer was installed underneath the model wind turbine to measure the dynamic loads (all three components of aerodynamic forces and the moment about each axis) acting on the wind turbine. The precision of the force-moment sensor cell for force measurements is $\pm 0.25\%$ of the full range (40 N). During the tests, sampling frequency is 1 kHz with sampling time of 60 seconds.

Model wind turbine



Figure 3-6 1:350 scaled wind turbine model to simulate a 2 MW wind turbine with 90 m rotor blades

Three bladed model wind turbine rotor has a diameter of 254 mm (10 inch) and the hub height is 225 mm (9 inch). Pitch angle of the blades is 10° . They are scaled down 350 times from the real life length scales. The blockage of the model is around 1% of the wind tunnel cross-section (Smaller blockage is important for the free expansion of the wakes).

3.3 EXPERIMENTAL RESULTS AND DISCUSSIONS



Figure 3-7 Schematic of the flow over steep hill or ridge, separation is likely to occur on the lee side depending on the slope

The flow decelerates at the upwind foot of the hill, before it accelerates to the top of 2D-Ridge. This explains the reduction in the power output of the wind turbine placed on the foot of the 2D-Ridge as shown in Table 3-1 below. The reduction in the power output of the wind

turbine located on the foot of high sloped 2D-Ridge ($\alpha=22^\circ$) is significantly higher especially for the no spire case due to the fact that slowdown of the flow is more pronounced for steeper ridges.

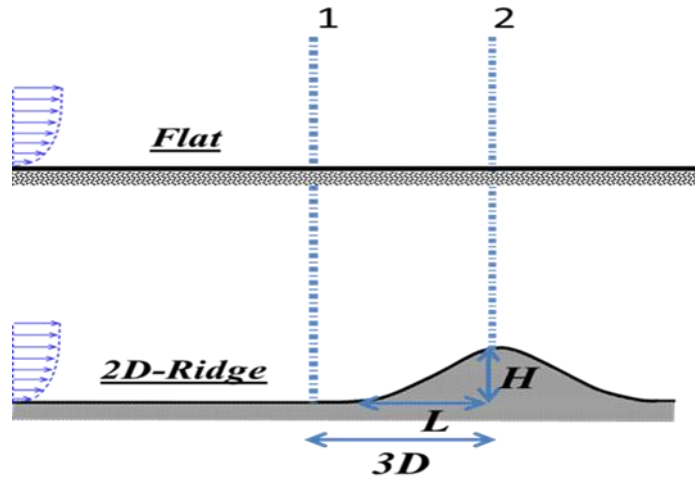


Figure 3-8 Locations where a model wind turbine was installed in the flat and complex (2D-Ridge) terrain

Power*1000 (mWatts)	Terrain type	(no spire case)	position 1	position 2	
	Flat terrain			0.66	0.67
	2D-Ridge	Moderate slope ($\alpha = 12^\circ$)		0.52	1.29
High slope ($\alpha = 22^\circ$)			0.38	1.04	

Power*1000 (mWatts)	Terrain type	(spire case)	position 1	position 2	
	Flat terrain			0.30	0.29
	2D-Ridge	Moderate slope ($\alpha = 12^\circ$)		0.29	0.63
High slope ($\alpha = 22^\circ$)			0.20	0.64	

Table 3-1 Comparison of wind turbine performances at location 1 and location 2 in the flat and complex terrain for the spire and no spire flow case

Table 3-1 shows the power output measurement results for a wind turbine located on the foot of 2D-Ridge (position 1) and on the top of the 2D-Ridge (position 2) with the results obtained in the same locations for flat terrain. The power output measurements on these

locations support the fact that flow decelerates at the upwind foot of the hill, before it accelerates to the top of 2D-Ridge.

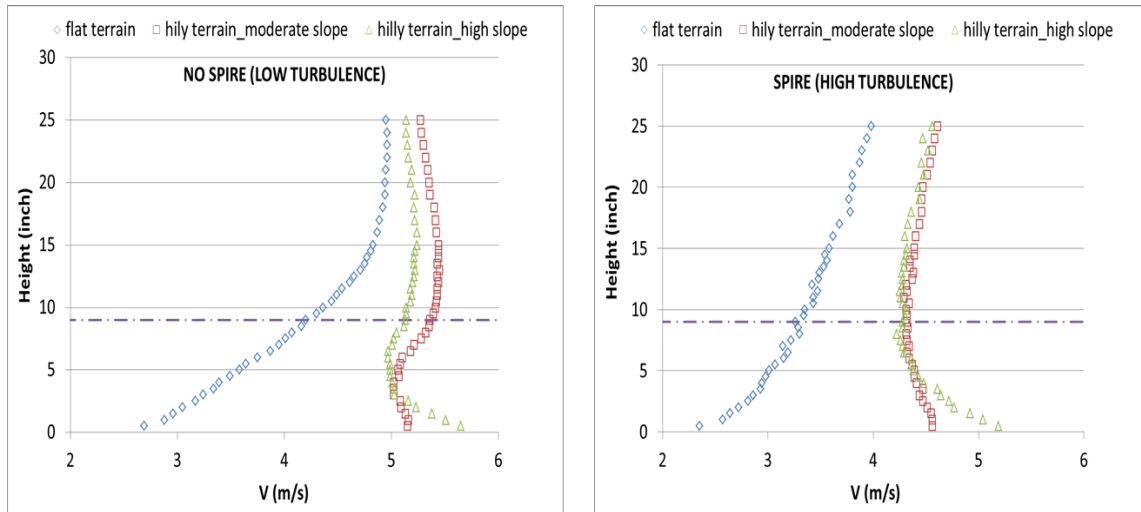


Figure 3-9a Measured mean velocity profile on the top of the 2D-Ridge in comparison with flat terrain for the spire and no spire flow case

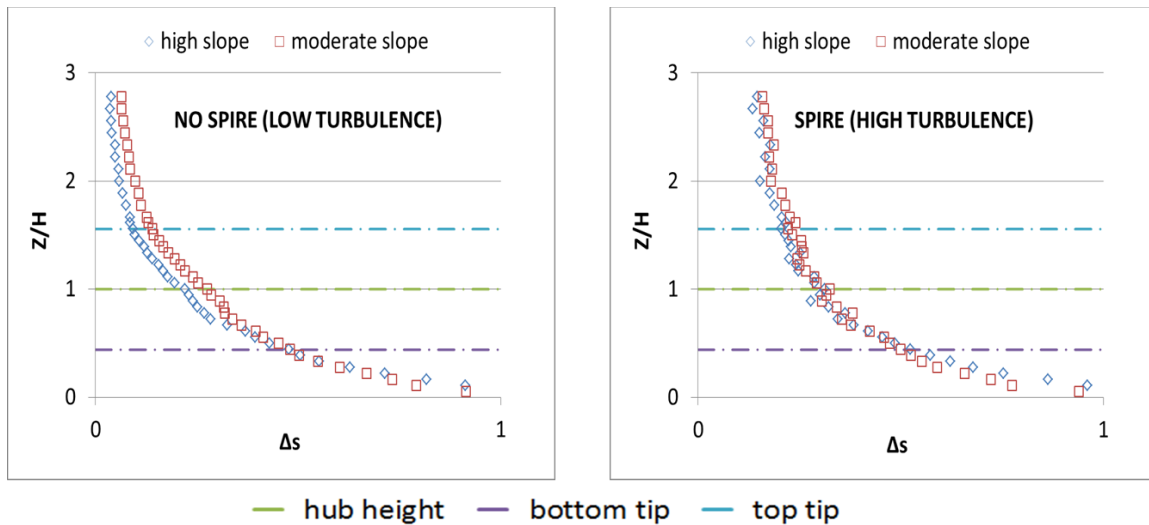


Figure 3-9b Fractional speed up ($\Delta s = \Delta U/U_0$) on the top of the moderate and high sloped 2D-Ridge for the spire and no-spire flow case

The turbine located on the top of the 2D-Ridge produces higher power output compared to the one in the flat terrain because it experiences higher wind speeds (speed-up effect) as shown in Figure 3-9a. However, for high sloped ridge ($\alpha=22^\circ$), the separation in the wake region is affecting the whole flow field over the ridge thus reducing the speed-up on the top of the 2D-Ridge when compared to the moderate sloped ridge ($\alpha=12^\circ$). The effect of slope on

the fractional speed up (ΔS) is more pronounced in the no spire case, causing a significant drop in the fractional speed up at the top of the high sloped ridge (Figure 3-9b).

Figure 3-9b illustrate that no significant difference was observed between the fractional speed up curves on the top of moderate and high sloped ridges in the spire case due to highly turbulent nature of the flow (strong vertical mixing).

Fractional speed-up (ΔS)	no spire case	spire case
Moderate slope ($\alpha = 12^\circ$)	0.28	0.33
High slope ($\alpha = 22^\circ$)	0.22	0.31

Table 3-2 Fractional speed up (at the hub height) on the top of the moderate and high sloped 2D-Ridge for the spire and no spire flow case

Higher fractional speed ups are observed on the top of the moderate sloped 2D-Ridge in comparison to the high sloped ridge, especially for the no spire case. Thus, the power output of the turbine on the top of the moderate sloped ridge is almost 25% greater than the one on the top of the high sloped ridge for the no spire case. However, for the spire case, fractional speed up for the moderate and high sloped ridge is not showing a significant difference throughout the rotor so does the power output of the wind turbine.

Mean flow velocity is considerably smaller for the spire case due to the fact that flow is disturbed and obstructed by the presence of spires. This is the ultimate reason behind the reduction in the power output of the turbine in the spire case.

Fractional speed up at the hub height is higher for the spire case when compared to the no spire case and the effect of the turbulent character of the incoming flow is more pronounced for the high sloped ridge ($\alpha = 12^\circ$).

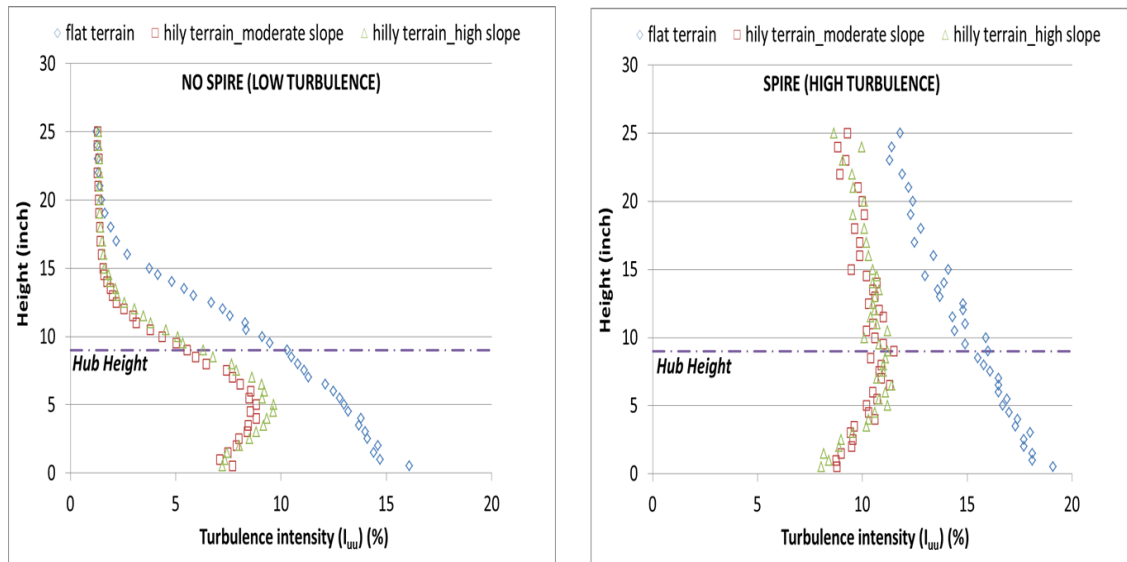


Figure 3-10 Measured turbulence (I_{uu}) profile on the top of the moderate and high sloped 2D-Ridge in comparison with flat terrain for the spire and no spire flow case

Figure 3-10 illustrates the turbulence intensity profiles for the spire and no spire cases. Reduced turbulence levels are observed on the top of the 2D-Ridge when compared to the flow in flat terrain. For the high sloped ridge, turbulence is slightly higher compared to the moderate sloped ridge due to the effect of separation. This slight difference can be observed in the no spire case especially below the hub height.

The fluctuations in the power output of the wind turbine were found to be closely related with the turbulence intensity profile of the incoming flow (Table 3-3).

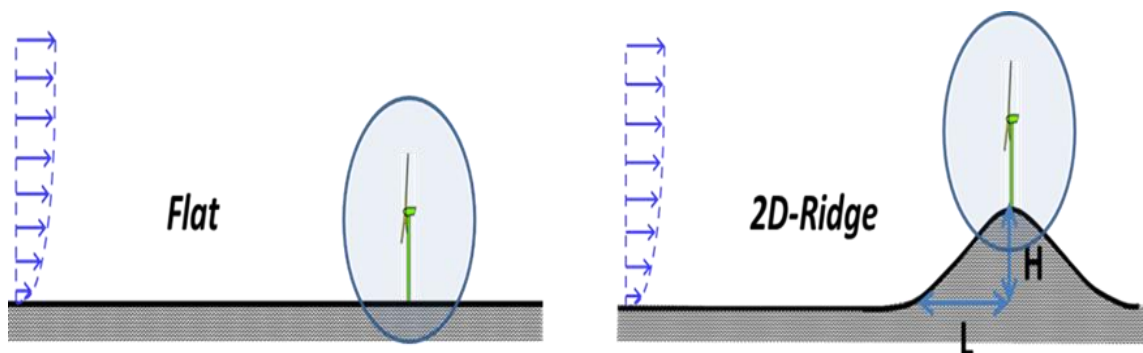


Figure 3-11 A schematic representation of a turbine located on a flat and complex terrain

Power analysis	no spire case		
	Flat terrain	2D-Ridge (Moderate slope)	2D-Ridge (High slope)
average power*1000 (mWatts)	<i>0.67</i>	<i>1.29</i>	<i>1.04</i>
standard deviation (std)	<i>0.070</i>	<i>0.123</i>	<i>0.105</i>
A.F. (std / average power)	<i>0.104</i>	<i>0.095</i>	<i>0.100</i>

Power analysis	spire case		
	Flat terrain	2D-Ridge (Moderate slope)	2D-Ridge (High slope)
average power*1000 (mWatts)	<i>0.29</i>	<i>0.63</i>	<i>0.64</i>
standard deviation (std)	<i>0.064</i>	<i>0.090</i>	<i>0.095</i>
A.F. (std / average power)	<i>0.211</i>	<i>0.14</i>	<i>0.148</i>

Table 3-3 Performance of a turbine (average power output with the deviations) on a flat and complex terrain for the spire and no spire flow case

Power output values of the wind turbine were measured for 120 seconds with a sampling frequency of 1 kHz. Table 3-3 compares the fluctuations in the power output of the wind turbine placed on a flat and complex (top of a high and moderate sloped ridge) terrain.

The amplitude of fluctuations (A.F.) in the power output is calculated by dividing the standard deviation in the power output to the average power output. The fluctuations in the power output for the spire case is higher when compared to the no spire case since the flow is highly turbulent for the spire case. Furthermore, the amplitude of fluctuations in the power output of a turbine placed on the top of a 2D-Ridge is less than the amplitude of fluctuations in the power output of a turbine in a flat terrain (Table 3-3) due to the reduced turbulence intensity levels observed on the top of the ridge (Figure 3-10).

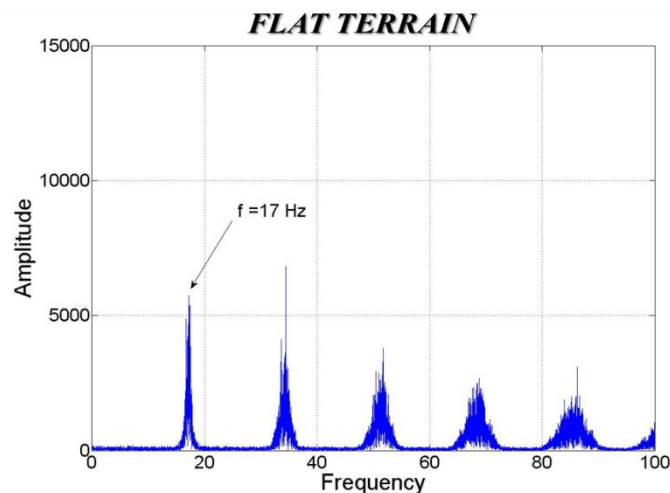
The amplitude of fluctuations in the power output of a turbine placed on the top of the high sloped 2D-Ridge ($\alpha=22^\circ$) is slightly higher when compared to the amplitude of fluctuations in the power output of a turbine placed on the top of the moderate sloped 2D-Ridge ($\alpha=12^\circ$) since the flow separation, affecting the flow field (enhanced turbulence) over the entire ridge, is more pronounced for the high sloped ridge.

The amplitude of fluctuations in the power outputs of the turbine placed in flat and complex (moderate and high sloped ridge) terrains are in agreement with the measured turbulence profiles proving the fact that there is a close relation between turbulence intensity (I_{uu}) levels of the flow and the power fluctuations of a wind turbine.

A model wind turbine located on the top of the ridge has higher power output compared to the one in flat terrain (Table 3-1) due to the speed up effects as shown in Figure 3-9a and Figure 3-9b. In addition, power output of the turbine on the top of the moderate sloped ridge ($\alpha=12^\circ$) is 25% higher than the one on high sloped ridge ($\alpha=22^\circ$) for the no spire case due to the fact that separation is affecting the flow over the ridge for steeper slopes. However, slope of the ridge did not show any significant effect on the power output of the model wind turbine for the spire case.

The power output of a turbine can also be inferred from the rotational frequency of the turbine. The rotational frequency of the turbine is measured by the optical tachometer during the experiments. In order to get an accurate estimate, voltage time series from the tachometer is recorded and the rotational frequency is estimated through the FFT analysis of the voltage time series.

Figure 3-12 illustrates the power spectrum of the recorded voltage time series obtained through a fast Fourier transform (FFT) analysis procedure. A dominant peak identified at a specific frequency which corresponds to the rotational frequency of the rotor blades of the wind turbine model. Other peaks represent the harmonic frequencies of the rotational frequency of the turbine rotor blades.



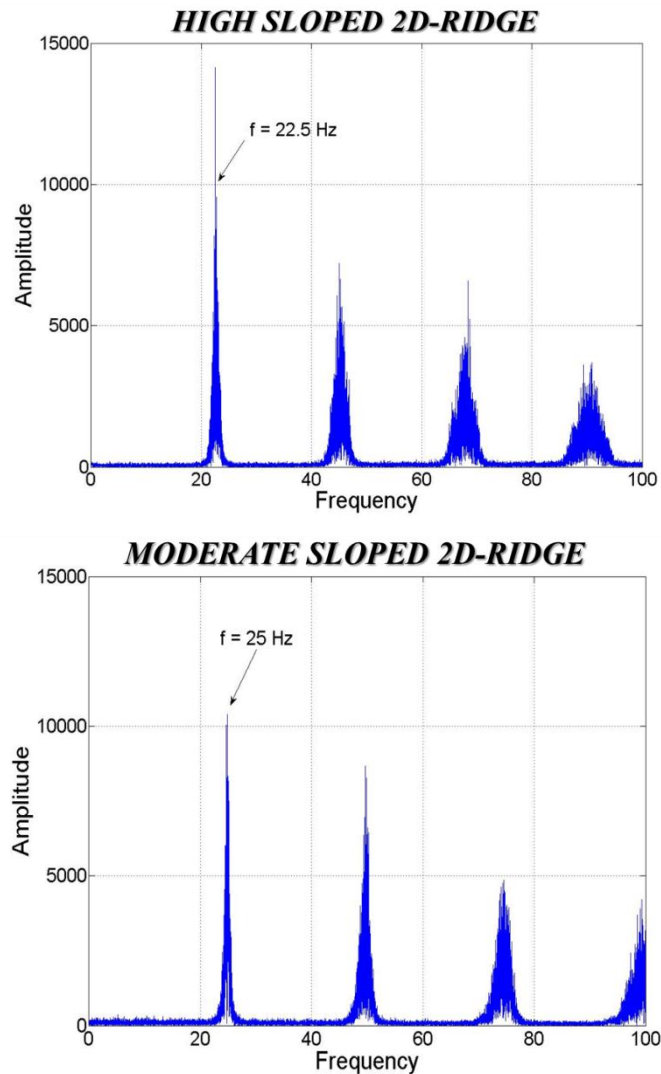


Figure 3-12 Power spectrum analysis of the measured voltage from the tachometer for a turbine in a flat and complex (top of the ridge) terrain (no spire flow case)

$$f (\text{moderate sloped ridge}) > f (\text{high sloped ridge}) > f (\text{flat terrain})$$

The rotational frequency of a wind turbine (f) is directly related to the power output of a wind turbine (P). The rotational frequency of the wind turbine in different terrains are in good agreement with the turbine power output results in these terrains for the no spire case.

$$P (\text{moderate sloped ridge}) > P (\text{high sloped ridge}) > P (\text{flat terrain})$$

Also Tip Speed Ratios (TSR) were calculated using the hub height velocities and rotational frequencies.

$$TSR = \frac{\pi f D}{U_{hub}} \quad (\text{eq. 3-1})$$

f (Hz) - rotational frequency of model wind turbine

D (m) - diameter of rotor of model wind turbine

U_{hub} (m/s) – Hub height velocity

TSR (moderate sloped ridge) > TSR (high sloped ridge) > TSR (flat terrain)

The thrust force (F) acting on a wind turbine in the flow direction is also measured by using a force transducer. The thrust coefficient (C_F) is calculated by using the formula;

$$C_F = \frac{8F}{\rho\pi(U_{hub})^2 D^2} \quad (\text{eq. 3-2})$$

ρ (kg/m^3) - density of air

F (N) - thrust force acting on a wind turbine

Terrain type	(no spire case)	U_0 (hub) (m/s)	Tip Speed Ratio (TSR)	Power*1000 (mWatts)	Force coefficient (C_F)
Flat terrain		4.20	3.3	0.67	0.155
2D-Ridge	Moderate slope ($\alpha = 12^\circ$)	5.36	3.7	1.29	0.176
	High slope ($\alpha = 22^\circ$)	5.13	3.5	1.04	0.162

Terrain type	(spire case)	U_0 (hub) (m/s)	Tip Speed Ratio (TSR)	Power*1000 (mWatts)	Force coefficient (C_F)
Flat terrain		3.26	3.2	0.29	0.156
2D-Ridge	Moderate slope ($\alpha = 12^\circ$)	4.32	3.6	0.63	0.178
	High slope ($\alpha = 22^\circ$)	4.28	3.4	0.64	0.183

Table 3-4 Model wind turbine performance in flat and complex (top of a 2D-Ridge) terrain for the spire and no spire flow case

As it is seen from the equation 3-2, thrust force acting on a turbine is proportional to the square of the velocity (hub height velocity). As the flow velocity through the rotor blades of

the wind turbine increases, the thrust force acting on the turbine increases so does the power output of the wind turbine. Thus, thrust force on the turbine is also an indicator of the power output of the turbine since both are proportional to the incoming velocity ($F \sim V^2$, $P \sim V^3$). The thrust force acting on the turbine placed on the top of the 2D-Ridge is greater due to speed-up effect in comparison to the wind turbine in the flat terrain (Table 3-4). Therefore, the wind turbine sited on the top of the 2D-Ridge would experience higher wind loads compared to those sited in the flat terrain.

For the no spire case, the speed up effect is more pronounced for the moderate sloped ridge compared to the high sloped ridge; therefore, the wind turbine was found to experience higher wind loads on the top of the moderate sloped ridge (Table 3-4).

For the spire case (highly turbulent flow), the power output of the turbine on the top of the ridge does not show significant difference with the change in the slope of the 2D-Ridge so does the thrust force. However, speed up effect on the top of the 2D-Ridge in comparison to the flat terrain resulted in a significant increase in the power output and thrust force coefficient (wind loading) of the turbine placed on the top of the ridge (Table 3-4).

Complex (2D-Ridge) terrain cobra probe measurements on the wake

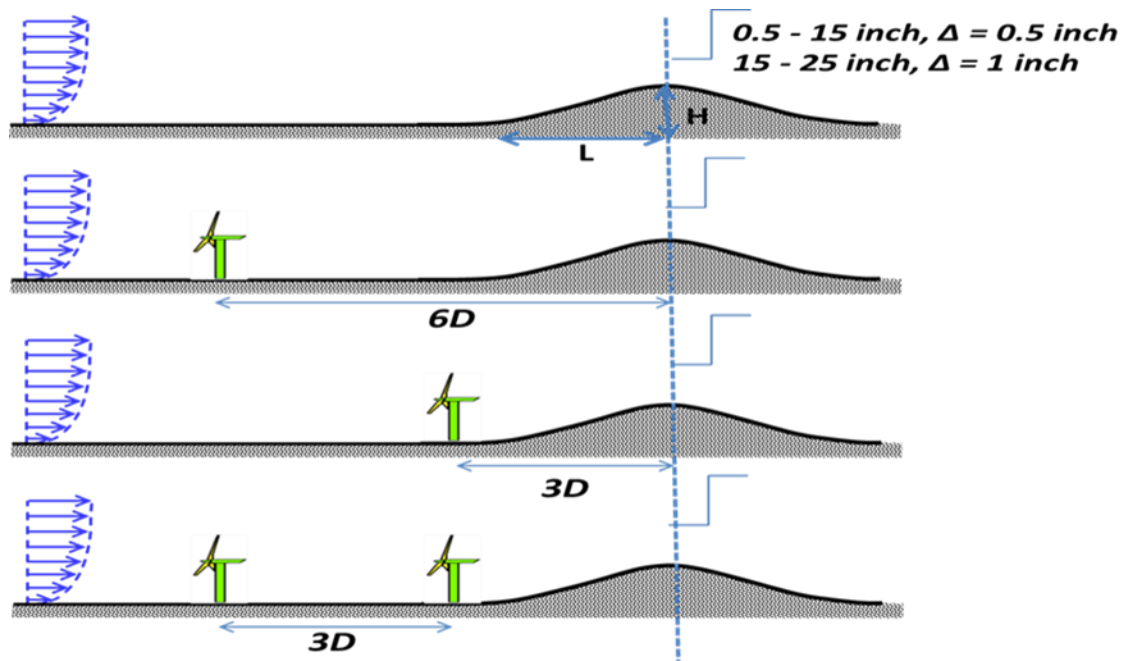


Figure 3-13 Wake measurements on the top of the 2D-Ridge in the vertical plane for different upstream turbine(s) configurations

Cobra probe measurements were conducted on the top of the moderate and high sloped 2D-Ridge in order to observe the wake effects (velocity deficit and enhanced turbulence) from the upstream turbine(s) with different spacing as shown in Figure 3-13. Then, the results were compared with the wake measurements on the flat terrain (Figure 3-15).

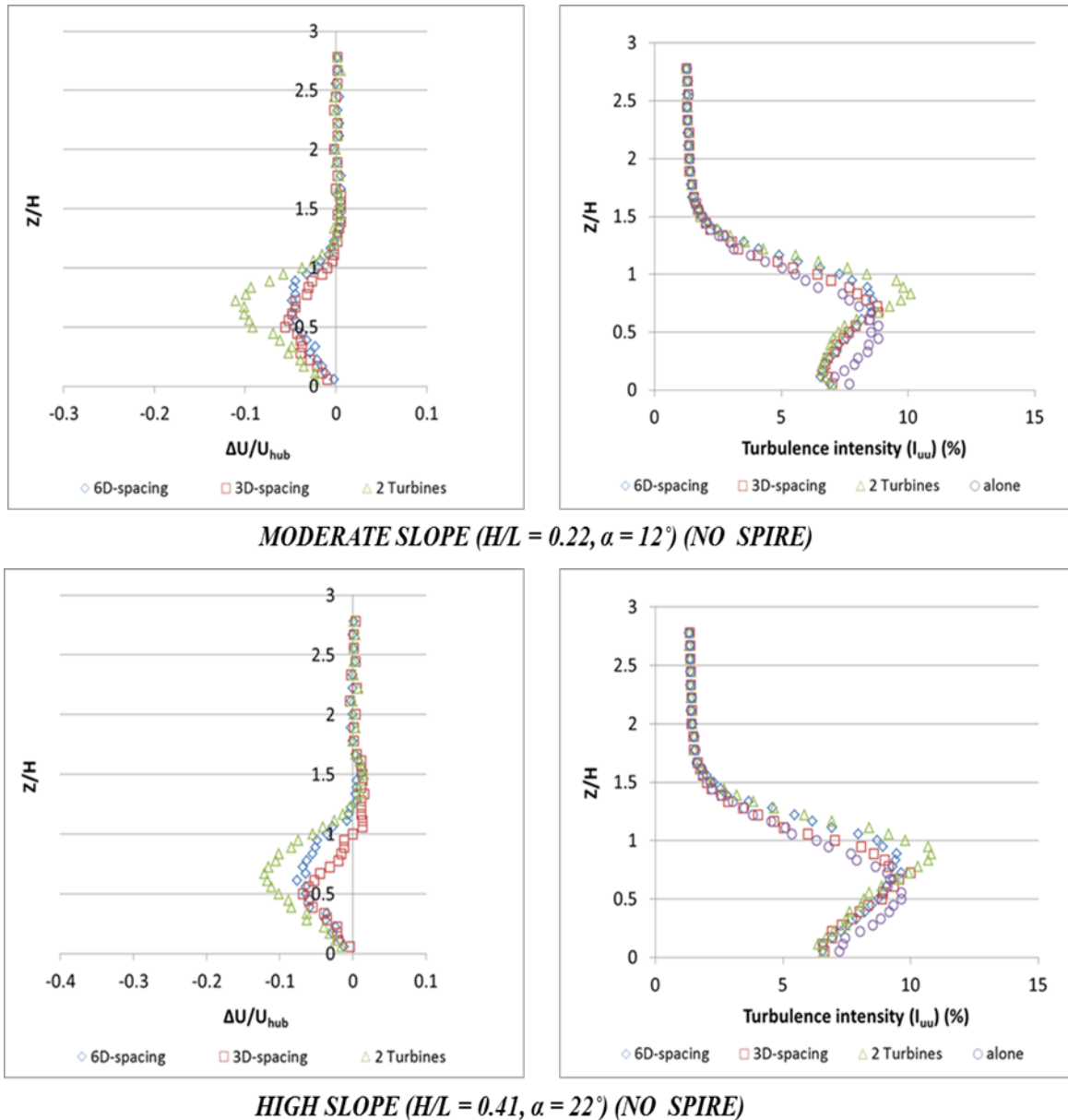


Figure 3-14 Normalized mean velocity deficit and turbulence intensity profile on the top of the moderate and high sloped 2D-Ridge for different upstream turbine(s) configurations (no spire flow case)

Flat terrain cobra probe measurements on the wake

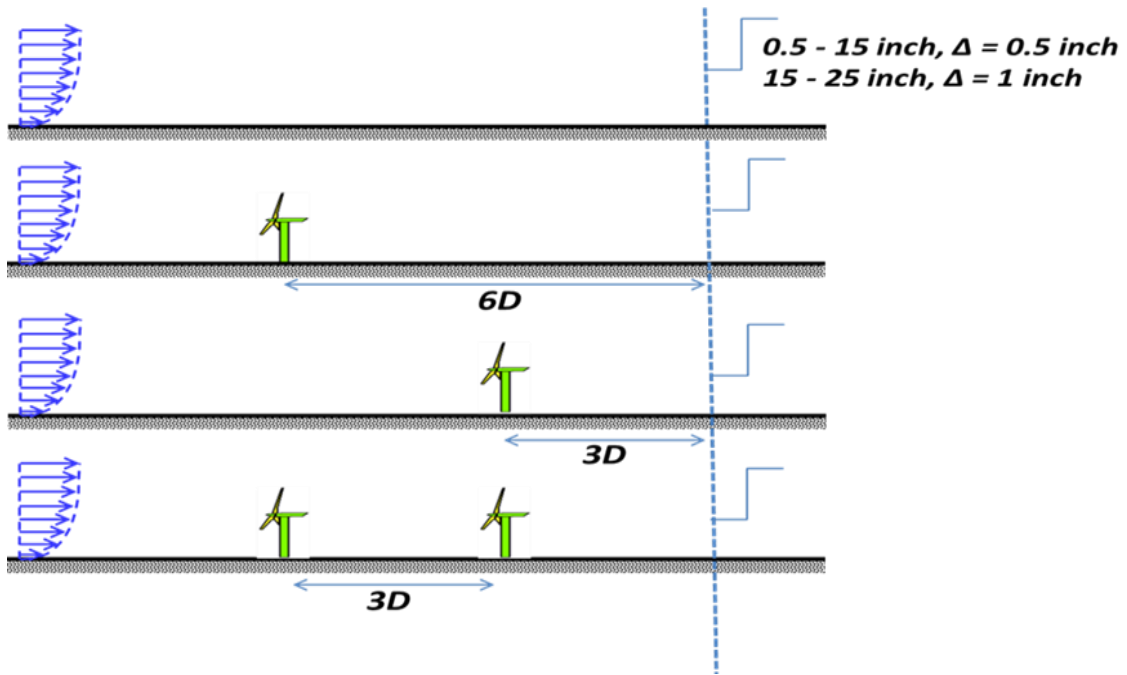


Figure 3-15 Wake measurements over a flat terrain in the vertical plane for different upstream turbine(s) configurations

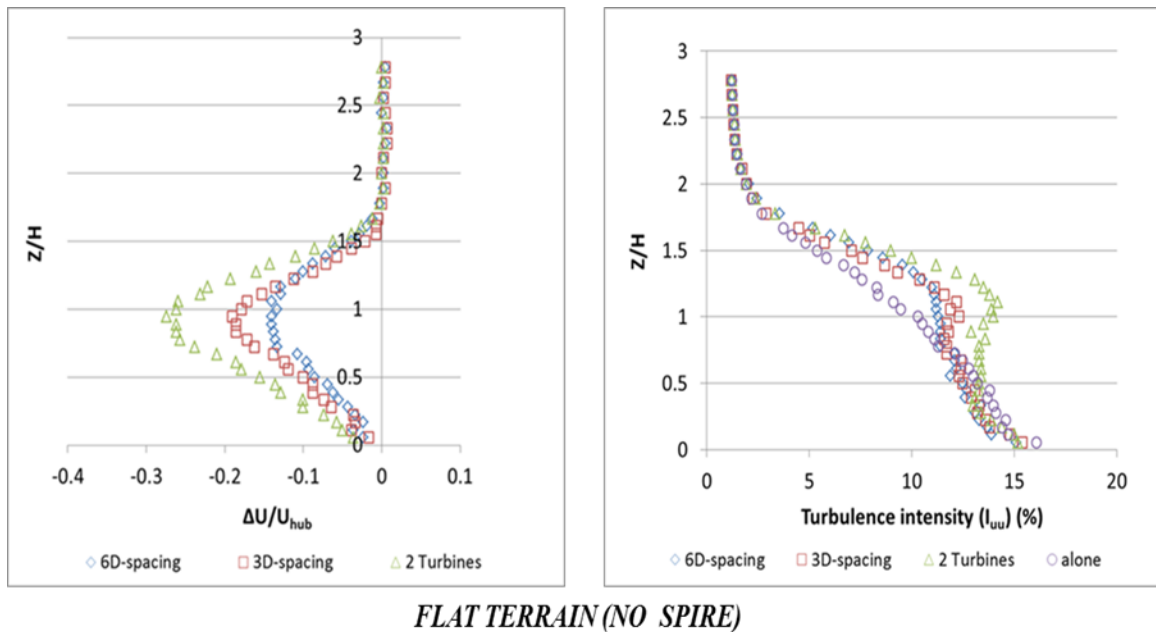


Figure 3-16 Normalized mean velocity deficit and turbulence intensity profile over a flat terrain for different upstream turbine(s) configurations (no spire flow case)

When the wake effects (velocity deficit and enhanced turbulence) are compared in the flat and complex (2D-Ridge) terrain for the no spire case, it can be deduced from Figure 3-14 and Figure 3-16 that the normalized velocity deficits measured in the wake of turbine(s) with different upstream turbine spacing is greater in the flat terrain that would lead to significant losses in the power output of downstream turbine. In addition, turbulence intensity levels in the wake are much greater in the flat terrain causing fluctuations in the power generated by the model wind turbine.

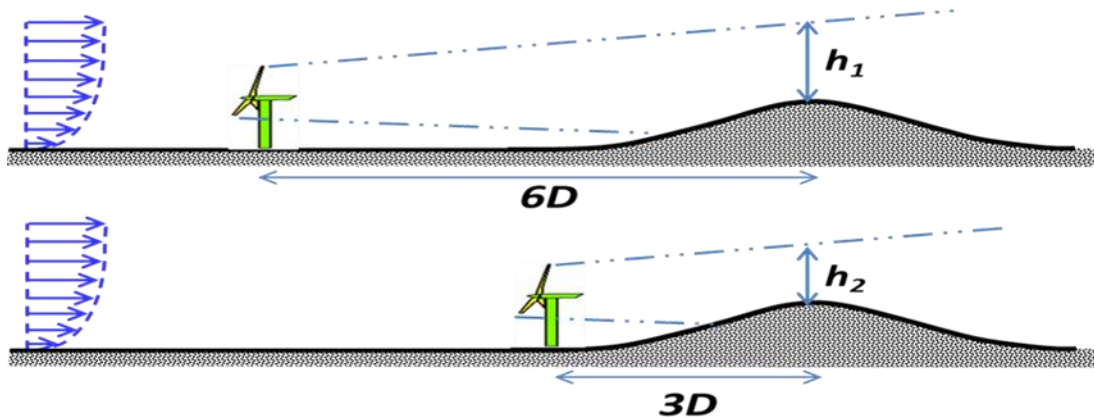


Figure 3-17 Schematic representation of wake expansion over a 2D-Ridge

It was also observed from the wake measurements that the effect of upstream turbine spacing on the wake profiles differs for flat and complex (2D-Ridge) terrain. For the measurements done on the top of the 2D-Ridge, 3D or 6D spacing of upstream turbine does not make a significant change in the wake profile. This would be due the fact that when upstream turbine placed at 3D spacing, most of the wake effects (especially below the hub height – largest velocity deficit due to the tower) are blocked by the ridge itself; however, when upstream turbine placed at 6D spacing, wake expands and recovers at the same time due to larger spacing. Wake expansion can be seen from Figure 3-14 that velocity deficit lasts for larger vertical distances for 6D spacing ($h_1 > h_2$). This effect is more pronounced for the high sloped 2D-Ridge.

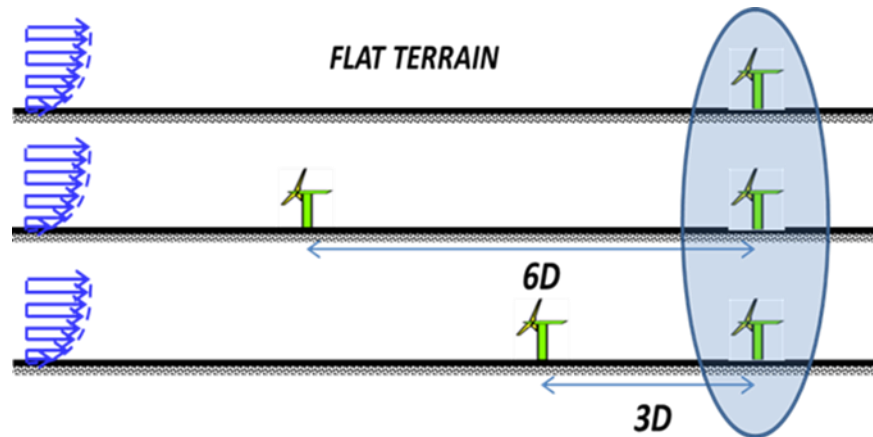


Figure 3-18 Performance (power and wind loading) measurements on the downstream turbine for different upstream turbine configurations in a flat terrain

Power*1000 (mWatts)	Alone		3D-spacing		6D-spacing	
Terrain type	No Spire	Spire	No Spire	Spire	No Spire	Spire
Flat	0.67	0.29	0.48	0.23	0.51	0.25
Percent decrease (%) in Power			28	21	24	14

Table 3-5 Wake effects on the performance (power) of a downstream turbine depending on different upstream turbine spacing for the spire and no spire flow case in a flat terrain

The wake effects on the power output of downstream turbine were observed depending on the spacing of the upstream turbines. The velocity deficit in the wake may lead to significant losses in the power output of the downstream turbine depending on its distance from the upstream turbine. As the distance between the turbines gets larger, downstream turbine could be less affected from the wake generated by the upstream turbine since wake recovers more efficiently in longer distances (Table 3-5).

For the spire case, the flow is highly turbulent and due to the vertical mixing (pulling the high speed air down – reducing velocity deficit), wake is recovered faster so the losses in power output is lower in comparison to the no spire case. However, the performance of the turbines in relatively low turbulent flow (no spire) is better than their performance in highly turbulent flow (spire) since the flow velocity is significantly reduced in the spire case (Table 3-4).

Force coefficient (C_F)	Alone		3D-spacing		6D-spacing	
Terrain type	No Spire	Spire	No Spire	Spire	No Spire	Spire
Flat	0.155	0.156	0.119	0.142	0.126	0.152
Percent decrease (%) in C_F			23	9	19	3

Table 3-6 Wake effects on the performance (wind loading) of a downstream turbine depending on different upstream turbine spacing for the spire and no spire flow case in a flat terrain

Wake effects on the wind loading of the downstream turbine are shown in Table 3-6. Since both power and wind loading of the wind turbine are dependent on the incoming velocity, the velocity deficit in the wake affects both power and wind loading. However, power is proportional to the cube of velocity and wind loading is proportional to the square of velocity; therefore, percent decrease in the power output of the turbine due to velocity deficit is higher in comparison to the percent decrease in the wind loading of the turbine in the wake.

For the spire case, due to the highly turbulent nature of the incoming flow, wake is recovered faster and at 6D-spacing, percent decrease in the thrust force acting on the turbine goes down to 3%.

As the spacing between turbines increases, wake is recovered at larger distances thereby reducing the loss in power and wind loading of the downstream turbine.

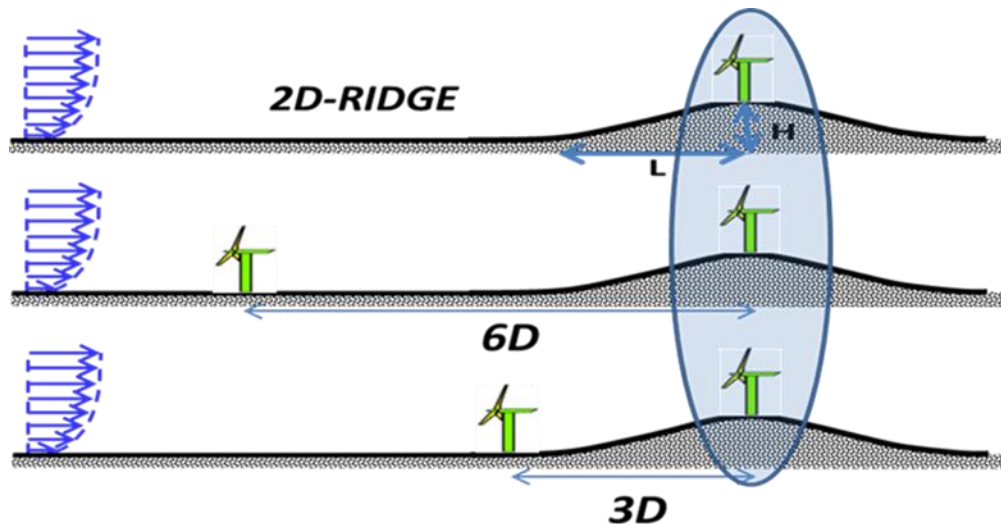


Figure 3-19 Performance (power and wind loading) measurements on the downstream turbine for different upstream turbine configurations in complex (2D-Ridge) terrain

Power*1000 (mWatts)	Alone		3D-spacing		6D-spacing	
	No Spire	Spire	No Spire	Spire	No Spire	Spire
2D-Ridge (moderate slope, 12°)	<i>1.29</i>	<i>0.63</i>	<i>1.21</i>	<i>0.58</i>	<i>1.20</i>	<i>0.60</i>
2D-Ridge (high slope, 22°)	<i>1.04</i>	<i>0.64</i>	<i>0.92</i>	<i>0.63</i>	<i>0.91</i>	<i>0.62</i>
Percent decrease (%) in Power (moderate slope, 12°)			<i>6</i>	<i>8</i>	<i>7</i>	<i>5</i>
Percent decrease (%) in Power (high slope, 22°)			<i>12</i>	<i>2</i>	<i>13</i>	<i>3</i>

Table 3-7 Wake effects on the performance (power) of a downstream turbine in a complex (top of a 2D-Ridge with moderate and high slope) terrain depending on different upstream turbine spacing for the spire and no spire flow case

The model wind turbine on the top of the 2D-Ridge has almost the same power output for 3D and 6D spacing of the upstream turbine. Thus, turbines would be placed closer in complex terrains (2D-Ridge) regardless of the dependence of the wake effects on spacing; however, there is a trade-off since the turbines on the foot of the 2D-Ridge suffer from the decelerated flow as mentioned earlier in this chapter.

It is deduced from the results that higher power outputs are observed for the turbine on the top of the 2D-ridge and losses due to wake effects are reduced when compared to the flat terrain.

For the no spire case, turbine on the top of the high sloped ridge experiences greater losses in the power output due to wake effects compared to the turbine on the moderate sloped ridge as shown in Table 3-7 although no significant difference observed in the normalized velocity deficit profile in the wake (needs further investigation).

Force coefficient (C_F)	Alone		3D-spacing		6D-spacing	
	No Spire	Spire	No Spire	Spire	No Spire	Spire
2D-Ridge (moderate slope, 12°)	0.176	0.178	0.170	0.174	0.165	0.174
2D-Ridge (high slope, 22°)	0.162	0.183	0.148	0.165	0.143	0.176
Percent decrease (%) in C_F (moderate slope, 12°)			3	2	6	2
Percent decrease (%) in C_F (high slope, 22°)			9	10	12	4

Table 3-8 Wake effects on the performance (wind loading) of a downstream turbine in a complex (top of a 2D-Ridge with moderate and high slope) terrain depending on different upstream turbine spacing for the spire and no spire flow case

As shown in Table 3-8, percent decrease (due to wake effects) in the wind loading of the turbine on the top of the ridge is relatively smaller than the percent decrease in the wind loading of the turbine in a flat terrain. This difference is more pronounced in relatively low turbulent (no spire) flow. Furthermore, in the no spire flow case, the turbine on the top of the high sloped ridge experiences greater losses in the wind loading due to wake compared to the turbine on the top of the moderate sloped ridge which was also observed in the power output measurements.

3.4 CONCLUSION

Wind turbine performance would be affected significantly by the terrain of the wind farm. It was found out that wind turbines sited on the top of the 2D-Ridge take advantage of higher wind speeds thus having more power output and also experiencing much higher wind loads compared to those sited over the flat terrain. Moreover, they are exposed to reduced turbulence levels compared to the turbines over the flat terrain.

The speed-up over a complex terrain, a 2D-Ridge in our case, is influenced by the slope of the ridge. It was observed that largest speed-up was observed on the top of the moderate sloped 2D-Ridge since no significant separation was observed on the lee side of the hill. As

slope increases, the separation is more likely to happen, affecting the entire flow over the ridge (reduced mean flow and enhanced turbulence).

The effect of the terrain and the incoming flow character on the wake interference was also investigated. Losses due to wake effects are significantly reduced on the top of the 2D-Ridge with moderate slope ($\alpha=12^\circ$). Furthermore, the turbine sited on the top of the ridge performed almost the same for 3D and 6D spacing of the upstream turbine revealing the fact that turbines would be placed closer in complex terrains (2D-Ridge) regardless of the dependence of the wake effects on spacing; however, there is a trade-off since the turbines on the foot of the 2D-Ridge suffer from the decelerated flow. This effect is more pronounced on the foot of steeper ridges.

In addition, usage of spires added turbulence to the flow thereby making the vertical mixing mechanism dominant in the flow. Therefore, wake recovers faster in the spire case, reducing the wake effects induced by the upstream turbines.

CHAPTER 4. MULTIPLE WAKE INTERACTIONS

4.1 FIVE TURBINES IN A LINE / EFFECT OF SPACING

4.1.1 INTRODUCTION

Each turbine operates in order to extract the power available in the wind (limited by Betz limit). However, the flow is disturbed during the power extraction process and wake, characterized by velocity deficit and enhanced turbulence, is generated behind the turbine. Thus, the downstream turbines in the wake of upstream turbines suffer from reduced power output and enhanced fatigue loading. As analyzed in the previous chapters, power losses due to wake depends on many factors including spacing between turbines, arrangement of turbines (wind farm layout) and incoming flow characteristics. The losses can be significantly higher for the first turbine immediately downstream of the most upstream turbine depending on the spacing between turbines (Adaramola & Krogstad, 2011; Barthelmie, et al., 2009; Dahlberg & Thor, 2009). However, power losses decrease slowly for the subsequent downstream turbines until an equilibrium condition is reached in the boundary layer (Dahlberg & Thor, 2009; Beyer, Pahkle, Schmidt, Waldl, & de Witt, 1994; Adaramola & Krogstad, 2011; Chamorro, Arndt, & Sotiropoulos, 2011).

It has been a controversial issue at what spacing the turbines will be placed far apart from each other to get the maximum output from the downstream turbines. In this experiment, we investigated the performance of the downstream turbine by using two turbines in tandem arrangement at different spacing (Figure 4-1).

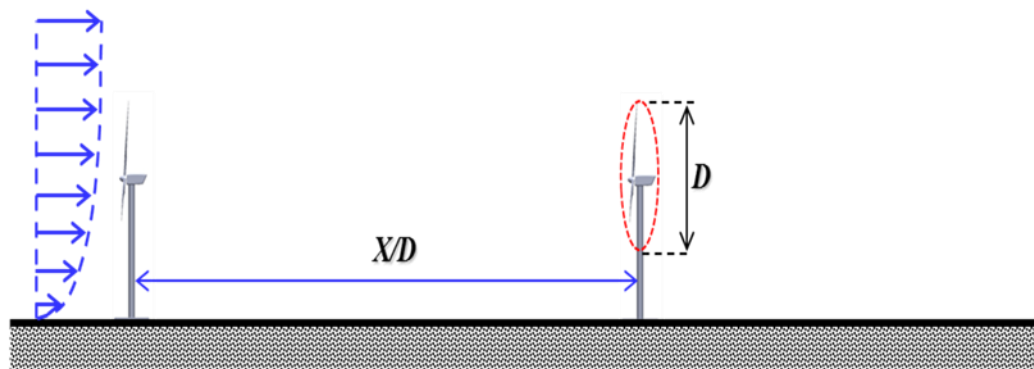


Figure 4-1 A schematic representation of two turbines in tandem arrangement (distance between the turbines is defined in terms of the diameter of the turbine)

The current streamwise spacing between turbines in the large wind farms is around 7 rotor diameters. Meneveau and John Meyers stated, “in the correct spacing, the turbines alter the landscape in a way that creates turbulence, which stirs the air and helps draw more energy from higher altitudes” (Johns Hopkins University, 2011). According to them, placing the turbines 15 rotor diameters apart - more than twice as far apart as in the current layouts - results in a more efficient power generation. However, there is always a trade - off due to the space and economic constraints.

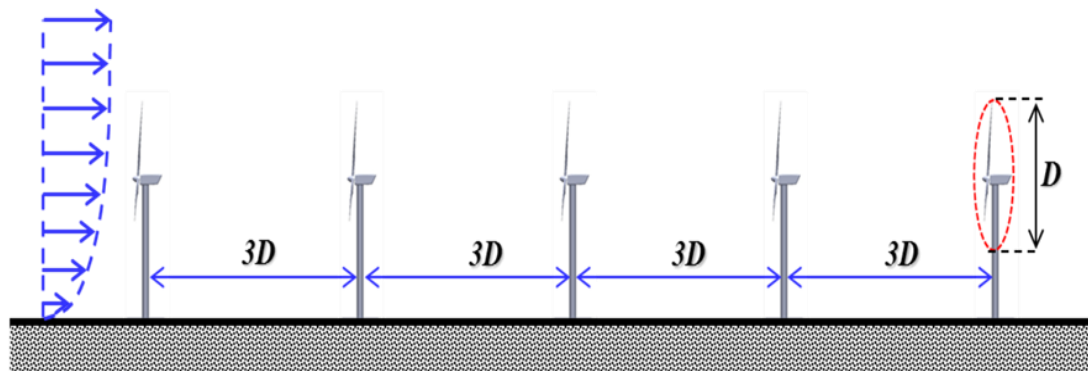


Figure 4-2 A schematic representation of five turbines with 3D streamwise spacing in tandem arrangement

In addition, 5 model wind turbines were installed in a tandem arrangement with 3D streamwise spacing as shown in Figure 4-2. The purpose was to observe the wake effects on the performance of the subsequent downstream model wind turbines. There are two parameters reflecting the performance of a wind turbine: thrust force acting on a wind turbine (in prevailing wind direction) and power output of a wind turbine. Both parameters are dependent on the wind speed; however, the effect of velocity deficit due to wake on the power output is more pronounced as mentioned in the previous chapters. In this experiment, these parameters were measured for the turbines located in each row. Furthermore, these measurements shed light on the development of an internal boundary layer within the rows. Moreover, effects of the incoming flow character (turbulence) on the wake were investigated.

4.1.2 EXPERIMENTAL SET-UP

Model wind turbines were installed in the AABL Wind Tunnel located at the Aerospace Engineering Department of Iowa State University as shown in Figure 4-3. The AABL wind tunnel is a closed circuit wind tunnel with a test section of 20m and a cross section of

2.4m*2.3m. A turbulent boundary layer was developed with the help of spires at the beginning of the test section and the wind tunnel floor was covered with chains to simulate the flow conditions similar to atmospheric boundary layer winds under thermally neutral conditions. Spires were used to change the turbulent character of the incoming flow.



Figure 4-3 Five turbines in tandem arrangement with 3D spacing (left) and spires at the onset of the test section of the wind tunnel (right)

3 bladed horizontal axis wind turbines (HAWT) were used during the experiments. All model wind turbines used are of the same kind and have the same dimensions. They have a rotor diameter of 254 mm and their hub height is 225 mm with a blade pitch angle of 10° . They are scaled down 350 times from the real life length scales.

The measurements (power and force) were done for two inflow conditions; spire case with highly turbulent incoming flow and no spire case with relatively lower turbulence levels in comparison to the spire case. Figure 4-4 shows the measured normalized mean velocity and turbulence intensity profiles (vertical) of the simulated boundary layer in the wind tunnel. The turbulence intensity (I_{uu}) at the hub height is around 10% for the no spire case and 17% for the spire case.

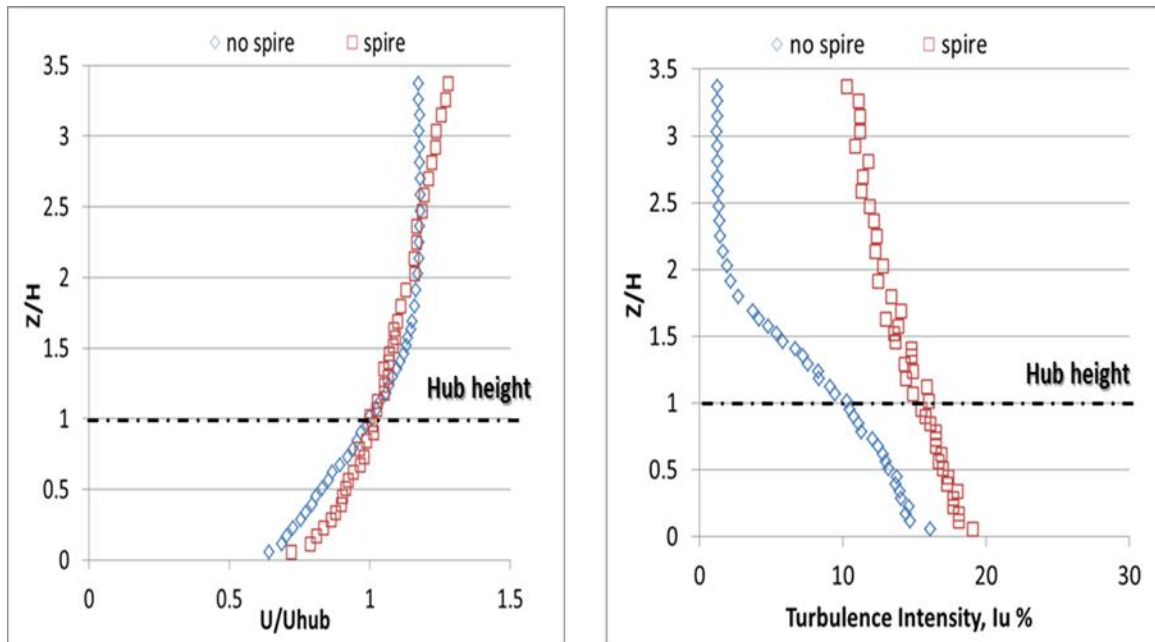


Figure 4-4 Normalized mean velocity and turbulence intensity profiles of the simulated atmospheric boundary layer

The electrical voltage through the DC motor installed inside the turbine nacelle was measured for different resistance values ranging from 1ohm to 1000ohm. Resistance was adjusted by using a variable resistance box connected to the DC motor via special wiring equipment. Optimum electrical power output of a wind turbine was then calculated for an optimum resistance value. The voltage output data were acquired for 180 seconds at a sampling rate of 1 kHz.

Force transducer (JR3) was installed underneath the model wind turbine in order to measure the dynamic wind loads acting on the wind turbine. During the experiments, the wind loads data were acquired for 60 seconds at the sample rate of 1 kHz for each case.

Rotational frequency of the model wind turbine was also measured using the optical tachometer (Monarch Instrument). FFT analysis of the voltage time series taken from the tachometer was used to get an accurate estimate of the turbine rotational frequency.

Labview is used as data acquisition software in the experiments. Two different codes exist for force and voltage measurements. Voltage measurements were then used to determine the power output (from DC motor) and the rotational frequency (from optical tachometer) of a model wind turbine. Thus, voltage readings from both DC motor and optical tachometer were taken at the same time using the same labview code.

4.1.3 EXPERIMENTAL RESULTS AND DISCUSSIONS

First, the thrust force and power measurements were done to observe the effect of spacing on the performance of the downstream wind turbine. The effects of turbulence levels of incoming flow were also investigated.

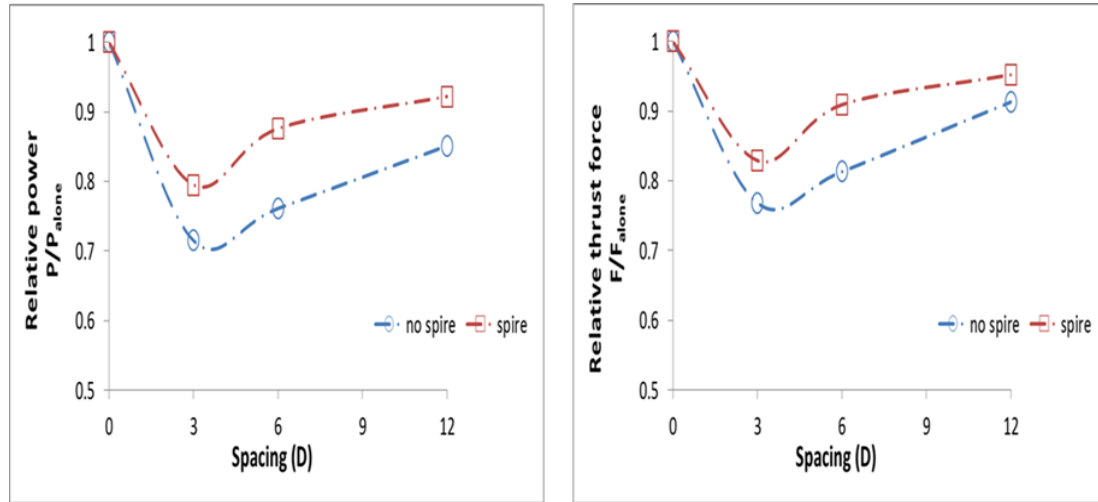


Figure 4-5 Normalized (Relative) power and thrust force variation for different turbine spacing ($X/D=3$, $X/D=6$ and $X/D=12$)

The measurements were done at $X/D=3$, $X/D=6$ and $X/D=12$ and compared with the individual performance of turbine without any wake effects. Thus, the relative power (P/P_{alone}) and the relative thrust force (F/F_{alone}) were used in Figure 4-5.

At $X/D=12$, the power losses is around 15% for the no spire case. However, in the spire (highly turbulent flow) case, recovery is faster due to the turbulent mixing so losses are reduced down to 8% as shown in Table 4-1.

Percent decrease (%) in Power	3D-spacing	6D-spacing	12D-spacing
No spire (low turbulence, 10%)	28.5	23.9	14.9
Spire (high turbulence, 17%)	20.5	12.4	7.8

Percent decrease (%) in thrust force	3D-spacing	6D-spacing	12D-spacing
No spire (low turbulence, 10%)	23.2	18.7	8.7
Spire (high turbulence, 17%)	17.1	9.1	4.8

Table 4-1 Percent decrease (%) in the power and thrust force for the spire and no spire flow case depending on the spacing between turbines

As the spacing between the turbines is increased, improvement in the performance (power and thrust force) of the downstream wind turbine was observed. Since, the power is affected more severely from the velocity deficit compared to the thrust force, mentioned earlier, the reduction in the power output of the downstream turbine is more than the reduction in the thrust force acting on the turbine.

At $X/D=12$, the effect of the wake introduced by the rotor is almost diminished; however, the presence of tower and nacelle is also an important source of disturbance for the incoming flow. We stopped the upstream turbine in order to observe the effect of solely the presence of tower and nacelle on the downstream turbine at $X/D=12$ for the no spire case. The disturbance introduced by tower and nacelle was still noticeable at $X/D=12$ causing a power loss around 10% for the downstream turbine.

Then, five turbines were installed in tandem arrangement with 3D streamwise spacing in order to investigate the multiple wake interaction effects on the subsequent downstream turbines.

Power output of the turbine in each row was calculated from the voltage readings for different resistance (load) values ranging from 1 ohm to 1000 ohm. Optimum performance was observed at an optimum resistance around 5 – 6 ohm (Figure 4-6).

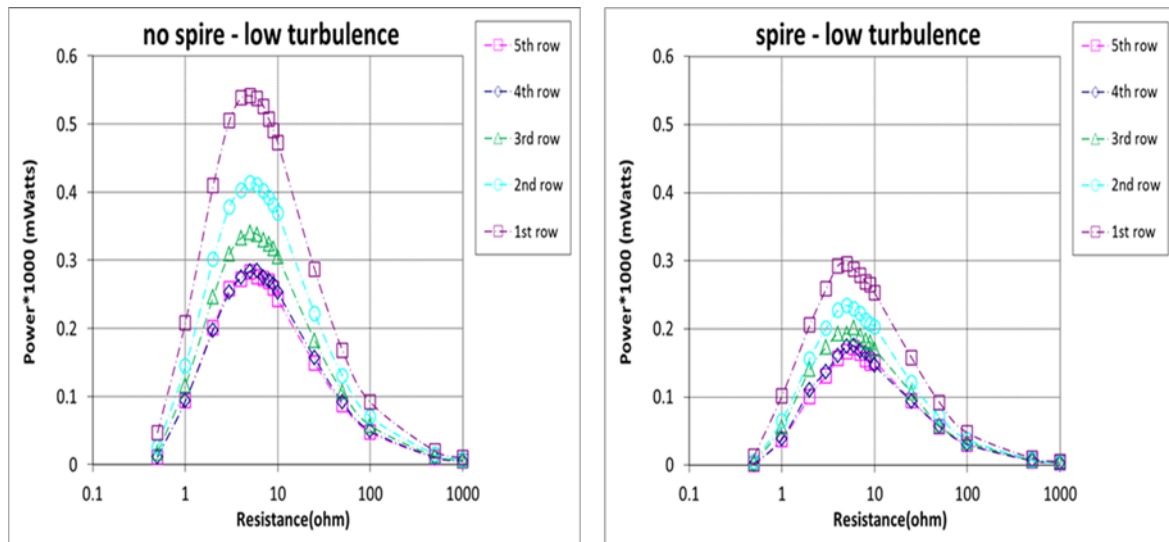


Figure 4-6 Variation of the power output of the wind turbine with different loading in each row for the spire and no spire flow case

For highly turbulent (spire) inflow, power output of the model wind turbine was reduced due to the reduced velocity up to 25% at the top tip height. Losses in the optimum power output of the model wind turbines located in the subsequent downstream rows can be seen clearly from Figure 4-6. Power loss is significantly higher for the first turbine immediately downstream of the most upstream one. It can be up to 28% for the no spire (low turbulence) case. After then, it gradually decreases in the following rows until an equilibrium in the boundary layer is reached. The equilibrium was reached starting with the fourth row of wind turbines.

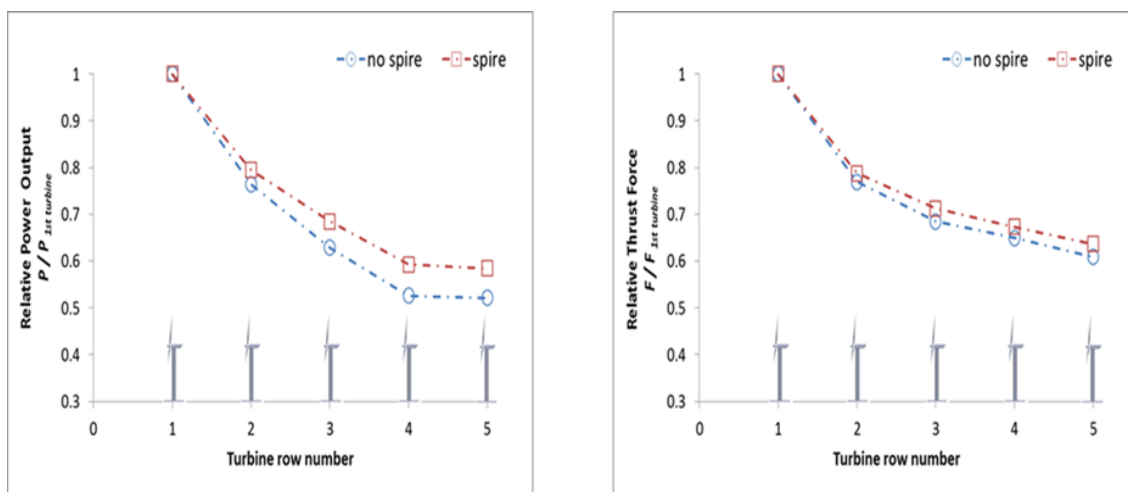


Figure 4-7 Normalized (Relative) power and thrust force variation throughout the rows

The reduction in the normalized power and thrust force for the turbines in the subsequent downstream rows was shown in Figure 4-7. This is due to the fact that turbines in the downstream rows see considerably lower freestream velocity due to the wake effects (velocity deficit) induced by the upstream turbines.

Although power output of the turbines in highly turbulent (spire) flow is considerably lower due to the reduced velocity compared to the no spire case, highly turbulent character of the incoming flow help the wake recover faster due to the turbulent mixing. It is clear from Figure 4-7 that especially after the second row, the effect of turbulence on the relative power and the thrust force is more pronounced. Turbulence enables efficient mixing of air inside the wake with the air outside the wake so that the velocity deficit in the wake recovered faster in highly turbulent flow. Thus, percentage loss in the power output was reduced approximately 6% in the last (fifth) row for the spire (highly turbulent flow) case. The improvement in the

thrust force due to turbulence is comparably small due to the fact that thrust force is dependent on the square of the incoming flow velocity, whereas power is dependent on the cube of the incoming flow velocity. Thus, the improvement in the velocity deficit has a stronger effect on the power output of a turbine.

We also investigated the wake effects on the rotational frequency of the model wind turbine in the last row. Figure 4-8 illustrates the amplitude versus frequency plot for the turbines located in the first and the last (5th) row. Dominant peak in the amplitude was observed at the rotational frequency of the model wind turbine. Other peaks represent the harmonic frequencies of the rotational frequency.

The wake effects on the rotational frequency of the turbine in the last row were observed. Rotational frequency analysis is important since power output of a turbine can be inferred through its rotational frequency.

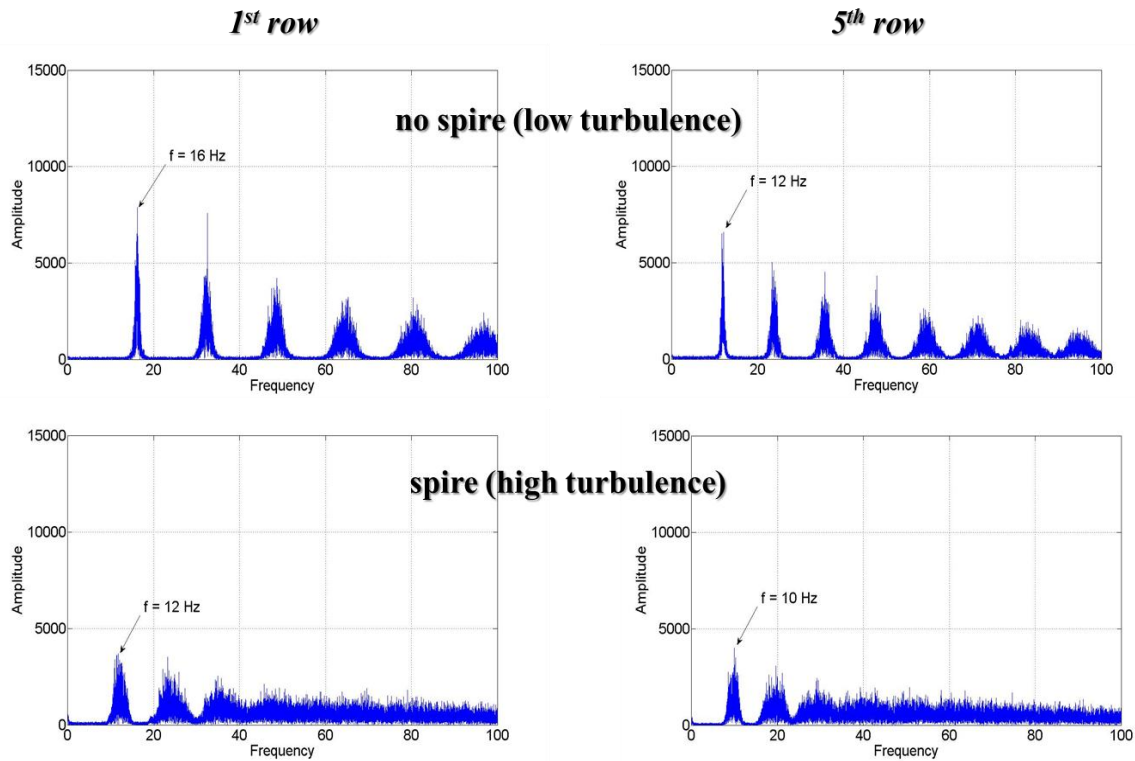


Figure 4-8 Power spectrum analysis of the measured voltage from tachometer for the spire and no spire flow case (comparison between the turbines located in the 1st and the last (5th) row)

In the spire (highly turbulent flow) case, the turbines rotate at lower frequencies due to the reduced velocity. In addition, reduction in the rotational frequency was observed for the

turbine in the last row compared to the turbine in the first row. The level of fluctuations in the rotational frequency is higher for the spire case thus making it hard to accurately estimate the rotational frequency.

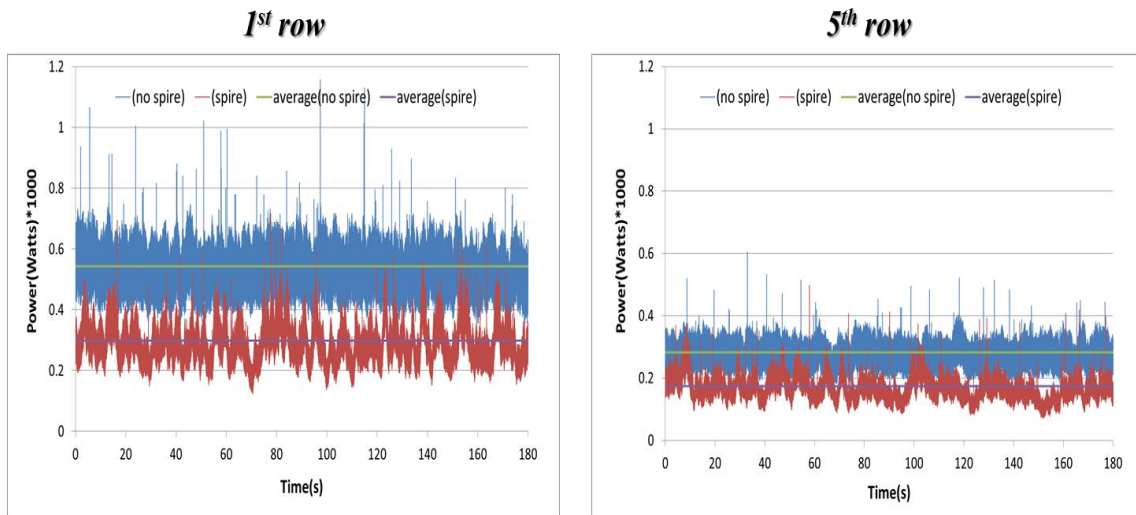


Figure 4-9 Time sequence of the measured power output of the turbine located in the 1st and last (5th) row for the spire and no spire flow case

The fluctuations in the wind speed and direction can be induced by both the turbulent character of the incoming flow and wake interference effects. Fluctuations in the wind speed and direction are more pronounced in highly turbulent flow causing higher rate of change in the angle of attack of the turbine blades. This will lead to fluctuations in the forces acting on the turbine blades thereby shortening the lifetime of the wind turbines drastically.

As shown in Table 4-2, for the spire (highly turbulent flow) case, turbulence generated by the spires lead to higher fluctuations in the power output. Thus, standard deviation in the power output increases while average power output decreases, thereby making the amplitude of fluctuations (A.F.) much higher for the spire case.

Power analysis	No Spire (Low turbulence, 10%)		Spire (High turbulence, 17%)	
	1st row	5th row	1st row	5th row
average power*1000 (mWatts)	<i>0.54</i>	<i>0.28</i>	<i>0.30</i>	<i>0.17</i>
standard deviation (std)	<i>0.057</i>	<i>0.031</i>	<i>0.059</i>	<i>0.036</i>
A.F. (std / average power)	<i>0.105</i>	<i>0.111</i>	<i>0.197</i>	<i>0.205</i>

Table 4-2 Performance of the turbine (average power output with the deviations) located in the 1st and last (5th) row for the spire and no spire flow case

When turbines are placed one behind another as in the case of 5 turbines in a line experiment, the wake effects (velocity deficit and enhanced turbulence) not only reduce the energy production but also lead to fluctuations in the wind forces (thrust and torque) acting on the blades. The latter will cause fluctuations in the overall power output and also it will make the downstream turbines more prone to wear and tear due to dynamic loading (fatigue). A slight increase in the amplitude of fluctuations (A.F.) for the turbine in the last (5th) row can be seen in Table 4-2 for the spire and no spire cases.

4.1.4 CONCLUSION

Effect of spacing on the performance of the downstream turbine (power and thrust force) was investigated. As the spacing between turbines increases, wake effects could be diminished so that performance of the downstream turbine could be increased. Furthermore, wake is recovered faster for highly turbulent (spire) incoming flow due to the turbulent mixing.

In addition, the development of wake and wake interference effects on the performance of wind turbines located in the subsequent downstream rows were investigated for different incoming flow character. Significant reduction was observed in the power and thrust force for the turbines in the subsequent downstream rows due to the fact that turbines in the downstream rows see considerably lower freestream velocity due to the wake effects (velocity deficit). Furthermore, spires introduced turbulence and eddy to the incoming flow, increasing the turbulent character of the flow. Highly turbulent incoming flow helps the wake recover faster so that percentage loss in the power output was reduced approximately 6% in

the last row for the spire case compared to the no spire case. However, highly turbulent nature of the incoming flow together with the wake generated turbulence lead to fluctuations in the wind forces acting on the blades which makes the turbines suffer from excessive dynamic loading (fatigue).

4.2 WAKE EFFECTS ON WIND TURBINE PERFORMANCE

4.2.1 INTRODUCTION

There are several factors affecting the overall power performance in a wind farm. One is the spacing between wind turbines and their arrangement pattern. As the spacing between wind turbines increases, the performance of the downstream wind turbines increases since more space gives the wake enough time for the recovery of the velocity deficit and enhanced turbulence levels, which are the main contributors for the power loss and fatigue loading especially for the downstream turbines. Second is the operating condition of the upstream turbines. Adaramola and Krogstad (2011) investigated the change in the power output of the downstream turbine by operating the upstream turbine slightly outside its optimum settings or changing the yaw angle of the upstream turbine. They found out that increasing the yaw angle of the upstream turbine up to 30° has a positive effect on the wind farm efficiency (maximum gain in the total power output is around 12%) for the two turbines in tandem arrangement.

Changing the yaw angle of the upstream turbine changes the orientation of the wake so that the downstream turbine stays completely out of the wake region or less affected. In the present study, the effect of changing the upstream turbine yaw angle on the downstream turbine performance was investigated for different inflow conditions (high and low turbulence) and for different separation distances (2D and 4D) by using two wind turbines in tandem arrangement.

4.2.2 EXPERIMENTAL SET-UP



Figure 4-10 Two turbines in tandem arrangement with upstream turbine yawed with 50° on the turntable

The 3-bladed wind turbine models used in the experiment have a diameter of 381 mm and the tower is 305 mm high with a pitch angle of 10° (Figure 4-10). Inflow conditions were changed by using spires and also chains were used on the wind tunnel floor to obtain the logarithmic velocity profile similar to atmospheric flow conditions. Figure 4-11 shows the measured profiles of normalized flow velocity and turbulence intensity for the two cases; spire (high turbulence) and no spire (low turbulence) cases.

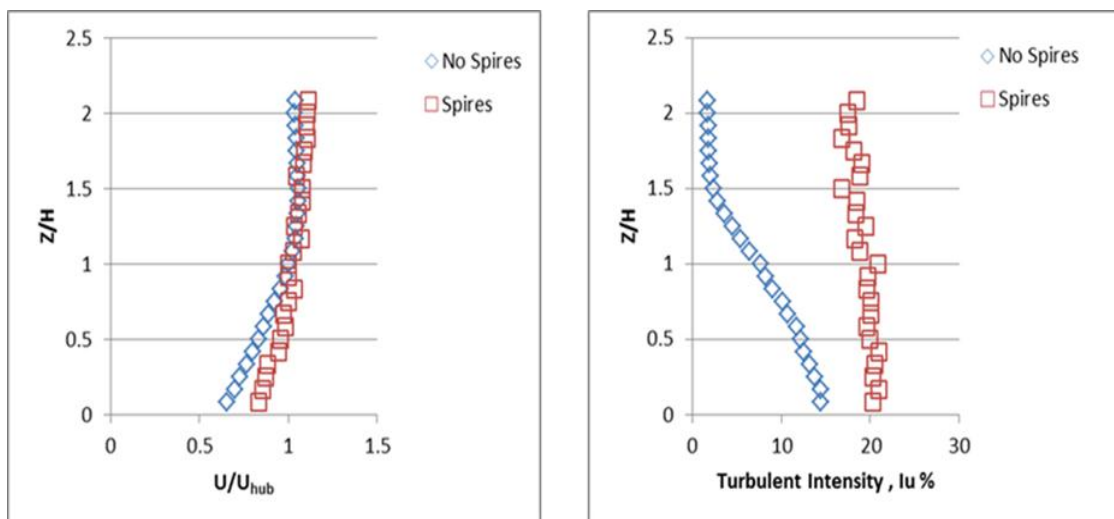


Figure 4-11 Measured profiles of normalized mean velocity and turbulence intensity

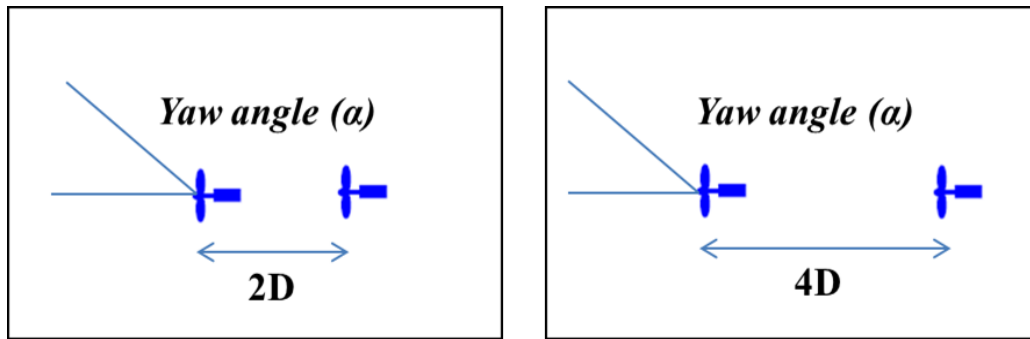


Figure 4-12 A schematic of two turbines (yawing the upstream turbine) in tandem arrangement with different spacing

As it is also shown in Figure 4-12, upstream turbine is yawed from 0° to 50° with an increment of 10° . Then power measurements were done on upstream and downstream turbines for two separation distances ($2D$ and $4D$) with different inflow conditions (high and low turbulence). The electrical voltage through the DC motor installed inside the turbine nacelle was measured for an optimum resistance value then electrical power was calculated. Turbine angular frequency was also obtained through the FFT analysis of voltage time series taken from the tachometer. Sampling frequency for the power and rotational frequency measurements were 1 kHz and sampling time was 120 seconds.

4.2.3 EXPERIMENTAL RESULTS AND DISCUSSIONS

The effect of operating the upstream wind turbine in yaw on the performance of the upstream wind turbine is shown in Figure 4-13. As the yaw angle of the upstream turbine increases, the performance of the upstream wind turbine degrades due to the fact the rotor blades will experience lower wind speeds ($U \cdot \cos(\alpha) < U$) perpendicular to the rotor plane. It can be easily seen from Figure 4-13 that power output and rotational frequency of the wind turbine are reduced by operating the upstream wind turbine in yaw. The effects of the turbulence character of the incoming flow on the normalized power output of the upstream turbine at various yaw angles are also shown in Figure 4-14. The normalized (relative) power output of the upstream turbine did not show significant change up until a yaw angle of $\alpha=20^\circ$ for highly turbulent (spire) incoming flow. However, a sudden drop in the normalized power was observed after then. Moreover, looking at the change in the normalized power output of the upstream turbines at various yaw angles for the spire and no spire case, it can be

concluded that more gradual decrease is observed in the no spire case with increasing yaw angle of the upstream turbine compared to the spire case.

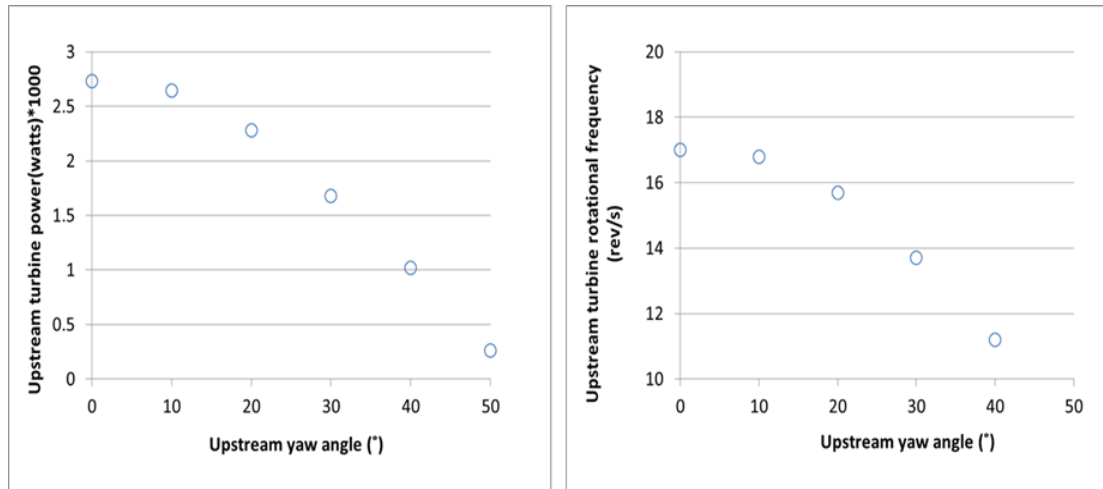


Figure 4-13 Variation in the power output and rotational frequency of the upstream turbine at various yaw angles for the no spire (low turbulence) case

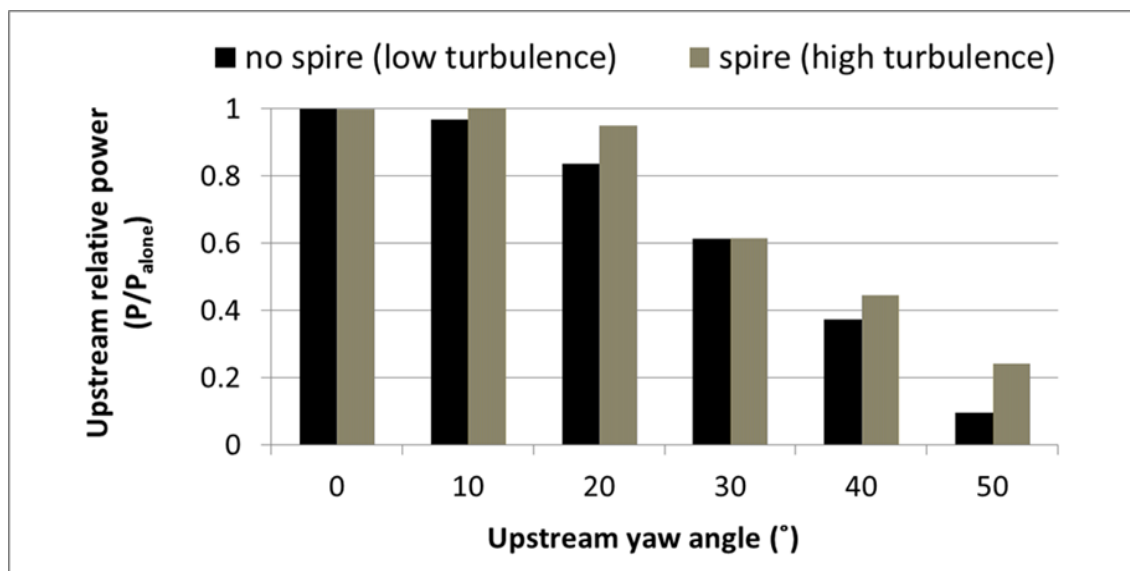


Figure 4-14 Normalized (Relative) power of the upstream turbine at various yaw angles for the spire and no spire flow case

Although increasing the yaw angle of the upstream turbine lead to reduction in the power output of the upstream turbine, downstream turbine can take advantage of that situation since it is no longer going to be under the direct effect of the upstream turbine wake. Therefore, downstream turbine sees comparably higher wind speeds and generate more power.

Figure 4-15 shows how the normalized power output of the downstream turbine changes with the increase in the yaw angle of the upstream turbine at different turbine spacing ($X/D=2$ and $X/D=4$). The figure clearly indicates that by increasing the yaw angle of the upstream turbine, there is a corresponding increase in the power output of the downstream turbine. The gain obtained in the power output of the downstream turbine by increasing the upstream turbine yaw angle is significantly influenced by the distance of separation between the turbines. The gain in the power output of the downstream turbine is around 42% for $X/D=2$ and 12% for $X/D=4$ at an upstream turbine yaw angle of $\alpha=50^\circ$ (the largest yaw angle used in the experiment).

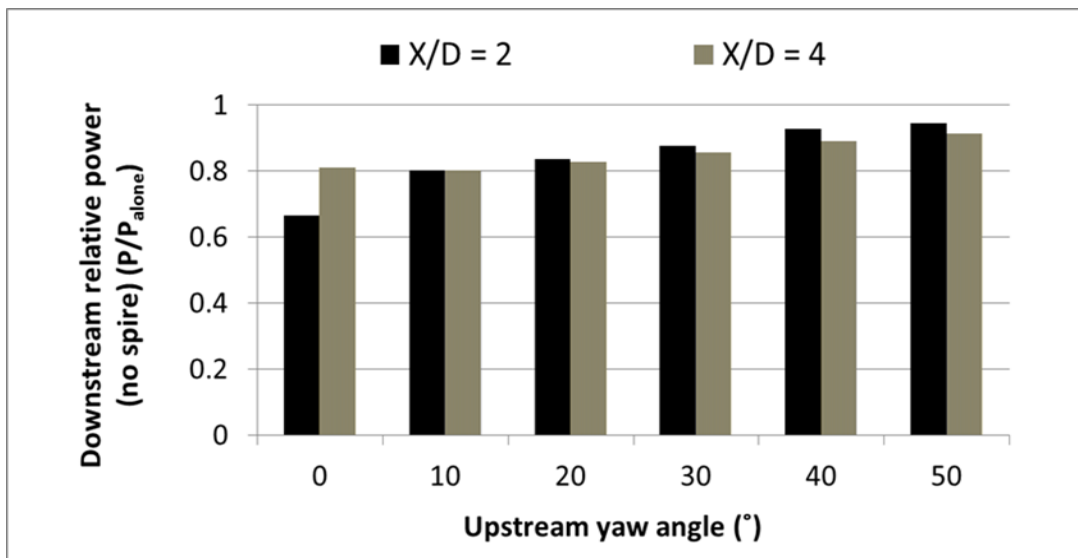


Figure 4-15 Normalized (Relative) power of the downstream turbine at $X/D=2$ and $X/D=4$ with the first upstream turbine operating at various yaw angles

The effect of increasing the yaw angle of the upstream turbine on the overall power output from two turbines at different turbine spacing ($X/D=2$ and $X/D=4$) was investigated for different incoming flow conditions. Figure 4-16 and Figure 4-17 shows how the overall efficiency of the wind farm (two model wind turbines in tandem arrangement) is affected by the distance of separation between the turbines and upstream turbine yaw angle in different incoming flow conditions.

As shown in Figure 4-16, maximum increase in the overall power output obtained for an upstream yaw angle of $\alpha=10^\circ$ at $X/D=2$ (the gain in the overall power is around 9%). At a yaw angle of $\alpha=20^\circ$, the gain is only about 4.5%. However, further increase in the yaw angle

of the upstream turbine leads to reduction in the overall power output since the drop in the power output of the upstream turbine becomes more dominant on the overall power output. The figure also shows that the overall power output obtained by operating the upstream turbine at an appropriate yaw angle ($\alpha=10^\circ$ or $\alpha=20^\circ$) at relatively small distance of separation ($X/D=2$) is comparable with $X/D=4$ (separation distance is doubled) and upstream turbine is not yawed. Considering the space and economic constraints related to the wind turbine siting in large wind farms, operating the upstream turbine at an appropriate yaw angle will not only improve the array efficiency but also save the space and money.

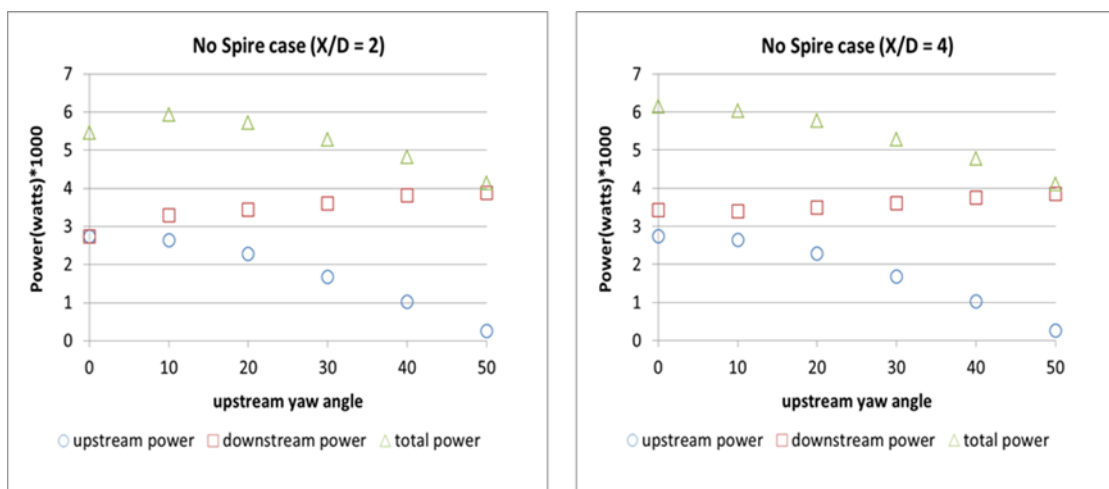


Figure 4-16 Variation in the total power output from two turbines at various upstream yaw angles depending on the separation distance for the no spire flow case

The effect of the turbulence character of the incoming flow on the overall power output from the two turbines with increasing upstream turbine yaw angle can be deduced from Figure 4-16 and Figure 4-17. In highly turbulent (spire) flow, increasing the upstream turbine yaw angle did not show any significant effect on the power output from the downstream turbine due to the fact that turbulent mixing mechanism is more effective on the performance of the downstream turbine than changing the yaw angle of the upstream turbine. Thus, the change in the overall power output with increasing upstream yaw angle is strongly dependent on the change in the power output of the upstream turbine (Figure 4-17). In addition, overall power output at an upstream yaw angle of $\alpha=10^\circ$ and $\alpha=20^\circ$ is almost the same with the case when upstream turbine is not yawed and a sudden drop in the overall power output was observed after $\alpha=20^\circ$ in highly turbulent (spire) flow.

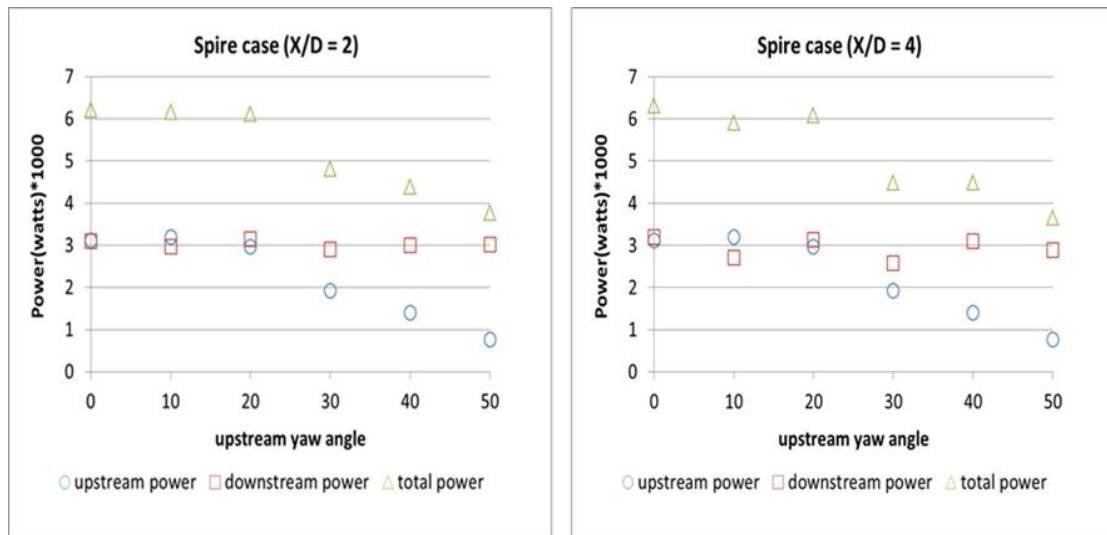


Figure 4-17 Variation in the total power output from two turbines at various upstream yaw angles depending on the separation distance for the spire flow case

4.2.4 CONCLUSION

This experimental study was conducted in order to see how yawing the upstream turbine will affect the overall power output from two turbines as well as the power output of the upstream and downstream turbines. A gain in the power output of the downstream turbine was observed with an increase in the upstream turbine yaw angle; however, there is a corresponding decrease in the power output of the upstream turbine. Thus, overall power output can be improved only at appropriate upstream yaw angle ($\alpha=10^\circ$ or $\alpha=20^\circ$). Besides, operating the upstream turbine at an appropriate yaw angle will reduce the distance between the turbines in a wind farm, thereby saving space and money. In addition, effect of incoming flow turbulence should be taken into account while changing the operating conditions of the upstream turbine.

BIBLIOGRAPHY

(2008). 20% Wind Energy by 2030. U.S. Department of Energy.

Major Wind Energy Countries. (2012). Retrieved April 13, 2012, from The Wind Power: Wind turbines and wind farms database: http://www.thewindpower.net/index_country_en.php

Adaramola, M., & Krogstad, P. (2011). Experimental Investigation of wake effects on wind turbine performance. *Renewable Energy*, 2078-2086.

Alfredsson, P., & Dahlberg, J. (1979). A preliminary wind tunnel study of windmill wake dispersion in various flow conditions. Stockholm, Sweden: The Aeronautical Research Institute of Sweden.

Arya, S. (1988). *Introduction to Micrometeorology*. Academic Press.

Arya, S., Capuano, M., & Fagen, L. (1987). Some fluid modeling studies of flow and dispersion over two-dimensional low hills. *Atmospheric Environment* Vol.21, No. 4, 753-764.

Barthelmie, R., Folkerts, L., Ormel, F., & et al. (2003). Offshore wind turbine wakes measured by SODAR. *Journal of Atmospheric and Oceanic Technology*, 30, 466-477.

Barthelmie, R., Hansen, K., Frandsen, S., Rathmann, O., Schepers, J., Schlez, W., et al. (2009). Modelling and measuring flow and wind turbine wakes in large wind farms offshore. *Wind Energy*, 431-444.

Beurskens, J. (2005, September). The evolution of wind turbines and wind park concepts. Petten, Netherlands: ECN.

Beyer, H., Pahle, T., Schmidt, W., Waldl, H.-P., & de Witt, U. (1994). Wake effects in a linear wind farm. *Journal of Wind Engineering and Industrial Aerodynamics*, 303-318.

Cao, T., & Tamura, T. (2006). Experimental study on roughness effects on turbulent boundary layer flow over a two-dimensional steep hill. *Journal of Wind Engineering and Industrial Aerodynamics*, 1-19.

Cao, T., & Tamura, T. (2007). Effects of roughness blocks on atmospheric boundary layer flow over a two-dimensional low hill with/without sudden roughness change. *Journal of Wind engineering and Industrial Aerodynamics*, 679-695.

- Chamorro, L., & Porte-Agel, F. (2009). A wind-tunnel investigation of wind-turbine wakes: Boundary- Layer turbulence effects. *Boundary - Layer Meteorology*, 129-149.
- Chamorro, L., & Porte-Agel, F. (2010). Effects of thermal stability and incoming boundary - layer flow characteristics on wind-turbine wakes: A wind-tunnel study. *Boundary - Layer Meteorology*, 515-533.
- Chamorro, L., & Porte-Agel, F. (2010a). Effects of Thermal Stability and Incoming Boundary- Layer Flow Characteristics on Wind Turbine Wakes: A Wind-Tunnel Study. *Boundary Layer Meteorology*, 515-533.
- Chamorro, L., & Porte-Agel, F. (2010b). Flow characterization of wind-turbine wake(s) developed in a boundary layer flow with different thermal stratifications:A wind-tunnel study. The fifth international symposium on computational wind engineering. North Carolina, USA, May 23-27.
- Chamorro, L., Arndt, R., & Sotiropoulos, F. (2011). Turbulent flow properties around a staggered wind farm. *Boundary - Layer Meteorology*, 349-367.
- Coeffe, J. (2011). Master Project: Wind tunnel investigations on wind farms. Lausanne, Switzerland: Wind Engineering and Renewable Energy Laboratory.
- Corten, G., Schaak, P., & Hegberg, T. (2004). Turbine interaction in large offshore wind farms. Wind tunnel measurements. Netherlands Agency for Energy and Environment.
- Dahlberg, J., & Thor, S. (2009). Power performance and wake effects in the closely spaced Lillgrund offshore wind farm. European Offshore Wind Conference. Stockholm.
- Fink, D. (2005). Small Wind Turbine Basics. *Energy Self Sufficiency Newsletter*, 21.
- FS Turbines Aerodynamic Efficiency Improvement. (n.d.). Retrieved April 13, 2012, from IQwind: <http://www.iqwind.com/index.php?categoryId=43263>
- Hoffmann, R. (2002). A comparison of control concepts for wind turbines in terms of energy capture. Darmstadt: Ph.D. Dissertation.
- Hu, H., Yang, Z., & Sarkar, P. (2011). Dynamic Wind Loads and Wake Characteristics of a Wind Turbine Model in an Atmospheric Boundary Layer Wind. *Experiments in Fluids*.

- Jenkins, M. (2008). Unit 7: Atmospheric Stability and Instability . Retrieved April 13, 2012, from USU: http://ocw.usu.edu/Forest__Range__and_Wildlife_Sciences/Wildland_Fire_Management_and_Planning/Unit_7__Atmospheric_Stability_and_Instability_1.html
- Jensen, L. (2007). Array efficiency at Horns Rev and the Effect of Atmospheric Stability. Dong Energy Presentation.
- Johns Hopkins University (2011). Better turbine spacing for large wind farms. ScienceDaily. Retrieved April 18, 2012, from <http://www.sciencedaily.com-/releases/2011/01/110120111332.htm>
- Kaimal, J., & Finnigan, J. (1994). Atmospheric Boundary Layer Flows: Their structure and measurement. New York: Oxford University Press.
- Lebron, J., Cal, R., Kang, H., Castillo, L., & Meneveau, C. (2009). Interaction between a wind turbine array and a turbulent boundary layer. 11th Americas Conference on Wind Engineering. San Juan, Puerto Rico.
- Linacre, E., & Geerts, B. (1999, April). Roughness length. Retrieved April 13, 2012, from <http://www-das.uwyo.edu/~geerts/cwx/notes/chap14/roughness.html>
- Madsen, H., Larsen, G., & Thomsen, K. (2005). Wake flow characteristics in low ambient turbulence conditions. Copenhagen Offshore Wind 2005.
- Manwell, J. F., McGowan, J. G., & Rogers, A. L. (2010). Wind Energy Explained: Theory, Design and Application, 2nd edition. Wiley.
- Massouh, H., & Dobrev, I. (2007). Exploration of the vortex wake behind of wind turbine rotor. Journal of Physics Conference Series 75.
- Meada, T., Yokota, T., Shimizu, Y., & Adachi, K. (2004). Wind tunnel study of the interaction between two horizontal axis wind turbines. Wind Engineering Volume 28, No. 2, 197-212.
- Meneveau, C., & Meyers, J. (2012). Optimal turbine spacing in fully developed wind-farm boundary layers. Wind Energy 15, 305-317.

- Pacella, R. M. (2010, March 26). How It Works: The Next-Gen Wind Turbine. Retrieved April 13, 2012, from POPSCI: <http://www.popsci.com/technology/article/2010-03/next-gen-wind-turbine>
- Ragheb, A., & Ragheb, M. (2010). Wind Turbine Gearbox Technologies. 1st International Nuclear and Renewable Energy Conference (INREC10). Amman, Jordan.
- Sanderse, B. (2009). Aerodynamics of wind turbine wakes: Literature review. Energy Research Center of the Netherlands (ECN).
- Transparency Market Research. (2012). Global Direct Drive Wind Turbines Market (2011-2016): Key trends and opportunities, new Installations and product developments and lower-maintenance requirements will drive market growth.
- U.S. Department of Energy. (2012, April 2). Wind Powering America. Retrieved April 13, 2012, from http://www.windpoweringamerica.gov/wind_installed_capacity.asp
- Venas, B. (1998). Experiments and numerical realizations of complex turbulent flows. Norwegian university of Science and Technology: Ph.D. Dissertation.
- Vermeer, L., Sorensen, J., & Crespo, A. (2003). Wind turbine wake aerodynamics. Progress in Aerospace Sciences, 467-510.
- Wharton, S., & Lundquist, J. (2010). Atmospheric Stability Impacts on Power Curves of Tall Wind Turbines - An Analysis of a West Coast North American Wind Farm. Lawrence Livermore National Laboratory.
- Wieringa, J. (1992). Updating the Davenport roughness classification. Journal of Wind Engineering and Industrial Aerodynamics 41-44, 357-386.
- Wu, Y., & Porte-Agel, F. (2010). Large-eddy simulation of wind-turbine wakes: Evaluation of turbine parametrisations. Boundary - Layer Meteorology, 345-366.